TESIS DE LA UNIVERSIDAD DE ZARAGOZA

2017

89

Pablo Andrés Piedrahita Salom

Non-linear models on complex networked systems: from synchronization phenomena to activity patterns and cascades

Departamento
Física Teórica

Director/es
Moreno Vega, Yamir
Borge Holthoefer, Javier

ISSN 2254-7606

Prensas de la Universidad
Universidad Zaragoza

ISSN 2254-7606

Universidad Zaragoza
1542

Tesis Doctoral

NON-LINEAR MODELS ON COMPLEX NETWORKED SYSTEMS: FROM SYNCHRONIZATION PHENOMENA TO ACTIVITY PATTERNS AND CASCADES

Autor

Pablo Andrés Piedrahita Salom

Director/es

Moreno Vega, Yamir
Borge Holthoefer, Javier

UNIVERSIDAD DE ZARAGOZA

Física Teórica

2017

Non-linear Models on Complex Networked Systems:

From Synchronization Phenomena to Activity Patterns and Cascades

Pablo Piedrahita Salom

A thesis submitted for the degree of

Doctor of Philosophy

Advisors

Dr. Yamir Moreno Vega

Dr. Javier Borge Holthoefer

Department of Theoretical Physics

University of Zaragoza

2017

A mi madre, no en vano ha sido todo tu esfuerzo, paciencia y dedicación.

En memoria de mi padre, tu partida marcó el inicio de este camino.

Agradecimientos

En primer lugar quiero agradecer a mi madre, la única persona en el mundo cuyo apoyo ha sido incondicional y sin la que no sería quien soy.
Quiero dar las gracias al resto de mi familia, a mi hermana Irene, y a mis sobrinos, David y Simón. Aunque el tiempo lejos de ustedes ha sido un enorme sacrificio, su presencia en vida es un constante estímulo para seguir adelante.
Me gustaría agradecer a mis directores de tesis, Yamir Moreno y Javier Borge Holthoefer, poco es lo que mis palabras pueden expresar respecto a su labor, ha sido un gran apredizaje a su lado y estoy seguro de que las lecciones nunca acabarán.
Estoy agradecido con todo el grupo de Física Estadística y No lineal, Fernando Falo, Jesús Gómez, David Zueco, Maria Carmen Moron, Alessandro Fiasconaro, Pedro J. Martínez, y en especial Juan J. Mazo y Luis Mario Floría, por todo su apoyo y dedicación desde el máster.
A mis preciados colaboradores, Sandra González-Bailón, Alex Arenas, James Gleeson y Davide Celai, siempre los recordaré por sus intachables y oportunas contribuciones.
Quieron reconocer a todos los miembros del BIFI, el lugar donde tuve la oportunidad de iniciar y dar mis primeros pasos dentro de la investigación científica. En concreto, gracias Guillermo, Arturo, Pedro y Patricia porque su trabajo y esfuerzo ayudaron a obtener los resultados más complejos de esta tesis. Así mismo, a mis compañeros del grupo COSNET, a Raquel, Joaquín, Emanuele, Sergio, Sandro, Guilherme y Carlos, con quienes tuve el placer de compartir innumerables comidas, viajes, salidas, discusiones y silenciosas horas de trabajo.
Por último, muchas gracias a mis amigos más cercanos, a Jesús, Jaime, Eduardo, Jorge, Verónica, Hector, Aura, Germán, Sofía, Gustavo, Alejandro, y Elizabeth, son incontables las veces que tuve que acudir por su ayuda y consejo a lo largo del tiempo que duró esta etapa.

Abstract

This dissertation articulates concepts from different disciplines and incorporates a comprehensive study of complex systems. Many dynamical and structural processes exhibit forms of emergent behaviors, often unspecified in the equations of motion. One of such effects is known as *synchronization*, a salient phenomenon that stands out for its ubiquitous occurrence in both numerical and experimental settings. Although a lot of research has been done to elucidate the intricate mechanisms underlaying the diverse types of synchronization reported thus far, many questions remain open to date, especially for networked systems. Here we propose to work at two distinct levels: (i) At the microscopic level, networks display recurrent structures named *motif*, one of which, denominated *relay*, enables two separate units to interact indirectly. This first instance of a rudimentary structure of interactions is ideal to study the communication of oscillating elements, where two different types of synchrony arise naturally: complete and generalized. To provide the system with dynamical complexity, we consider a regime in which the interacting oscillators describe chaotic trajectories, tuned by a continuous and instantaneous coupling. This approach allowed us to determine the exact onset of generalize synchrony and the specific mathematical conditions to identify it. (ii) At the macroscopic level, we increase not only size of the system but also its randomness. Several well-known complex topologies are examined for dynamical units that interact intermittently. This pulse-coupled populations of elements are analyzed and characterized from two perspectives: a neuronal approach (in the excitatory regime) and a sociological interpretation (in the oscillatory regime). In either case, the systems of interest displayed a wide variety of behaviors; regular, irregular and coherent patterns of oscillations, including regimes where system-wide synchronization is attainable. At the network level, we also managed to derive significant analytical predictions and descriptions of large activity events and other average estimations, rendering relevant discussions on their practical applications.

Contents

List of Figures

Resumen

La presente tesis doctoral se enmarca dentro de la física estadística y de sistemas complejos, haciendo especial énfasis en el estudio de fenómenos emergentes como la sincronización de elementos oscilatorios y excitables. Específicamente, esta investigación abarca el análisis de dinámicas no lineales en sistemas discretos cuyas interacciones están regidas por redes. En consecuencia, esta memoria de tesis puede ser dividida en dos componentes interconectados: En la primera parte se introducen conceptos básicos de la teoría de grafos, los cuales son necesarios para la comprensión de los demás contenidos de esta disertación ya que todos ellos versan sobre sistemas con *topologías* complejas subyacentes. En la segunda parte se presentan los resultados de las *dinámicas* no lineales sobre dichas estructuras (reales y sintéticas) y el análisis comparativo entre éstas y lo observado en fenómenos reales de tipo neuronal, social y experimental (circuitos electrónicos).

En síntesis podemos afirmar que, una vez ambos componentes (topología y dinámica) han sido implementados y perfeccionados, el principal objetivo de este trabajo de investigación es estudiar y analizar exhaustivamente modelos de dinámicas no lineales sobre redes (simples y complejas) en aras de determinar todos los posibles comportamientos de dichos sistemas, abordando aspectos como la predicción analítica de la aparición de fenómenos globales (cascadas) y de comportamientos colectivos (sincronización), así como la ulterior comparación con la actividad observada en fenómenos naturales y humanos.

Parte I: Redes complejas

Una vez introducidas diversas nociones generales sobre *complejidad* y comportamientos emergentes, se procede a revisar exhaustivamente un amplio número de investigaciones relativas a temas afines. La primera parte de la tesis está dedicada a examinar en detalle la teoría estándar de redes complejas, vital para el desarrollo de

los posteriores resultados. Concretamente, se introduce la definición formal de red a manera de *grafo* matemático, así como varias alternativas para representar convenientemente dichas redes (matriz de adyacencia, lista de adyacencia, etc.). Además, se describen conceptos fundamentales del formalismo de la teoría de grafos como el grado, camino, distancia, subgrafo, componente, etc. Seguidamente proponemos cuatro descriptores, ampliamente usados, para caracterizar la estructura de este tipo topologías: (i) distribución de grado, (ii) grado medio de los vecinos más cercanos, (iii) longitud media del camino más corto y (iv) agrupación media. Así, habiendo incluido estas herramientas, procedemos entonces definir cuatro tipos de topologías extensamente estudiadas a lo largo de este trabajo, y para las cuales ya existen muchos desarrollos analíticos. A saber, por un lado tenemos las redes regulares, que son 1D lattices, configuración todos-a-todos y k-regulares aleatorias. Por otro, las redes aleatorias tipos Erdős-Rényi, mundo pequeño y libres de escala. Adicionalmente, se describe brevemente una elemental versión de las hoy populares redes multicapas, a manera de generalización de los modelos antes mencionados. Por último, dos procesos combinatorios son introducidos en relación con la estructura de las redes. En primer lugar, para generar redes con una distribución de grado arbitraria, se propone el *modelo de configuración* que corresponde a la implementación algorítmica del formalismo conocido como *función generadora* (con el que es posible deducir rigurosamente importantes propiedades de la estructura de las redes). En segundo lugar, presentamos una revisión de la *teoría de percolación*, indispensable para entender cómo se pueden dañar y desintegrar las redes, tanto por fallos aleatorios como por ataques dirigidos.

Parte II: Dinámicas no lineales

Sincronización en sistemas caóticos de relevo

Al inicio de esta parte del trabajo se especifican la imprescindible noción de sincronización y las formas de sincronía que han sido detectadas en sistemas caóticos a lo largo de las pasadas décadas. Posteriormente, se definen los sistemas de relevo (también conocidos como relay, en inglés), que consisten en una estructura de red microscópica (tipo *motif*) en la que dos unidades o subsistemas separados interaccionan indirectamente a través de una tercera unidad o subsistema. Este tipo de configuración es de gran importancia e interés científico ya que para ella existen diversas aplicaciones tecnológicas. Además, en dicha estructura simple se ha detectado la aparición de varias formas de sincronización, lo que incluye la elusiva *sincronización*

generalizada (SG), uno de los comportamientos de interés dentro de este estudio. Concretamente, se examinan osciladores caóticos tipo Rössler en la configuración de relevo para acoples no dirigidos, continuos e instantáneos, haciendo uso de reconocidas herramientas matemáticas como el espectro de Lyapunov y de dos indicadores de presencia de sincronía entre las trayectorias de dichas unidades. Como medida de la sincronización completa su utiliza una función simple de error vectorial que compara la distancia de los puntos en el espacio de fases, mientras que para la SG se introducen dos indicadores independientes, a saber, el porcentaje de puntos sincronizados (SPP, en inglés) y las inter-dependencias no-lineales (índice N). Finalmente, se realiza el estudio detallado desde dos perspectivas, numérica y experimental. En primer lugar, se analiza la dinámica conjunta del sistema numérico de 9 dimensiones (3 por cada oscilador), y se determina que existe un valor especifico del acople, llamado crítico, a partir del cual los osciladores no conectados directamente exhiben sincronización completa. Tras un análisis más profundo y detallado de dicha dinámica a través de técnicas espectrales e de los indicadores antes mencionados, se puede concluir que el inicio de la sincronización completa marca el punto donde la SG ocurre. Adicionalmente es posible establecer la condición de aparición de dicho fenómeno, caracterizada por un único exponente de Lyapunov positivo, así como que la mejor técnica para detectar SG está dada por el indicador SPP (ya que éste presenta cambio abrupto justo en el acople crítico). En segundo lugar, se procedió a analizar la robustez de los resultados numéricos a través de la implementación experimental de circuitos electrónicos (tipo Rössler, operando en régimen caótico). Con este enfoque, y a pesar de las típicas limitaciones instrumentales, se puede establecer para un conjunto significativo de circuitos en configuración de relevo la existencia de SG.

Modelos de neuronas en redes heterogéneas

El segundo sistema de estudio tiene sus raíces en dinámicas tradicionalmente asociadas al campo de la Neurociencia. En la primera parte de este contenido se hace una significativa revisión de los modelos de neuronas desarrollados a lo largo del siglo XX, lo cual incluye neuronas puntuales (sin distribución espacial), modelos de compartimentos (con distribución espacial), dinámicas multidimensionales, etc. Finalmente nos centramos en el tipo concreto de dinámica a adoptar, llamada de integración-y-disparo (o integrate-and-fire, en inglés), que puede ser interpretada como una versión simplificada de modelos más realistas (como el modelo Hodgkin-Huxley). De esta

forma, se hace una descripción detallada de las diversas versiones que han sido propuestas para este modelo, con especial énfasis en aquellos ingredientes que intentan capturar los aspectos más relevantes de los sistemas reales. En cuanto a la red subyacente de interacciones y en aras de introducir complejidad estructural, se consideran sistemas de gran tamaño con obvias propiedades emergentes: Distribución de grado tipo libre de escala. Específicamente, nuestro modelo consiste en un conjunto de elementos excitables cuyas interacciones ocurren como pulsos (con retrasos) y están regidas por la estructura de una red compleja heterogénea y no correlacionada. Tras proponer algunas definiciones básicas, procedemos a realizar extensas simulaciones numéricas para caracterizar el sistema y examinar los efectos paramétricos. De esta forma, es posible determinar la existencia de varios regímenes de actividad autosostenida dependiendo tanto de los valores puntuales del acople como de la forma matemática de éste:

- **Acoples homogéneos:** En primer lugar, para acoples homogéneos (iguales para todos los elementos de la red), existe una actividad denominada *estándar* en la cual cada neurona es capaz de alcanzar su umbral de disparo con un sólo input de sus vecinos. Mientras que para valores pequeños del acople, en los cuales las neuronas requieren múltiples inputs para disparar, el sistema presenta un tipo de actividad de bajo nivel que podemos llamar *anormal* o *patológica*. Este último tipo de actividad se requiere que la dinámica inicie como consecuencia de la activación simultánea de varias zonas de la red. Ahora bien, la instancia más extrema de actividad anormal la denominamos *crítica* y corresponde al resultado de utilizar el valor más bajo del acople homogéneo para el cual la red presenta actividad de disparos alguna (es decir, el estado de actividad más patológica). Este estado es de actividad crítica es muy significativo ya que permite hacer estimaciones analíticas que resultan muy precisas.

  Con el objetivo de probar y examinar la robustez del sistema, introducimos dos estudios de perturbaciones: dinámicas y estructurales. (i) Perturbaciones dinámicas: Se propone una estrategia para probar la respuesta del sistema a los estímulos globales de excitación e inhibición. El mecanismo consiste en activar o desactivar el estado de un gran número de neuronas (escogidas al azar) y observar el cómo evoluciona el sistema. Se pudieron detectar tres escenarios principales: estímulos inhibitorios para extinguir toda actividad, estímulos excitatorios que no ocasionan cambios en la actividad global irregular, y estímulos

excitatorios e inhibitorios para aumentar y reducir, respectivamente, las oscilaciones de señales regulares (asociadas a acoples fuertes). (ii) Perturbaciones estructurales: Se introducen perturbaciones de tipo percolativo, de modo que una vez se remueven nodo aleatoriamente, se ejecuta la dinámica y se observa la respuesta del sistema. De este modo se puede encontrar transiciones de fallo de la actividad global cuya fracción crítica escala con el tamaño de la red. Así, se demuestra que las redes libres de escala son, una vez más, muy resilientes dinámica y estructuralmente a fallos aleatorios.

- **Acoples inhomogéneos:** En segundo lugar, cuando se correlaciona la amplitud de los pulsos que un nodo recibe con su grado se obtiene una excelente forma de homogenizar la actividad de un sistema heterogéneo. Las señales globales de disparos de la red se vuelven periódicas como resultado de un fenómeno de sincronización que denominamos oscilaciones coherentes. Dadas ciertas condiciones iniciales, todos los elementos en el sistemas exhiben una misma frecuencia de disparo en este caso. No obstante, aspectos como la longitud del transitorio, el valor medio, la amplitud y la periodicidad de la señal de disparos global dependen sensiblemente de dichas condiciones iniciales. Por esta misma razón, el estudio de perturbaciones dinámicas producto de estímulos globales en el caso de acoples inhomogéneos implica que todos los aspectos de la actividad global pueden ser alterados por medio de estímulos con patrones triviales (aunque los efectos de éstos suelen ser irreversibles).

El resultado más importante de este apartado es la derivación de expresiones analíticas que permiten deducir aspectos de la dinámica al nivel de grandes poblaciones de neuronas y sin recurrir a simulaciones numéricas. Brevemente, a través de aproximaciones de campo-medio se determina una expresión para el valor medio del intervalo-entre-disparos de las neuronas de conectividad k, lo cual permite descomponer la actividad global en los diversos grados e inferir otros aspectos interesantes del modelo. Así mismo, se demuestra que existe una expresión aproximada entre la tasa de disparos globales de la red y el valor medio del intervalo-entre-disparos, con lo cual se pueden estimar todas las cantidades promedio relevantes de la dinámica del sistema. Estas aproximaciones resultan ser muy precisas para redes que presentan alta heterogeneidad de grado.

Dinámica neuronal en sistema socio-técnicos

El último sistema de estudio consiste en una dinámica de neuronas tipo integración-y-disparo en redes sintéticas y reales. Concretamente se trata de un modelo que pretende capturar el mecanismo conocido como *contagio complejo* y aplicarlo en el contexto de las interacciones sociales (a través de plataformas tecnológicas). En la primera parte de este capítulo se revisan conceptos y trabajos previos relacionados a la modelización de dinámicas sociales (difusión de la información, cascadas y el modelo clásico de umbrales). En contraste con el modelo de neuronas anteriormente presentado, este caso no se trata de una población de elementos excitables sino de osciladores cuya actividad está completamente determinada por sólo dos parámetros: el acople (la fuerza o amplitud de los pulsos) y la curvatura de la función de carga de los osciladores (que especifica qué tan rápido alcanzan éstos la zona próxima al umbral de disparo). Varios aspectos de esta propuesta pueden ser interpretados de manera simple y directa siguiendo estas aproximaciones. Los pulsos, por ejemplo, podrían simbolizar en determinados entornos los mensajes emitidos por los usuarios, mientras que los parámetros de la dinámica representan aspectos esenciales de las interacciones sociales como la *influencia* de los vecinos (acople) y la *motivación* o *propensión intrínseca* de los agentes del sistema para activarse (curvatura de la función de carga). Trabajos previos en el tema señalan que bajo ciertas condiciones el sistema tiende al estado sincronizado, por lo que se anticipa la aparición de eventos de disparos globales.

Tras la implementación y caracterización del sistema, se determina que existen varios regímenes de actividad. Dado un valor fijo de motivación y para una topología específica, es posible encontrar que existe un valor del acople por debajo del cual el sistema no exhibe cascadas de disparos globales. De modo que se trata de un valor *crítico* que establece comportamientos super- y subcríticos del sistema (que también es verificado mediante el análisis de la distribución de cascadas). Con esto en mente, se estudian dos tipos de espacios de parámetros con el fin de observar los efectos de la dinámica en cuatro topologías: 1D lattices, Erdős-Rényi, mundo pequeño y libres de escala. De lo cual se detecta claramente un patrón: Para redes homogéneas, cuanto más aleatoriedad existe en la estructura mejor para alcanzar la sincronización (frente a condiciones dinámicas adversas, como acoples pequeños). En el caso de la topología heterogénea, las redes libres de escala mostraron ser muy restrictivas en cuanto a la aparición de sincronización, normalmente en ellas la sincronía o bien aparece rápido o no lo hace en absoluto. Ello puede ser explicado si se considera la así llamada

paradoja de la heterogeneidad.

Nuevamente, como en el caso anterior, se puede derivar una condición analítica que el sistema debe cumplir para que ocurra una cascada global, la cual se relaciona directamente con la condición de existencia de la componente gigante en redes. Este desarrollo permite predecir (con, por lo menos, un paso por adelantado) la ocurrencia de este tipo de eventos sistémicos. Para ilustrar esta derivación, se ejecutan múltiples simulaciones numéricas en las redes con los comportamientos extremos: Erdős-Rényi (las más tolerantes) y libres de escala (las más restrictivas). De esta manera se muestra que el método propuesto produce resultados precisos para un amplio rango de valores del grado medio de dichas redes.

La última parte de este estudio se enfoca en una aplicación en una (sub) red de la plataforma Twitter correspondiente a la actividad de un fenómeno de protesta en España conocido como el 15M. El primer aspecto que se aborda es la determinación del comportamiento periódico de los usuarios, para lo cual se analizan las señales individuales de los mismo con la densidad espectral. Los resultados de esta pruebas son indiscutibles, en cuanto a que dichos agentes en efectos exhiben múltiples periodicidades. El segundo aspecto que se examina es una estrategia para estimar los valores de los parámetros del modelo a fin de reproducir el comportamiento observado. Se concluye que el valor del intervalo-entre-disparos es aproximadamente inversamente proporcional a la propensión intrínseca de los agentes. El último aspecto que se estudia es la distribución de cascadas correspondiente a periodos de alta y baja actividad en el sistema real. Se determinó que este modelo puede describir fielmente las características estadísticas de los diversos regímenes que el sistema presenta. En este orden de idea, nuestra aproximación al problema de modelizar interacciones sociales extiende considerablemente todo el trabajo previo en el tema ya que incorpora elementos como la activación recurrente, el contagio complejo y las cascadas de información.

Chapter 1

Introduction

In recent years the term "*complexity*" has become a trendy word, which is particularly widely used in specialized fields. However, specifying such term in the context of technical research can be a tricky task, trait clearly reflected by the fact that there is no general consensus or universal definition for it. In our particular case, we will no try to provide a formal statement on the matter, though simply introduce a broad notion adopted in Physics and Mathematics. In consequence, a *complex system* always involves phenomena displaying at least one of the following aspects [3]:

i Circular causality, feedbacks, logical loops, self-referential rules or recursion.

ii Sensitivity to initial conditions, exponential propagation of perturbations and unpredictability.

iii Large populations of units characterized by interconnected and interdependent non-trivial relations.

iv Emergence: Self-organized global behaviors or large-scale structures that emerge from the interaction of –disordered– units.

Among these qualities and behaviors, *Emergence* is certainly the most puzzling. The concepts that such a methodological view involves contradict a philosophical standpoint called *Reductionism*. Generally speaking, reductionist thinking suggests that objects, phenomena, theories or even entire areas of knowledge can be reduced o decomposed into more basic parts, that in turn can be explained or accounted for by other –wider– theories or areas of knowledge. For example, in this tradition it is believed that chemistry is based on physics, biology based on chemistry, psychology on biology, and so on [4]. These ideas are not recent: Back in Newton's time the

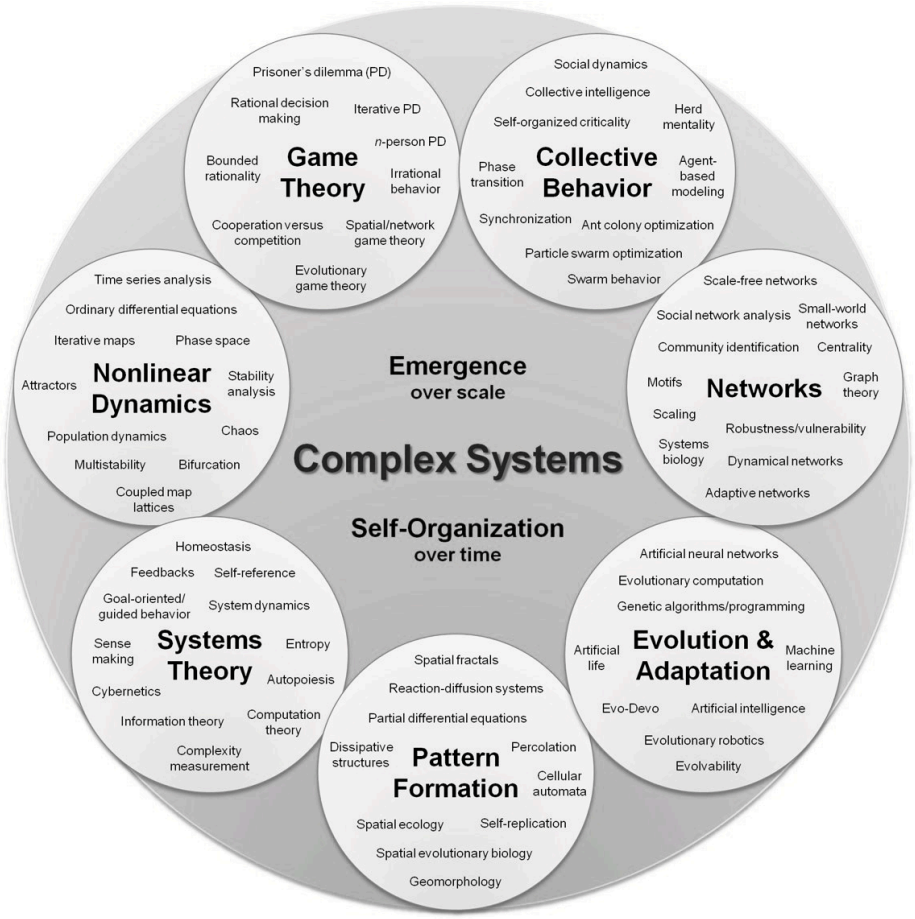

Figure 1.1: Graphical representation of Complex Systems.

mechanistic approach was the main trend and scientists use to believe that any phenomenon could be explained by the laws of motion. Up to this point, this posture is still an important methodology in fields like particle physics and molecular biology (though some changes are taking place) [5, 6]. In contrast, the idea of Emergence can be understood –informally– as prescribed by the Aristotelian principle: "The whole is more than the sum of its parts". In concrete practical terms, this view states that collective phenomena, that occur at macroscopic scales (typically in Complex Systems), are due to local interactions among its constituents but cannot be reduced or explained as a result of the properties observed at the microscopic level of the system. In other words, these emergent outcomes are (structural or dynamical) patterns not specified in the equations that describe the evolution of the system. Examples of collective phenomena can be found in a wide variety of natural and synthetic systems: dissipative processes (convection in liquids or gases), hydrodynamics (viscosity, elasticity and tensile strength), statistical physics (phase transitions in materials), biology

(organization of living cells), neuroscience (activity patterns in the brain), man-made settings (failure cascades in power-grids), among many others [7].

To illustrate how extensive complex systems is, Fig. 1.1 shows an organizational map of the field broken into seven sub-groups[1]. This schematic Figure summarizes some of the most recognizable phenomena in this field and provides an great compartmentation that comprises around 70 different sub-topics (that, in turn, also exhibit interdependences with each other). Obviously, the number of possible systems that this area comprises is quite large, so let us describe next a few limited scenarios, narrowing our attention to a relevant historical perspective.

Three entangled stories in one timeline

With the objective of establishing the precise context in which the present doctoral research is set, in what follows we overview some of the prior work on three related areas and provide brief yet illuminating comments on their salient history.

- **Nonlinear dynamics and chaos:** The study of dynamical systems and nonlinear models has a long history, which goes back to the formulation of the infinitesimal calculus in the 15th century [8]. However, it was not until the mid-20th century, and in the following decades, that a true explosion of knowledge and intense research activity began. Among many remarkable contributions, the seminal work by E. N. Lorentz on hydrodynamic flow (1963) [9], stands out. Lorentz observed that a simple set of coupled differential equations displayed a complicated behavior, quite sensitive to initial conditions, notion that eventually came to be known as *Chaos*[2]. During the late 1960's and the 1970s, thanks to the introduction of computers as research tools, the powerful concept of fractality was developed [10], and the first applications of nonlinear models appeared in fluid mechanics (turbulence) and biological systems (e.g. cardiac pacemakers, circadian rhythms, and other oscillators) [11, 12, 13, 14]. Today,

[1] Created by Hiroki Sayama, D.Sc., Collective Dynamics of Complex Systems (CoCo) Research Group at Binghamton University, State University of New York, CC BY-SA 3.0, `https://commons.wikimedia.org/w/index.php?curid=12191267`.

[2] Although the first person to discover a chaotic system was the mathematician and philosopher Henri Poincaré (1854–1912) with the paradigmatic *three-body problem*. Poincaré demonstrated that no general analytical solution exists for it in terms of algebraic expressions and integrals.

after having spent nearly 40 years developing countless significant contributions to multiple disciplines, the study of deterministic nonlinear dynamics has become one of the most solid and active scientific research fields.

- **Graphs:** Networks or graphs, as abstract mathematical objects, have also a long tradition. Even though the first studies on this subject can be traced back to the 18th century [15], which were mainly focused on topological aspects and navigability[3], the topic remained unpopular[4] until the introduction of statistical methods on random graphs by Paul Erdős and Alfréd Rényi in 1959 [16] and the extraordinary contributions by Frank Harary in the decades of the 1960's and 1970's [17]. Their emblematic works created what is known today as *Network Theory*, one of the fastest-growing areas of modern science. More recently, in the late 1990's and the early 2000's, graphs became more than an exclusive theoretical exercise for mathematicians with the introduction of novel topologies linked to real-world phenomena (e.g. small-world and scale-free models) [18, 19]. As of now, after two decades of intense research (devoted mainly to structural topics), network theory constitutes the standard framework upon which scientists build up their models of discrete interacting units [20, 21].

- **Mathematical neurons:** The first mathematical model of a neuron was proposed by a pioneer named Louis Lapicque in 1907 [22] and, for the most part of the 20th century, just a handful of remarkable researchers contributed to this field with abundant discoveries. Among all of these models and theories, the most relevant are those that attempt to capture in a simple manner intricate mechanisms of real neurons and to reproduce realistically the interactions among them. Let us mention a few of these prominent proposals: The synaptic plasticity introduced by Donald Hebb (1940s) [23], the spike generation mechanism by Alan Hodgkin and Andrew Huxley (1950s) [24], the cable theory by Wilfrid Rall (1950s) [25, 26], the interacting neurons by David Marr (1960s-1970s) [27] and the working memory studies by Daniel Amit (1980s-1990s) [28, 29] are some of the outstanding findings in Theoretical Neuroscience during this period of time. In the decades of the 1980's and 1990's, thanks to the massive progress on numerical simulations to model populations of interacting elements,

[3]The notable problem of the Seven Bridges of Königsberg, solved by Leonhard Euler in 1736.

[4]In the sense that during the 19th century and for the better part of the 20th century only a small group of researchers, mostly mathematicians, produced isolated developments in this area.

the scientific community developed a great interest in the study of neural systems at many different levels and scales (being random recurrent networks the most widely used approach when it came to capturing neural architectures) [30, 31, 28, 29]. In the past two decades, proposing dynamics of neurons became a popular phenomenon as a result of the network-approach, and also due to the realization that modeling and understanding the brain might be indeed the ultimate challenge in network science. This is the foundation of this relatively new interdisciplinary field of investigation, which, as in the previous cases, is also extremely active nowadays[5] [32, 33, 34, 35, 36].

Systems of interest

In the previous Section we presented the background in which this dissertation is rooted. Let us now turn our attention to the specific methodology and subjects on which our research will be mainly focused, namely deterministic processes that take place on top of random structures of interactions.

Networks

The interest in the study of complex networked systems has been steadily increasing over the past few decades, especially in Physics as a results of the prominent advantages provided by the standard techniques of the statistical mechanics. In our case, we will focus on discrete systems that can be modeled as static complex networks. As an emblematic example of structural complexity let us comment on the scale-free topology [19]. As its name indicates, these networks do not posses a characteristic scale (their degree distribution is a power-law), allowing certain structures to appear in all the scales (notion that connects with both fractals [10] and the scaling observed in phase transitions [37, 38]). These emergent topological properties, can be interpret as a collective behavior in terms of the so-called dynamical models (generating algorithms that involve growth), which is precisely one of the universal fingerprints of complexity.

As an illustration of their versatility, in the scientific literature there are numerous applications and significant results in various disciplines; ranging from physics (e.g.

[5]By a straightforward search on the website http://www.pubmed.com, it can be verified that the number of neuron-related articles published in 2016 is around 70.000 –papers containing any of the words: “neuron”, “neural” or “brain”.

cosmology, quantum mechanics, materials, etc.) and engineering (e.g. Internet, communication and power networks) to biology (e.g. proteins, genetics, neuroscience, epidemics, etc.) and sociology (e.g. real and online social networks, small world effect and authors' network, among others) [39, 21, 40, 20]. In Chapter 2 we will review basic properties and measures of the graph theory, incorporating a few essential complex networks models and structural-related processes.

Synchronization

Among all of the emergent behaviors that have been found in Complex Systems as yet, synchronization stands out for its ubiquitous nature. This phenomenon was originally observed by Christiaan Huygens, in the mid-17th century, from a set of coupled pendulum clocks, and it is still one of the most enigmatic outcomes detected in all kinds of coupled oscillating setting [41, 42]. Remarkable real-world examples of synchrony include flashing of fireflies, electric activity in the brain (epileptic seizures), activity patterns of cardiac cells (pacemakers), optical communications, arrays of electric and electronic circuits, and a broad family of dynamical systems (which includes, of course, chaotic oscillators) [43, 8]. Regarding this last example, that is, systems consisting of units operating in chaotic regime, there has been made an enormous effort in developing a vast amount of research over the past three decades [44, 45, 46, 47, 48, 49, 50]. Many of these developments aimed to establish a general framework that could account for and classify the numerous kinds of synchronized states reported in the literature, whereas others to introduce novel mathematical indicators of synchrony. At the network level a lot of works have also been devoted to studying synchronization phenomena, particularly on diverse types of deterministic oscillators, with outstanding rigorous findings that have spread to other disciplines as a consequence of their practical implications [31, 51, 52, 43, 39, 42, 53, 54, 55, 56, 57].

In our particular case, we will examine thoroughly two types of synchronization, complete and generalized [58], in a configuration[6] that allows two separate units to communicate –indirectly– through a third one (in which the channels of interactions are instantaneous and bidirectional). This setting has been considered by other authors to study a few different forms of synchrony (mostly lag-synchronization) [59, 60, 61, 62], and to analyze experimental systems like circuits [63, 64], Lasers [61, 62], brain dynamics [65, 66, 67] and underwater acoustic sensors [68]. However, many questions

[6] A simple structure that resembles a water molecule.

remain open concerning the appearance of generalized synchronization in relay systems; specifically the conditions that determine the onset of relay synchronization and the derivation of mathematical tools and measures that enable us to detect accurately hidden behaviors in coupled chaotic systems. All of these questions, and some other, will be addressed in Chapter 3.

Neural dynamics

In living systems of neurons there are many kinds of cell architectures, and that they all exhibit a broad range of behaviors (diverse regimes of activity, firing mechanisms, adaptation, spikes, and so on) [69, 70]. Over the years our models of individual neurons have evolved into a high-level of sophistication as an attempt to capture such diversity, and nowadays it is possible to perform extensive and expensive simulations on large populations of these independent units. Regarding the interactions among real neurons, it is indeed an essential and elusive aspect to reproduce realistically, yet networks provide a useful and simple framework to this end. A great deal of research has been devoted precisely to study emergent properties of ensembles of neurons that interact according to both simple and complex topologies [71, 72, 73, 74], a topic that continues to be an attractive interdisciplinary subject for physicists, mathematicians and neuroscientists [34, 35, 33, 75]. Most of these works capitalize on numerical approaches that have demonstrated to be quite versatile; one can generate various underlying structures of interactions and include many realistic ingredients like chemical synapses, ion currents, compartments, stochastic currents, noise and adaptative parameters [76, 77].

However, numerical models also have many limitations and, at the network level, analytical results are scarce, particularly for sparsely connected systems (which resemble the actual structure of the brain [78]). To illustrate this point, that is the lack of rigorous results on networks, let us consider some of the most common constraints imposed on the system of study. As far as we know, the vast majority of the analytical approaches already published for spiking models of neurons require some sort of *diffusion approximation*, so that the membrane potential can be described approximately as a random process [79, 80, 81]. For this attribute to be true, the density of links of the network has to be high [28, 29, 30, 82], which, by definition, is not the case for sparse network. A second mathematical technique is the so-called "spike-train statistics", which is a framework developed to analyze and fit spike patterns

of population of neurons[7] by means of a characterizing probability function [83, 84]. Even though this attempt seems promising, especially to study activity patterns of living neurons, it is a proposal that is far from fully developed (there is no general strategy to derive such probability function from data, and the precise mathematical form of it is required –as well as a procedure to fit accurately the many parameters that are needed) [85].

Finally, concerning the popular family of neural dynamics known as integrate-and-fire[8], numerous studies devoted to numerical explorations were performed over the past four decades [86, 71, 28, 79, 80, 87, 77, 36], whereas just a handful were published on developing analytics (mostly based on mean-field approximations) [88, 89, 81, 72, 90, 91, 92, 93]. These limited theoretical developments also hinge on similar assumptions as the ones mentioned above, namely densely connected networks or stochastic approximations (useless for sparse graphs). In contrast, in Chapter 4 we will examine large ensembles of excitable elements on heterogeneous topologies, providing both numerical findings and novel analytical estimations.

There is warning on the vernacular here: To honor a long tradition we use in this Thesis expressions like "neural model" or "model of neurons" to refer to a group of mathematical frameworks that mimic –to some extent– the behavior of real neurons. However, in our view, such models are not strictly limited to be a representation of the some biological cell. Consequently, in a more general sense, we consider them as pulse-coupled dynamical units that should never be constrained by the features that real neurons exhibit. As an observation related to this viewpoint, very often one finds in the literature authors trying to justify these mathematical models by comparing their findings, on clearly unrealistic scenarios, with the activity observed in live populations of neurons. Be certain that this is not what we aim to do here. On the contrary, we believe there is no need for us to follow that path because these versatile dynamics have an intrinsic value that extends far beyond their application as a plain description of what such cells typically do.

Socio-technical environment

The proliferation of social networking tools –and the massive amounts of data associated to them– has evidenced that modeling social phenomena demands a com-

[7] Generally driven by external stimuli or noise.

[8] Two of these models are studied in depth in the present dissertation.

plex, dynamic perspective. Physical approaches to social modeling are contributing to this transition from the traditional paradigm (scarce data and/or purely analytical models) towards a data-driven new discipline [94, 95, 96, 97]. This shift is also changing the way in which we can analyze social contagion and its most interesting consequence: the emergence of information cascades in the Information and Communication Technologies (ICT) environment. Theoretical approaches, like epidemic and rumor dynamics [98, 99, 100], reduce these events to physically plausible mechanisms. These idealizations deliver analytically tractable models, but they attain only a qualitative resemblance to empirical results [101], for instance regarding cascade size distributions. The vast majority of models to this end –including the threshold model [102], overviewed in Chapter 5– are based on a dynamical process that determines individuals' activity (transmission of information), and this activity is propagated according to certain rules usually based on the idea of social reinforcement, i.e. the more active neighbors an individual has, the larger his probability to become also active, and thus to contribute to the transmission of information. Yet, the challenge of having mechanistic models that include more essential factors, like the self-induced (intrinsic, spontaneous) propensity of individuals to transmit information, still remains open –though some contributions emerge in this fast-growing field [103, 104]. Furthermore, the availability of massive amounts of microblogging data logs, like Twitter, places scholars in the position to scrutinize the patterns of real activity and model them. These patterns indicate that avalanche phenomena are not isolated events. Instead, users engaged in a certain topic repeatedly participate, affecting each other and giving rise to an heterogeneous collection of cascades emerging over time, which can not be modeled independently from each other.

As a consequence of these observations, in Chapter 5 we propose a dynamical threshold model that is able to display a broad variety of behaviors and reproduce the activity patterns detected in online platforms, extending our comprehension of social interactions and our ability to predict the occurrence of system-wide events.

Chapter 2

Complex networks

In order to better understand the models, descriptions, and results relative to the underlying complex topologies that will be studied throughout this Thesis, some of the standard framework of graph theory has to be introduced. Consequently, in this Chapter we report on basic concepts, notation and formalism that will allow us to grasp the importance of all the theoretical developments and findings that the present work encompasses. There is a warning, though: The following sections are, by no means, a full review on the subject of graph theory, and we strongly suggest reading references [40, 20, 39, 105, 21, 106] for further insight into the topic.

The Chapter is structured in the following way: In Sect. 2.1 we bring forward the notion of graph and provide a set rigorous definitions, mandatory for the study of networks. Four structural-related descriptors to characterize networks are presented in Sect. 2.2 and, in Sect. 2.3, we report on several simple and complex topologies (providing the formal description of their defining features). The last two Sections of the Chapter are devoted to describing models on how to build and break down graphs respectively, both processes are of major importance in theoretical and empirical understanding of complex systems.

2.1 Simple definitions and notation

In a wide sense the term "*Network*" refers to an abstraction usually represented as a set of points connected by lines or arrows. This notion can also be stated in a more formal way by introducing a mathematical entity known as *graph* (from now on we shall use indistinctly the words graph and network). A graph $\mathcal{G}$ is simply a pair of sets $(\mathcal{V}, \mathcal{E})$, where $\mathcal{V} \neq \varnothing$ is a countable set whose elements are named *nodes* or *vertices* and, $\mathcal{E}$ is a set of pairs of different nodes denominated *links* or *edges*. If these pairs

are ordered we say that the graph is *directed* (also called *digraph*), if not, we say the graph is *undirected*. The cardinality of $\mathcal{V}$, usually denoted by N, is the *size* of the graph, and the cardinality of $\mathcal{E}$ is symbolized by $\mathcal{L}$. Now, if $\mathcal{L} \ll N^2$ the network is said to be *sparse* and if $\mathcal{L} \approx N^2$ we say it is *dense*.

A second way to represent a network is by its *adjacency matrix*, A, a square matrix of order N with entries $a_{ij} \neq 0$ whenever $(i,j) \in \mathcal{E}$ and $a_{ij} = 0$ otherwise. Note that our definition of graph includes two implicit constraints, first, $a_{ii} = 0$ since $(i,i) \notin \mathcal{E}$, and second, no matter the value of $a_{ij} \neq 0$ only one edge is allowed between two nodes (i.e. for the same pair of nodes multiple edges are forbidden). If A happens to be binary or boolean (its entries are either 1 or 0), then we call this network *unweighted*, and if not, it is *weighted* (and commonly represented as W instead). Two nodes, i and j are considered *neighbors* (or *adjacent*) when $a_{ij} \neq 0$.

By letting $\mathcal{V}_i$ denote the set of all neighbors of node i, we find a third way to represent a network. This representation is known as the *adjacency list* and can be defined as a set of 3-tuples of the form $(i, j \in \mathcal{V}_i, a_{ij})\, \forall i, j$ (which is very useful when it comes to computer coding).
As for individual node properties, the most salient feature of all is the *degree* (or *connectivity*), that we can specify as in-degree and out-degree of node i by the expressions,

$$k_i^{in} = \sum_j a_{ij} \quad \text{(incident links)} \qquad \text{and} \qquad k_i^{out} = \sum_i a_{ij} \quad \text{(emergent links)}\,. \tag{2.1}$$

For undirected networks A is symmetric, so obviously $k_i^{in} = k_i^{out} = k_i$ (which is also the cardinality of $\mathcal{V}_i$). In a similar manner, still for undirected networks, the *average nearest neighbors degree* of node i can be described as follows,

$$k_{nn}^i = \frac{1}{k_i} \sum_{j \in V_i} k_j = \frac{1}{k_i} \sum_{j=1}^{N} a_{ij} k_j = \frac{\sum_{j=1}^{N} a_{ij} \sum_{h=1}^{N} a_{jh}}{\sum_{j=1}^{N} a_{ij}}\,, \tag{2.2}$$

expression that allows us to compute easily a network descriptor that will be introduced in the next section.

The word *path* is defined as an ordered set of $n+1$ nodes $\mathcal{V}_p = \{i_0, i_1, ..., i_n\} \subseteq \mathcal{V}$ and n edges $\mathcal{E}_p = \{(i_0, i_1), (i_1, i_2), ..., (i_{n-1}, i_n)\} \subseteq \mathcal{E}$ (n is called *path length* or *distance*). When $n > 0$ and $i_0 = i_n$ the path receives the name of cycle or loop. If there is a path between any two nodes of a undirected network we say that it is *connected* (in the case of digraphs the name is *strongly connected network*). If there is no path between

two nodes, we say that the distance between them is infinite ($n \to \infty$).
Finally, a set $\mathcal{G}' = (\mathcal{V}', \mathcal{E}')$ is said to be a *subgraph* of a graph $\mathcal{G} = (\mathcal{V}, \mathcal{E})$ if $\mathcal{V}' \subseteq \mathcal{V}$ and $\mathcal{E}' \subseteq \mathcal{E}$. A connected subgraph is named *component*, and the largest component of a network is called *giant component*, whose size scales with the size of the network.

2.2 Characterizing networks

There are many sound and accurate descriptors reported in the literature to characterize networks (at both local and global level), but since we will not use most of them in this Thesis here we only describe four of them and suggest further reading for more details. In the rest of the chapter all definitions are introduced for undirected networks unless noted otherwise.

2.2.1 Degree distribution

In network science, it is customary to characterize (uncorrelated) graphs by what is commonly known as *degree distribution*, $p(k)$, which is simply the fraction of nodes having degree k (although this is not the only definition there is, it is the simplest one). For uncorrelated networks the *average degree* is thus,

$$\langle k \rangle = \sum_k k p(k) = \frac{1}{N} \sum_i k_i = \frac{2L}{N} \ , \tag{2.3}$$

and in the same fashion it is possible to express any *moment* of the distribution as,

$$\langle k^n \rangle = \sum_k k^n p(k) \ , \tag{2.4}$$

which are very useful to extract information about the shape and location of such distribution (its characterization) and will play an important role when making predictions for the models we study in following chapters.

For digraphs, of course, there are two kinds of degree distributions (one for in-degree and another for out-degree) and all relevant quantities relating to them can be computed analogously to undirected graphs ($p(k^{in}), p(k^{out}), \langle k^{in} \rangle, \langle k^{out} \rangle$, etc.).

2.2.2 Average degree of the nearest neighbors

The *average degree of the nearest neighbors for nodes having degree* k, $k_{nn}(k)$, can be computed directly from Eq. 2.2 as follows,

$$k_{nn}(k) = \frac{1}{N_k} \sum_{\forall i | k_i = k} k_{nn}^i \ , \tag{2.5}$$

where $N_k = Np(k)$ represents the total number of nodes of degree k. This quantity is most relevant since it is related to the conditional probability, $p(k^{'}|k)$, that a node of connectivity k is linked to a node of degree $k^{'}$,

$$k_{nn}(k) = \sum_{k^{'}} k^{'} p(k^{'}|k) \ . \tag{2.6}$$

When a network exhibits *degree-degree correlations* the probability $p(k^{'}|k)$ has a dependence on k, whereas for *uncorrelated* networks $p(k^{'}|k)$ is just a function of $k^{'}$ (it can be proved easily that $k_{nn}(k) = \langle k^2 \rangle / \langle k \rangle$, constant when there are no correlations). If $k_{nn}(k)$ increases with k, the network is said to exhibit an *assortative mixing*, and if $k_{nn}(k)$ decreases with k, the network is considered to have a *dissortative mixing*. Clearly the average degree of the nearest neighbors for nodes of degree k is a simple measure –easy to interpret– that can be used to detect the presence of such correlation in networks.

2.2.3 Diameter and average shortest path length

The *shortest path length* between nodes i and j is the number of edges of the shortest path between them, which is a measure of distance usually represented as a matrix whose entries are l_{ij}. This matrix leads to the concept of *diameter* of the network, that corresponds to its largest entry $d = \max_{(i,j)}\{l_{ij}\}$. Another important and defining measure of networks' metrics is the *average shortest path length* that can be expressed as,

$$\langle l \rangle = \frac{1}{N(N-1)} \sum_{\forall i \neq j} l_{ij} \ . \tag{2.7}$$

The behavior of this measure with the size of the graph is often studied and used to identify networks' topology. Unfortunately this quantity, as defined above, has one disadvantage: it diverges when there are unreachable nodes (i.e. when the network has more than one component). One option to sort this out is to perform the average over nodes in the so-called giant component, and this is the definitions we will assume from now on (other options require slightly different definitions that we shall not consider here). The same constraint is to applied for the diameter of the network.

2.2.4 Average clustering

It has been observed that networks (both real an synthetic) tend to form "triangles" naturally (cycles of length 3), which can be express formally by the notion of clustering of node i, C_i, as the number of links existing between nodes in $\mathcal{V}_i$ (nearest neighbors), symbolized by e_i, divided by the total possible number of edges,

$$C_i = \frac{2e_i}{k_i(k_i-1)} = \frac{\sum_{jh} a_{ij}a_{jh}a_{hi}}{k_i(k_i-1)} \ . \tag{2.8}$$

Consequently, the *average clustering*, also known as *clustering coefficient*, of the network is given by,

$$\langle C \rangle = \frac{1}{N}\sum_i C_i \ . \tag{2.9}$$

Again, as in previous cases, we can many find in the literature numerous definitions of clustering, specially those that adopt the notion of *transitivity*, and regarding this it is worth emphasizing that the value of clustering depends on the particular formula we use.

2.3 Network models

Over the past decades the scientific community has either discovered or developed an enormous amount of network topologies and algorithms to generate synthetic configurations with desired features (probably as an attempt to mimic real graphs). In this section we will introduce the main aspects of topologies that will be studied in this Thesis and some of the methods to construct them.

2.3.1 Regular graphs

An elementary definition of a regular graph states that it is a network where each vertex has the same degree. Under such a general statement there can be found a wide variety of topologies, being of interest three of them:

- *1D lattices* or *ring networks* (RN): where each node is connected to the same number, ι, of nearest neighbors on each side (having periodic boundary conditions). This configuration possesses a high clustering coefficient and a large average shortest path length ($\langle l \rangle = \mathcal{O}(N)$) [105]. To generate this graph the specific algorithm is not relevant, and apart from N, the only extra parameter

needed is $\iota \geq 1$ (so each node has connectivity $k = 2\iota$). See Fig. 2.1 for an illustrative diagram.

- *Complete networks* or *all-to-all*: where each vertex is connected to the other $N-1$ nodes of the network [105]. This graph has a high clustering coefficient and the smallest average shortest path length possible ($\langle l \rangle = 1$). Again, the algorithm implemented to generate this network is irrelevant since the structure of the graph is not affected by it, and no extra parameters are required.

- *Random* $k-$ regular *networks* (RRN): In this case each node is connected to their k neighbors, chosen uniformly at random from the N vertices. These graphs tend to exhibit a low clustering coefficient and a small average shortest path length. Several methods have been proposed to generate this topology efficiently, in our case we will use the configuration model –described in the Sect. 2.4– (apart from N and $k \geq 2$ no extra parameters are needed to obtain connected networks).

2.3.2 Erdős-Rényi topology

Random graphs, also referred to as Erdős-Rényi netwoks (ERN), were the first complex topologies ever studied and come from a long tradition in mathematics [16]. Although there have been proposed several frameworks to define them, here we will focus on two of the simplest versions (see Fig. 2.1 for an illustrative diagram).

The "*ensemble-of-networks*" approach is a well-known and widely used strategy to introduce what a random network is [16, 107, 105]. Briefly, by fixing either the pair $(N, \mathcal{L})$ or the pair (N, p) (where p represents the probability of edges between vertices) one can construct a family of graphs that satisfy such constraints, and then by selecting –at random– one graph among our collection of graphs it is said that a random network is created. In fact, fixing (N, p) leads to the ensemble of graphs having size N –family generally represented by $\mathcal{G}(N, p)$–, and in which a graph having $\mathcal{L}$ links appears with probability $p^{\mathcal{L}}(1-p)^{\frac{N}{2}-\mathcal{L}}$ (binomial distribution). Following these ideas one can derive a powerful theory that allows us to calculate many of the properties of random graphs, for instance the degree distribution [21]:

$$p_k = \binom{N-1}{k} p^k (1-p)^{N-1-k} \quad \text{(binomial distribution)} \,, \tag{2.10}$$

which, in the limit of $N \to \infty$ (for $\langle k \rangle$ constant), can be written as,

$$p_k = e^{-\langle k \rangle} \frac{\langle k \rangle^k}{k!} \quad \text{(Poisson distribution)} \; . \tag{2.11}$$

Let us point out now some relevant remarks about this model. On the one hand, these networks display degree homogeneity, no correlations, and a small clustering coefficient, given by $\langle C \rangle = \langle k \rangle / N$ –that vanishes in the thermodynamic limit, qualities rarely found in real complex networks [39, 21]. On the other hand, it can be proved that the average shortest path length scales as $\langle l \rangle = \mathcal{O}(\log N)$ as $N \to \infty$ [20], which is small compared to 1D lattices, and often a desirable property also present in real-world networks.

The second approach to generate this graph observes the notions prescribed for the so-called generalized random networks model (topologies having arbitrary degree distributions and constructed by the configuration model) that can be found in Sect. 2.4.

Many other results of this model were left out of this brief definition, again in Sects. 2.4 and 2.5 we review some structural-related properties and its relation to percolation (a second order –structural– transition) respectively.

2.3.3 Small-world topology

Some of the key features of this model have a long history that goes back to Milgram's experiments, about fifty year ago, and have been used widely for researchers in many fields of Science [20, 105]. Now, the two essential aspects that are included in this class of networks are: (i). A small average shortest path length that scales logarithmically with the size of the network (i.e. $\langle l \rangle = \mathcal{O}(\log N)$ as $N \to \infty$), and (ii). A high clustering coefficient ($\langle C \rangle \approx 1$) [39, 106].

Here we focus on three models to generate small-world networks (SWN):

- Watts-Strogatz model: Being the most studied version of SWN in history, this method has received a great deal of attention, partly because it interpolates between 1D lattices (RN) and completely random networks (ERN), but mostly because it exhibits some of the properties observed in real systems. Its simplest version goes as follows [108],
  - Generate a ring network of size N and $\iota \geq 1$ (which is considered a large world).

– Remove edges with probability $p \in [0, 1]$ and replace them with edges that join vertices selected uniformly at random from the N nodes. These new edges are called *shortcuts* or *bridges* and the process of replacing them is known as *rewiring*.

At $p = 0$ no rewiring takes place, so the network is simply the underlying 1D lattice. For small values of the parameter p the small-world effect is created (the shortcuts reduce significantly the average shortest path length while the remaining regular structure maintains a high value of clustering). At $p = 1$ vertices are connected independently at random, which is an Erdős-Rényi graph.

The degree distributions, rarely included in description of the method, can be derived analytically [109],

$$p_k = \sum_{n=0}^{\min(k-\iota,\iota)} \binom{\iota}{n} (1-p)^n p^{\iota-n} \frac{(p\iota)^{k-\iota-n}}{(k-\iota-n)!} e^{-p\iota} \quad (\text{for } k \geq \iota) \,, \tag{2.12}$$

which becomes a Poisson distribution when $p \to 1$. For an illustrative diagram of a SWN see Fig. 2.1.

- Newman model: This is a variation of the Watts-Strogatz model, the only difference is that in this case instead of rewiring we add undirected shortcuts to the ring network [21]. The obtained configuration is very useful to perform analytics, but has one downside: At $p = 1$ we do not create an Erdős-Rényi network. However this shortcoming entails no significant problem since we are only interested in networks for which $p \ll 1$.

- Roxin-Riecke-Solla model: This is a variation of the Newman model. In this case the structure is the same as in the previous model, but with one small difference: shortcuts are directed [72]. Again, the disadvantage of not creating an Erdős-Rényi graph at $p = 1$ is present here. Another drawback of this approach is that our adjacency matrix is not symmetric, so performing analytic calculations is much more difficult.

2.3.4 Scale-free topology

This model is strongly related to the concept of scale invariance. A function f is said to be scale invariant when $f(cx) \propto f(x)$. Only one particular set of functions satisfies

this property: power laws. These mathematical relations can be easily defined as a function,

$$f(x) = Cx^{-\beta} \quad \rightarrow \quad \log(f) = -\beta \log(x) + \log(C) \ , \tag{2.13}$$

which in a log-log plot is clearly a line with negative slope equals to β.

Power laws shine in their own right because they appear as important results in many fields of Science, ranging from physics (e.g. scaling functions related to phase transitions), mathematics (fractals), and economics (Pareto's law) to social science (Zipf's law) and biology (Kleiber's law). Network science is no exception. The scale-free configuration –illustrative diagram is shown in Fig. 2.1– is a random graph whose degree distribution is a power-law of the form, $p(k) \sim k^{-\gamma}$ $(k \geq 1)$ [19], which is a behavior also exhibited by many real-world networks (with exponents in the range $2 < \gamma < 3$, for the most part) [40, 39].

Now, a distribution such as this one, in theory, entails some restrictions. For instance, both the first and second moment of the degree distribution diverge for $\gamma < 2$ and $\gamma < 3$, respectively [105]. Nevertheless, it is possible to calculate finite values for other ranges of the exponent as we will see next. Let k_{min} be the smallest degree of network, then we can derive the following approximate expressions (exact in the thermodynamic limit),

$$\langle k \rangle \approx \frac{\gamma - 1}{\gamma - 2} k_{min} \quad (\gamma > 2) \ , \tag{2.14}$$

$$\langle k^2 \rangle \approx \frac{\gamma - 1}{\gamma - 3} k_{min}^2 \quad (\gamma > 3) \ . \tag{2.15}$$

Another significant aspect prompted by the heterogeneous degree distribution is the presence of some nodes with large degree values, called hubs, a feature that ensures having a small average shortest path length according to $\langle l \rangle = \mathcal{O}(\log N)$ for $\gamma > 3$ and $\langle l \rangle = \mathcal{O}(\log \log N)$ for $2 < \gamma < 3$ [39, 110]. As for the clustering coefficient, it has been proved that $\langle C \rangle \sim N^{(7-3\gamma)/(\gamma-1)}$, so $\langle C \rangle$ vanishes for $\gamma > 7/3$ as $N \to \infty$ and increases for $\gamma < 7/3$ as $N \to \infty$ [20].

In a very general sense we can say that there are two kinds of methods to construct random networks with any degree distribution. First, the so-called *static approach* which hinges on the idea that no information is needed as to how edges are created (so connections are set at random) and that the topology can be generated by simply assuming that nodes have at least one defining property (e.g. degree, weight, etc.) [20]. Examples of this class of models are the configuration model and fitness models.

Second, the *dynamical approach*, in which some sort of evolution or growth is assumed (so the mechanism for connecting nodes has to be known in advanced). Examples of this type of model include the Barabási-Albert model and the Dorogovtsev-Mendes-Samukhin model [39]. In our case we will focus on static models, so the particular method that will be used to generate the scale-free topology is the same as the one for other random graphs –explained in Sect. 2.4, the configuration model (that, to ensure uncorrelated scale-free networks, includes additional constrains reported in [111]).

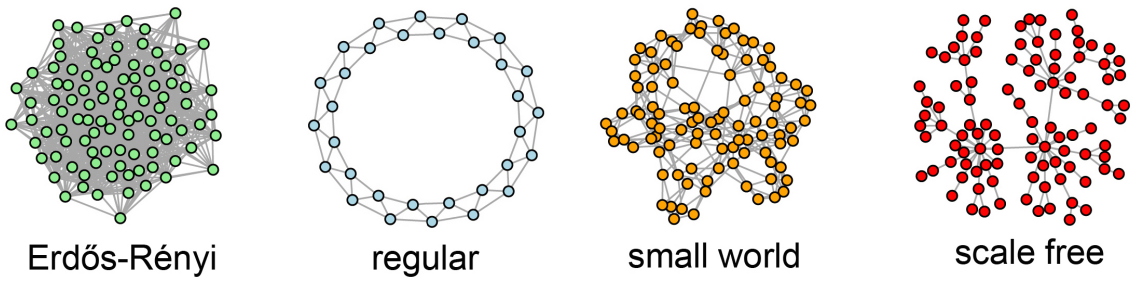

Figure 2.1: Illustrative example of network topologies.

2.3.5 Multilayer networks

In this section we introduce a more complex topology, but in no way we mean to present here a thorough mathematical description of such configuration (whose treatment requires a basic tensorial formalism). For a review on this subject we suggest references [112, 54]. By the expression "multilayer network" we denote a configuration of connected graphs arranged in layers (so these structures, in addition to nodes and edges, also incorporate layers). Assuming that each of the n_l layers have one single network of size N, then each node of the multilayer network is identified by two numbers, first, the usual node-index $1 \leq i \leq N$, and second, the number of the layer, $l \geq 1$, that contains the network it belongs to. As to the local topology (within each layer), it can be generated independently using any of the models described in the previous sections (approach that has been called "*Simple static model*" [54], and that is related to the configuration model described in the next Section). Furthermore, the degree sequences of single-layer-graphs can be specified in any desired manner to set, for instance, a degree correlation between different layers (i.e. node-indexes can be sorted in accordance to their degree values and the links between layer can be arrange in consequence). In Fig.2.2 the inter-links (dashed lines) join

exclusively vertices that have the same node-index i but that belong to different layers, thus each node is obviously connected to both their local neighborhood –within the same layer (solid lines)– and to $(n_l - 1)$ neighbors in other layers. However keep in mind that these inter-links are not constrained, in general, in such fashion and, thus, more complex connectivity patterns can be produced by considering other rules.

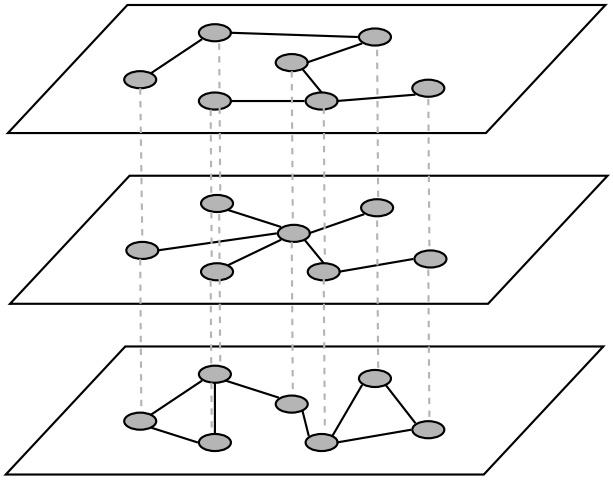

Figure 2.2: Illustrative diagram of a multilayer network having a graph of size $N = 7$ on each of its $l = 3$ layers. Inter-links connecting nodes of the top layer and nodes of the bottom layer are not shown.

Adding all these ideas together, and following the example exhibited in Fig.2.2, the total number of neighbors of any vertex i in layer l is given by:

$$k_i^l = k_{i,l}^{local} + n_l - 1 \; . \tag{2.16}$$

Clearly the numbers $\{k_{i,l}^l\}_{i=1,2,\ldots,N}$ follow the degree distribution of the chosen topology for the layer l, $\{k_{i,l}^{local}\}_{i=1,2,\ldots,N}$, but shifted to the right, which would be a power-law for scale-free networks, a Poisson distribution for Erdős-Rényi networks and so on.

A comment on the nature of nodes and links here compared to nodes and links of multiplex networks is in order. In this simple and illustrative definition nodes of different layers having equal node-index i are not necessarily the same entity, in fact, they can have independent properties and display behaviors. For instance, the removal of node i in layer l at a particular moment does not imply necessarily that any of the nodes identified by the node-index i in any of the other $n_l - 1$ layers has to be removed as well.

2.4 The configuration model

Originally introduced in 1978 by the authors of reference [113], it has received a lot of attention since then because it can be used to derive many analytical results on random networks. The ideas behind this model are quite simple, following those related to ERNs, one can construct random networks with any desired degree distribution $p(k)$ as follows [20],

- Generate a degree sequence for the set of N vertices, $\{k_i\}_{i=1,\ldots,N}$ ($\sum_i k_i$ even), its histogram should fit $p(k)$ accurately as $N \to \infty$.
- Connect vertices by choosing pairs of nodes uniformly at random, adhering to previously assigned degrees (self- and multiple- connections are prohibited).

Clearly this algorithm is characterized, as other static models, by the absence of information about the principles that drive the creation of links between nodes.

Now,taking advantage of the randomness of these networks, a theory based on the so-called generating function formalism can be developed. This approach is essentially a powerful method that, instead of dealing directly with a combinatorial problem to derive properties of networks, introduces an alternative strategy transforming it into an algebraic problem (involving power series), which is much easier to solve[1]. In this regard, here are three interesting results on networks' structure [21], first:

$$\langle C \rangle = \frac{1}{N} \frac{(\langle k^2 \rangle - \langle k \rangle)^2}{\langle k \rangle^3}\,, \tag{2.17}$$

which is a general expression that can be used to prove all the results, regarding the clustering coefficient of random networks, mentioned above. Second, the average shortest path length can be expressed as,

$$\langle l \rangle \approx 1 + \frac{\log(N/\langle k \rangle)}{\log[(\langle k^2 \rangle - \langle k \rangle)/\langle k \rangle]}\,. \tag{2.18}$$

And third, the condition that guarantees having a giant component of size $\sim N$:

$$\frac{\langle k^2 \rangle}{\langle k \rangle} > 2\,. \tag{2.19}$$

This condition sets the minimum –average– connectivity that a network with arbitrary degree distribution is required to have in order to be connected. To illustrate this

[1]Originally proposed by Newman, Watts and Strogatz in references [114, 115], it is very useful to determine many properties of networks with arbitrary degree distribution.

point, let us consider the case of ERNs, where $\langle k \rangle = var(k) = \langle k^2 \rangle - \langle k \rangle^2$. Thus, Eq. 2.19 gives:

$$\frac{\langle k \rangle^2 + \langle k \rangle}{\langle k \rangle} = \langle k \rangle + 1 > 2\,, \tag{2.20}$$

which means that any ERN with $\langle k \rangle > 1$ exhibits a giant component of size $\sim N$.

Regarding the degree sequence, for non-uniform distributions, we follow *the inversion method* (also known as inverse transform sampling). Briefly, the inversion principle states [116]:

"*if Y is a continuous random variable uniformly distributed on* [0, 1] *and if X is a continuous random variable with a cumulative distribution represented by F_X, then the random variable $F_X^{-1}(Y)$ has the same distribution as X*".

Thus we propose a simple algorithm as follows,

- Generate a random number $0 \leq y \leq 1$.
- Calculate $x = F_x^{-1}(y)$.
- Repeat previous steps N times.

Obviously, to generate our degree sequences from uniformly distributed random variables this method requires that the inverse function of the desired cumulative distribution exists. In our case this restriction is irrelevant because the distributions we study throughout this Thesis can be easily inverted.

As an illustration of the advantages of the configuration model, and also to show further developments of the generating function approach, in the next Section we report on a structural-related process in random network.

2.5 Percolation theory

So far, we have reviewed some of the main characterizing properties of networks, their diverse topologies and also how to build them. Now let us describe how to disassemble them. In network science, a fascinating process known as *percolation* can be generally understood as a procedure to damage networks' structure. There are several ways to do that, and depending on what you chose to break down an how it is performed, the process takes different names. At the most basic level, a graph

comprise two kinds of entities, nodes and edges, and in order to damage its structure one or both constituents have to be removed (somehow). When the damaging process is performed only on nodes (which typically implies also removing the edges attached to them), it is called *site percolation*, and when only links are involved it is called *bond percolation*. The specific order to remove this elements is also an essential aspect of the process. Generally speaking when researchers talk about percolation, they mean *random percolation* which simply states that the parts to be removed are chosen uniformly at random. Of course, this is not the only way to do it. For instance, in the case of site percolation, if nodes are selected and removed in order by their degree this receives the name of *targeted attack* and it is a simple strategy that has proven very effective in inflicting catastrophic damage to scale-free networks[2] [20]. Although such a process might seem just like a theoretical exercise, it has many significant results and applications to biological systems, real-world infrastructures and engineering problems. To mention a few, percolation theory can be used to model (as an approximation) complex behaviors like disease spreading, power-grid failures and traffic congestion.

Fortunately, many rigorous approaches on the subject have been developed over the past decades (since, at least, the 1940s) and here we present a brief review on the main results provided by, again, the generating function formalism. By adopting this approach, one can obtain an expression for the critical value of the node-occupation probability ϕ in uncorrelated networks [21]:

$$\phi_c = \frac{\langle k \rangle}{\langle k^2 \rangle - \langle k \rangle} = \frac{1}{\langle k^2 \rangle / \langle k \rangle - 1}\,, \tag{2.21}$$

which is the minimum fraction of nodes still present in the damaged network (after a random removal of vertices is performed) required for the giant component to exist (derived rigorously under the configuration model).
In the case of ERNs, Eq. 2.21 simply reduces to:

$$\phi_c = \frac{1}{\langle k^2 \rangle / \langle k \rangle - 1} = \frac{1}{\langle k \rangle}\,. \tag{2.22}$$

Note also that, for scale-free networks, the second moment of the degree distribution diverges in the thermodynamic limit when $\gamma \leq 3$ (see Eq. 2.15), and in this case $\phi_c \to 0$, which means that the giant component exists even when most of the vertices are removed.

[2]This is a major finding in Network Science because, as mentioned previously, many real-world networks exhibit scale-free properties and thus the same structural vulnerabilities.

The inequality in Eq. 2.21, also called the percolation threshold, depends crucially on the size of the system [117], which sets a serious limitation for its application to real networks (whose sizes are always finite, of course). Nevertheless, it can be proved that a good approximation of ϕ_c for finite SFNs is given by [20]:

$$\phi_c \approx \left(\frac{\gamma - 3}{2 - \gamma}\right) k_{max}^{\gamma-3} \, k_{min}^{2-\gamma} \quad 2 < \gamma < 3 \,, \tag{2.23}$$

where k_{max} is the largest degree in the network.

For more information on percolation in complex networks we suggest reading references [21, 115, 110, 39, 20].

Finally, other relevant aspects of the basic network framework include centrality measures, mesoscale descriptors, community detection and modular structures, among many others. In this brief review such topics were left out because they are unrelated to the present work, and we encourage the reader to consult the references of this Chapter for further details.

Chapter 3

Synchronization in relay systems

At the local level, many networks exhibit recurrent structural patterns of connections, called *motifs* [39], that may enhance or hinder the appearance of complex behaviors. In this Chapter we focus on one of such microscopic structures to demonstrate there is a specific form of synchronization in configurations that act as mediators between two dynamical units (commonly referred to as relay systems). In particular, our approach to analyze the behavior of this elementary graph and elucidate when the global synchronized states appear[1] includes a well-known tool of the spectral theory, along with two useful indicators of synchrony. The robustness of our findings is illustrated experimentally using several electronic setups, which also allows to provide some insight into a few experimental technologies that are based on these ideas.

The Chapter is organized as follows: We introduce the notion of synchronization and discuss some of the most recognizable types of synchronized states that have been observed in chaotic systems (Sect. 3.1). Then, we describe the two kinds of synchronization to be studied in the present work, the relay synchronization and the generalized synchronization, along with a brief review on some of their current applications. In Sect. 3.2 we report on the system of interest, a set of three chaotic oscillators diffusively coupled (according to an elementary graph), and examine all of the mathematical and numerical tools that are used to characterize our setting and to determine the onset of the synchronized states. Main numerical simulations/analysis for a 9D Rössler dynamical system are reported in Sect. 3.3, as well as our experimental findings on electronic circuits (operating in chaotic regime) in Sect. 3.4. At the end of the Chapter, a detailed discussion on the results is presented, including –possible– new lines of research, and further examples of relay synchronization in optical and biological systems.

[1] As a function of the coupling strength that, of course, links our dynamical subsystems.

3.1 Synchronization

3.1.1 Basic notion

Synchronization is a common phenomenon in a diversity of natural and technological systems. Examples of synchronous behavior include biological phenomena (firing patterns of neurons in the brain, spike activity of fireflies, circadian rhythms, pacemaker cells in the heart, and so on), social activities (finance, opinion formation, dating patterns, and even hand clapping), engineering (lasers, electronic circuits, communications, etc.), and physics (coupled mechanical settings, dynamical systems, superconductive elements, etc.), and many others. [42, 41, 7].

Clearly the concept of "*synchronization*" is hard to pinpoint given the ubiquitous occurrence of this behavior. In what follows, we will not try to present a comprehensive report on the subject, but simply to offer some intuitive ideas that might shed some light on this topic. The word *synchronization* has an ancient root in Greek, that means syn = the same, and chronos = time [118]. In terms of modern natural languages, a wider notion of synchronization can be stated informally as "*agreement or correlation in time of different processes*", and more formally as "*a process wherein two (or many) systems (either equivalent or nonequivalent) adjust a given property of their motion or activity to a common behavior, due to coupling or forcing*" [43]. Yet other authors prefer to follow broader notions like: "*Synchronization as an adjustment of rhythms of oscillating objects due to their weak interaction*" [41], which, although intuitive, is rather vague for most purposes. In any case, from these ideas we are able to see distinctly that synchronization always involves three aspects: oscillations, coupling or interaction, and adjustment of rhythm or common behavior. However, as already stated, we never get to satisfy with our definitions every form of synchronization there is, for the trouble with this concept obviously lies in the fact that there exist several types of synchronization that have been observed in many systems of diverse nature.

3.1.2 Forms of synchronization

In the present Chapter we focus exclusively on synchronous states defined for chaotic elements (systems that are characterized as sensitively dependent on initial conditions [8]), though this phenomenon is also encountered and discussed in Chapters 4 and 5 for pulse-coupled elements. Here are some of these types [43]:

- Complete synchronization (CS): It is certainly a basic form of synchronization present in many kinds of systems (including non-chaotic ones). It consists of a perfect match of the trajectories of –at least– two coupled systems in the course of the time (which can be achieved by imposing a strong undirected interaction between them). Spectral analysis has shown that for two coupled identical chaotic units conditional Lyapunov exponents of the subsystem to be synchronized are all negative [58].

- Phase synchronization (PS): When considering two or more coupled nonidentical oscillators (whose motions can be characterized by amplitudes, frequencies and phases) there is a regime in which oscillators' phases are locked while correlations in the amplitudes remain weak.

- Lag synchronization (LS): This is an intermediate form of synchrony between PS and CS. For two or more non-identical oscillating elements, lag synchronization means that there exist locking between phases and between amplitudes, but with the presence of a time lag.

- Generalized synchronization (GS): Again, given at least two different oscillators, we say that GS takes place between them whenever the trajectory of one system can be mapped onto the trajectory of the other by a single global bijective function (see section 3.1.4).

- Intermittent lag synchronization (ILS): It is a state where the systems involved satisfy LS most fo the time, but occasionally their trajectories exhibit unsynchronized behavior (perhaps related to certain parts of the attractors).

- Imperfect phase synchronization (IPS): Obviously this type of synchronization refers to a state in which the oscillators involved exhibit PS most of the time but the phase locking might fail occasionally.

3.1.3 Synchronization in relay systems

A relay configuration is simply an undirected graph of size $N = 3$ and $\mathcal{L} = 2$, in which two –dynamically identical– nodes are connected to a third one but not to each other (see Fig. 3.1). This configuration, as stated above, can be interpreted as a network motif, which are subgraphs that repeat themselves in large networks [39]. Given the natural occurrence of these local structures, we believe it is most relevant to study synchronization phenomena in such systems providing them a dynamical complexity

to offsets their basic morphology (which is why we chose to study chaotic oscillators –two varieties of Rössler attractors are depicted in Fig. 3.1).

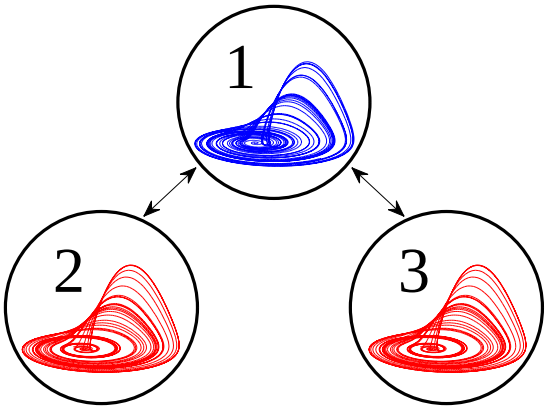

Figure 3.1: Relay configuration diagram displaying three chaotic oscillators joined as prescribed (for the 9-dimensional dynamical system, see Eqs. 3.1).

An elegant way to enhance synchronization is the use of a relay setting between the systems to be synchronized. This synchronous state of relay units, also known as relay synchronization (RS), involves achieving complete synchrony of the two dynamical subsystems (nodes 2 and 3 in Fig. 3.1) by means of the action of an indirect coupling through a third unit (node 1 in Fig. 3.1), whose dynamics does not necessarily join the shared state. This particular form of synchronization has many relevant effects on both theoretical studies and practical applications. For instance, RS is especially useful in undirected systems with a certain delay in the coupling line, where lag-synchronization has also been reported [59, 60, 61, 62]. In these cases, indeed, the coupling delay may induce instability of the synchronous state [119], which can be restored again thanks to a relay system. Lasers [59, 60, 61, 62] and electronic circuits [63] have been the benchmark for experimental demonstration of the feasibility of RS, showing its robustness against noise or parameter mismatch. In semiconductor lasers, for instance, zero-lag synchronization between two delay-coupled oscillators can be achieved by relaying the dynamics via a third mediating element, which surprisingly lags behind the synchronized outer elements. In electronic circuits, RS has been used as a technique for transmitting and recovering encrypted messages, which can be sent bidirectionally and simultaneously [64]. Apart from its technological applications, RS has also been proposed as a possible mechanism at the basis of isochronous synchronization between distant areas of the brain [65, 66, 67]. Despite such evidence

of RS, there are still open questions of a fundamental nature. The main issue is to characterize properly the relationship, established in RS, between the dynamics of the relay system and that of the fully synchronized identical systems it connects[2]. In this Chapter we provide evidence, among other results, that there exists indeed a correlation between them.

3.1.4 On generalized synchronization

Given that GS is one of the main concepts of this chapter, next we provide further details on this prominent phenomenon. Consider two systems whose dynamics are given, respectively, by $\dot{x}(t) = f(x(t), y(t))$ and $\dot{y}(t) = g(y(t), x(t))$. According to the definition of GS discuss above, this behavior is characterized by the existence of a one-to-one function $h(x(t))$, such that $\lim_{t\to\infty}\|y(t) - h(x(t))\| = 0$ [41], a condition rather difficult to prove –directly– in most instances. To illustrate this point, let us see some of the results reported on GS in the literature. In particular, for *directed* coupled units (master system $\rightarrow$ slave system) its existence has been proven by checking the ability of the response unit to react identically to different initial conditions of the same driver unit, which can be quantified by evaluating the mutual false nearest neighbors [46] or by measuring the conditional Lyapunov exponents [58]. More recently, GS has been also reported in networks of undirected coupled oscillators [120] and suggested that GS could occur when a *minimum* value of the coupling delay is guaranteed in a relay configuration [121] as well, but no proof of GS existed so far for systems that are *instantaneously* coupled through an additional relay unit.

3.2 Model and tools

In this section we report on the system of interest and three distinctive measures that are used to assess the existence of CS, RS and GS, all of this with the aim of determining whether GS is behind the role played by the relay unit in the RS process.

3.2.1 Dynamical system

Let us consider the case of three interacting Rössler oscillators [122] diffusively coupled according to the configuration diagram of Fig. 3.1. The generic route to complete

[2]A relay unit may have certain parameter mismatch with the identical units they link [50] or can even be a completely different system [63], and thus, typically, it exhibits a dynamical behavior that seems unrelated –a priori– to the one displayed by the systems fully synchronized.

synchronization of two Rössler oscillators is well known in the literature [41]. Here, instead, we incorporate a relay configuration where units 2 and 3 are identical (same parameters in Eq. 3.1), and unit 1 –the relay element– is set to have (one or more) different parameters with respect to them. Again, the edges are not only undirected but also instantaneous and RS is said to take place whenever CS between oscillators 2 and 3 occurs.

The equations of motion of the full 9D system are,

$$\begin{cases} \dot{x}_1 = -y_1 - z_1, \\ \dot{y}_1 = x_1 + a_0\, y_1 + \sigma(y_2 - y_1) + \sigma(y_3 - y_1), \\ \dot{z}_1 = 0.2 + z_1(x_1 - 5.7), \end{cases} \\ \begin{cases} \dot{x}_{2,3} = -y_{2,3} - z_{2,3}, \\ \dot{y}_{2,3} = x_{2,3} + a\, y_{2,3} + \sigma(y_1 - y_{2,3}), \\ \dot{z}_{2,3} = 0.2 + z_{2,3}(x_{2,3} - 5.7). \end{cases} \tag{3.1}$$

Although here we focus our results on the case $a_0 = 0.3$, $a = 0.2$, different parameter mismatches between unit 1-2 and 3 have also been tested (exhibiting the same qualitative results). In all cases considered, the existence of a stable chaotic attractor has been verified for the isolated systems.

3.2.2 Lyapunov exponents

A widely-used strategy to characterize the asymptotic behavior displayed by a dynamical system is the study the Lyapunov exponents (also known as Lyapunov spectrum). Basically, this framework offers an analysis based on the rate of divergence or convergence of nearby trajectories of the system [123]. To illustrate the concepts behind this proposal, let us describe briefly the leading Lyapunov exponent λ. Consider two initial points in the phase space of a dynamical system $\mathbf{x}_{t_0}$ and $\mathbf{x'}_{t_0}$ at t_0 such that $\delta\mathbf{x}_{t_0} = \|\mathbf{x}_{t_0} - \mathbf{x'}_{t_0}\| \ll 1$. Let $\mathbf{x}_t$ and $\mathbf{x'}_t$ be the images of $\mathbf{x}_{t_0}$ and $\mathbf{x'}_{t_0}$ after a suitable $t \gg 1$, and $\delta\mathbf{x}_t = \|\mathbf{x}_t - \mathbf{x'}_t\|$ the distance between these images, then the leading Lyapunov exponent is given by the expression:

$$\lambda = \lim_{t\to\infty} \frac{1}{t - t_0} ln\left(\frac{\delta\mathbf{x}_t}{\delta\mathbf{x}_{t_0}}\right) \approx \frac{1}{t - t_0} ln\left(\frac{\delta\mathbf{x}_t}{\delta\mathbf{x}_{t_0}}\right) , \tag{3.2}$$

which clearly quantifies how fast the images separate form each other. If $\lambda > 0$ the system exhibits exponential divergence of nearby orbits, a condition that characterizes

chaotic behavior (i.e. sensitivity to initial conditions [8]). On the other hand, $\lambda < 0$ is associated with a stable fixed point and $\lambda = 0$ with a stable limit cycle. The Lyapunov exponent thus defined is just an illustration concerning only local behavior (two local points of the phase space), and in order to characterize the whole system a global quantity is required (an average, as will be shown in the next paragraphs).

More formally, let $\dot{\mathbf{x}} = \mathbf{f}(\mathbf{x})$ be the dynamical system, where $\mathbf{f} : U \subseteq \mathbb{R}^n \to \mathbb{R}^n$ (smooth), then the leading Lyapunov exponent can be computed as follows:

$$\lambda = \lim_{t\to\infty} \frac{1}{t-t_0} ln \left(\frac{\|\mathbf{J}^t(\mathbf{x}_{t_0})\delta\mathbf{x}_{t_0}\|}{\|\delta\mathbf{x}_{t_0}\|} \right) = \lim_{t\to\infty} \frac{1}{t-t_0} ln\|\mathbf{J}^t(\mathbf{x}_{t_0})\hat{\mathbf{n}}\| \,, \tag{3.3}$$

where $\mathbf{J}^t(\mathbf{x}_{t_0})$ is the Jacobian matrix of the system, whose entries are $J^t_{ij}(\mathbf{x}_{t_0}) = \partial f_i(t)/\partial x_j(t_0)$, and $\hat{\mathbf{n}} = \delta\mathbf{x}_{t_0}/\|\delta\mathbf{x}_{t_0}\|$ is the unit vector oriented in direction of the initial perturbation. So the initial perturbation $\delta\mathbf{x}_{t_0}$ evolves as:

$$\delta\mathbf{x}_t = \mathbf{J}^t(\mathbf{x}_{t_0})\delta\mathbf{x}_{t_0} \,. \tag{3.4}$$

Provided that, in general, the Jacobian matrix is not symmetric, diagonal or even constant along the trajectory described by the system, from the geometric point of view, it maps –for instance– the unit sphere into an ellipsoid. Furthermore, it can be proved that this Jacobian deformation can be factored into a rotation ($\mathbf{R}^t(\mathbf{x}_{t_0})$, an orthogonal matrix) and a stretch ($\mathbf{S}^t(\mathbf{x}_{t_0})$, symmetric positive definite matrix), for which an orthonormal eigenbasis expands [124]:

$$\mathbf{S}^t(\mathbf{x}_{t_0})\hat{\epsilon}^t_i = \omega^t_i(\mathbf{x}_{t_0})\hat{\epsilon}^t_i \;\text{ where }\; 1 \le i \le n \,, \tag{3.5}$$

where $\omega^t_i(\mathbf{x}_{t_0})$ are the n positive real eigenvalues of $\mathbf{S}^t(\mathbf{x}_{t_0})$. For simplicity, let us consider an initial perturbation along the ith-axis (it can be computed –alternatively– by components), then $\hat{\mathbf{n}} = \hat{\epsilon}^t_i$ and from Eq. 3.3 one can define the finite-time ith-Lyapunov exponent:

$$\lambda^t_i(\mathbf{x}_{t_0}) \approx \frac{1}{t-t_0} ln\|\mathbf{R}^t(\mathbf{x}_{t_0})\omega^t_i(\mathbf{x}_{t_0})\hat{\epsilon}^t_i\| = \frac{1}{t-t_0} ln\left[\omega^t_i(\mathbf{x}_{t_0})\right] \,, \tag{3.6}$$

which is clearly the rate of stretching along the ith-axis (given $\mathbf{x}_{t_0}$ and t). Eq. 3.6 provides a strategy to compute the average ith-Lyapunov exponent along the trajectory of the dynamical system, for a suitable short interval T the Lyapunov spectrum is obtained iteratively [125]:

$$\lambda_i \approx \frac{1}{KT} \sum_{j=1}^{K} ln\left[\omega^j_i(\mathbf{x}_{t_0})\right] \,, \tag{3.7}$$

which should be calculated until they show convergence.

Note that there is a Lyapunov exponent for each dimension of the dynamical system, and that the eigenvalues $\omega_i^t(\mathbf{x}_{t_0})$, that quantify the stretching ($\omega_i^t(\mathbf{x}_{t_0}) > 1$) and compression ($0 < \omega_i^t(\mathbf{x}_{t_0}) < 1$), can also be computed as renormalization parameters resulting from the reorthogonalization process to "correct" the deformation that the Jacobian matrix causes to the initial basis [126].

3.2.3 CS measure

A useful yet simple quantity to detect the existence of complete synchronization between nodes i and j is the error function, $\langle e \rangle_{i,j}$, defined as,

$$\langle e \rangle_{i,j} = \lim_{\tau \to \infty} \frac{1}{\tau} \int_0^\tau \|\mathbf{x}_i(t) - \mathbf{x}_j(t)\| dt \ , \tag{3.8}$$

As mentioned above, in the case of CS the trajectories become identical after the transient, so this measure provides accurate confirmation of the presence of such behavior.

3.2.4 GS indicators

Direct evidence of the onset of GS between nodes 1 and 2 can be provided by the use of two indexes: the synchronization points percentage (SPP, for short) introduced by Pastur *et al.* in reference [49], and the non-linear interdependence (N-index) proposed by Quiroga *et al.* in reference [127]. Lets us describe both of them briefly:

- SPP quantifies the fraction of phase-space points of a given subsystem (in our case, Rössler attractors represented by nodes) for which there is a *local continuous function* to the phase-space of the other subsystem or unit. The essence of the method involves the analysis of the nearest neighbors of the points of the domain space (e.g. node 1), and the search of their images in the neighborhoods of time-related points of the codomain space (e.g node 2). In this way, one is able to assert the existence of local functions only for certain statistical confidence level (continuity statistics method) [45]. One way to optimize this search, suggested in reference [49], is performing the so-called time-delay reconstruction of the subspaces involved [128], due to the fact that, in higher dimensions, the size of these neighborhoods (the number of points inside co-domains required to assess the existence of the local function) is smaller. Note that, even though this

reconstruction is convenient in terms of time efficiency, it is just an optional step before SPP computation[3]. Whenever SPP = 1, there exists a unique, global, continuous synchronization function from one subsystem to the other [48], and thus we say that the two subsystems are in GS (see Ref. [49] for further details of the method).

- The second index we consider here is the N-index, an asymmetric measure of synchronization defined as,

$$N(\mathbf{x}|\mathbf{y}) = \frac{1}{P}\sum_{n=1}^{P}\frac{R_n(\mathbf{x}) - R_n^{(k)}(\mathbf{x}|\mathbf{y})}{R_n(\mathbf{x})}\ , \tag{3.9}$$

where $\mathbf{x}(t)$ and $\mathbf{y}(t)$ are the states of the two dynamical systems for which GS is being evaluated, and the subindex $n = 1, ..., P$ refers to a discrete-time sampling of the attractor. Furthermore, $R_n(\mathbf{x}) = (P-1)^{-1}\sum_{i\neq n}(\mathbf{x}_n - \mathbf{x}_i)^2$ is the mean squared distance to random points in the attractor, and $R_n^{(k)}(\mathbf{x}|\mathbf{y}) = k^{-1}\sum_{i=1}^{k}(\mathbf{x}_n - \mathbf{x}_{\mathbf{y}_{n,i}})^2$ is the mean squared distance to the k false nearest neighbors of $\mathbf{x}_n$, which are the points corresponding to the time indices $\mathbf{y}_{n,i}$ of the k nearest neighbors of $\mathbf{y}_n$. By definition, $N(\mathbf{x}|\mathbf{y}) \leq 1$, and it can be marginally smaller than 0 for totally unsynchronized dynamics. Values close to zero indicate that there is no synchronization, whereas values close to 1 mean that for any n a small cloud of neighboring points around $\mathbf{y}_n$ is mapped into a small cloud of neighboring points around $\mathbf{x}_n$, which hints again at the presence of GS in the system (as it indicates the existence of a continuous mapping from the phase space of system $\mathbf{y}(t)$ to that of system $\mathbf{x}(t)$).

3.3 Numerical results

For all numerical integrations, a 4th-order Runge-Kutta algorithm with an integration time step of 5×10^{-3} time units is used (a transient of 2×10^3 is also removed in

[3]Even though our findings using this index are sound, there is an important caveat: The method is quite sensitive to sampling parameters (due to the discrete nature of the neighborhoods used in the numerics), so a fine-tuning is required in order to compute the SPP based on the 3D spaces of the attractors. One option to avoid this problem is to project the attractors onto any of the axis and then perform the so-called time delayed reconstruction. When the chosen dimension for the reconstruction satisfies the condition $d_r > 2 \times d$ (where d is the dimension of the attractor), we do not find any false-nearest-neighbors [128]. In this manner, we get to use the SPP without having to select carefully our sampling parameters. To our knowledge this is the first time that such aspect of the SPP index has been reported in the literature.

all cases). Fig. 3.2[4] shows $\langle e \rangle_{1,2}$ (blue line) and $\langle e \rangle_{2,3}$ (red line), as a function of the coupling strength σ. It is clear that there is a critical value for the coupling, $\sigma_c \simeq 0.10$, above which RS occurs for any generic initial condition, where complete synchronization between nodes 2 and 3 takes place, whereas for nodes 1 and 2 still displays $e_{1,2} > 0$ (no synchrony of amplitudes between the relay node and the rest).

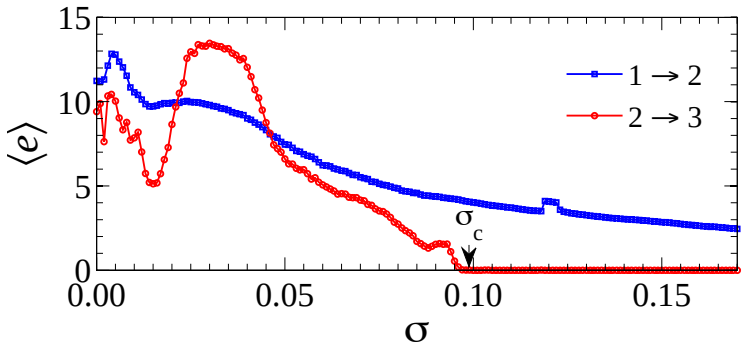

Figure 3.2: Synchronization error $\langle e \rangle$ between systems 1 and 2 (blue line), and between systems 2 and 3 (red line) as a function of the coupling strength σ (see Fig. 3.1). The critical coupling σ_c marks the beginning of the RS regime.

More insight into the role that the relay system plays in RS is gained by computing the Lyapunov spectrum of the full 9-dimensional system, which is here realized by means of the classical method[5] by Benettin et al. [126]. The results are reported in Fig. 3.3 (a), where the 6 largest Lyapunov exponents of the spectrum are plotted as a function of σ. The highlighted (grey) areas are windows where periodic dynamics might appear depending on the initial conditions (in the case of $\sigma \simeq 0.006$), or in all of them (around $\sigma \simeq 0.12$). Consequently, we do not consider any further these coupling regions where non-chaotic dynamical regimes accidentally emerge, as they do not add relevant information for the understanding of RS.
For negligible couplings, the set of Lyapunov exponents (labeled such that $\lambda_1 \geq \lambda_2 \geq \cdots \geq \lambda_9$) is divided into three positive ($\lambda_1 > 0$ and $\lambda_2 = \lambda_3 > 0$), three zero ($\lambda_4 = \lambda_5 = \lambda_6 = 0$), and three negative ($\lambda_7 < 0$ and $\lambda_8 = \lambda_9 < 0$) exponents. As the coupling increases, λ_6 becomes negative almost immediately. By checking the phase-space orbits of the systems, this corresponds to a phase synchronization regime

[4]Synchronization errors were computed for 2×10^4 time units, after an initial transient of 2×10^3 time units was disregarded. Curves in Fig. 3.2 depict averages over 30 independent realizations, each one starting from different random initial conditions.

[5]For the computation of the Lyapunov exponents, a time window of 2×10^4 time units was considered after an initial transient of 2×10^3 time units. Gram-Schmidt reorthonormalization was applied every 0.25 time units. Curves in Fig. 3.3 are the result of averages over 30 independent realizations, each one starting from a different random initial condition.

between systems 2 and 3. At $\sigma \simeq 0.04$, λ_5 also becomes negative, and just one effective phase remains in the system, corresponding to $\lambda_4 = 0$. So far the three largest Lyapunov exponents remain positive, suggesting that the three chaotic amplitudes are still not correlated. A further increase in σ determines the vanishing of λ_3 and the dropping below zero of λ_4. Eventually, for higher coupling strengths, λ_2 vanishes and λ_3 becomes negative. The coupling strength for which this latter scenario is observed is $\sigma = 0.100 \pm 0.001$, and therefore it almost perfectly matches the critical coupling strength for RS. In other words, the onset of RS corresponds to a regime with only one independent chaotic amplitude in the entire system. The fact that $\lambda_1 > 0$, $\lambda_2 = 0$ and $\lambda_i < 0$ for $i = 3, 4, \ldots, 9$ hints at the possibility that GS is taking place between both of the subsystems 2 and 3 (which are in complete synchronization with each other) and system 1 (i.e., the possibility that there is a functional relationship $\mathbf{x}_{2,3}(t) = h(\mathbf{x}_1(t))$, and the phase-space trajectories collapse onto a generalized synchronization manifold).

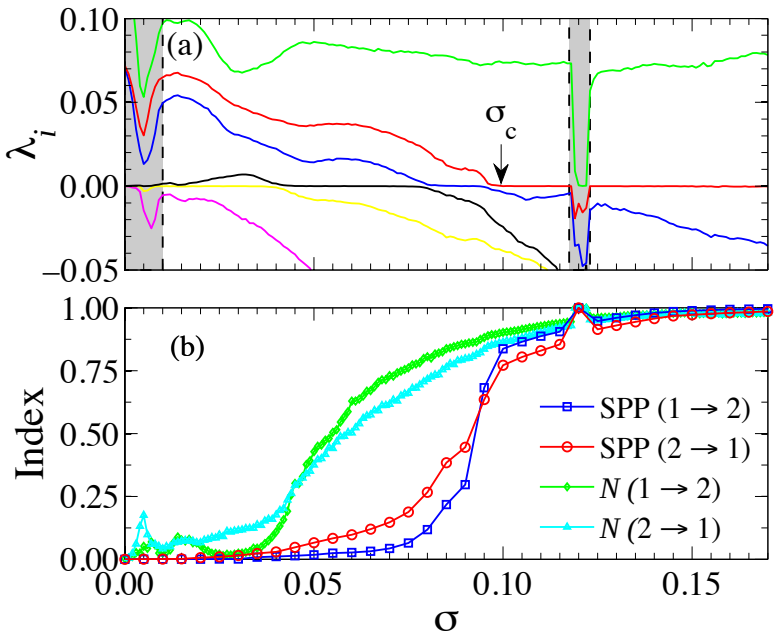

Figure 3.3: (a) Lyapunov spectrum as a function of σ (only the positive, zero and slightly negative Lyapunov exponents are shown). The gray filled areas are windows where the dynamics is periodic see the text for further explanations). The critical coupling σ_c coincides to a very high precision with the coupling strength at which the second largest Lyapunov exponent vanishes. (b) SPP and N-index (see text for definition) vs. σ, with system 1 as the domain set and 2 as the codomain set for the possible mapping (blue line for SPP and green line for N-index) and vice-versa (red line for SPP and light blue line for N-index).

Fig. 3.3 (b) shows the curves of both the SPP[6] and the N-index[7], for the case in which system 1 (2) is taken as reference and system 2 (1) is inspected for the existence of a functional relationship (denoted by $1 \to 2$ ($2 \to 1$) in the figure). The SPP curves clearly display a smooth behavior for almost every σ, and exhibit the transition to GS near σ_c, detecting the periodic dynamics at $\sigma = 0.12$ (discontinuous jump to SPP = 1.0). The curves of the N-index fluctuate slightly above zero for small couplings, while they reveal a clear monotonous growth with σ beyond $\sigma \simeq 0.04$. At $\sigma = \sigma_c$, the N-index values are very close to 0.90, and for higher coupling strengths they increase up to 0.98 for $\sigma = 0.17$, the changes being, from this point on, almost indistinguishable from numerical fluctuations. All this evidence confirm that a GS regime is associated to the setting of RS, with the function relating the states of the peripheral and relay units being invertible, which is not the general case of GS in unidirectionally coupled systems [46].

3.4 Experimental setup

Finally, we offer an evaluation of the robustness of these phenomena under realistic conditions, and we implement an experiment based on oscillating electronic circuits. The experimental setup is sketched in Fig. 3.4 and consists of three piecewise Rössler circuits operating in a chaotic regime. The dynamical system of the experimental setup is [129]:

$$\begin{cases} \dot{x}_1 = -\alpha\left(\Gamma\, x_1 + \beta\, y_1 + \xi\, z_1 - \sigma(x_3 - x_1) - \sigma(x_2 - x_1)\right), \\ \dot{y}_1 = -\alpha\left(-x_1 + \upsilon_a\, y_1\right), \\ \dot{z}_1 = -\alpha\left(-g\left(x_1\right) + z_1\right), \end{cases} \\ \begin{cases} \dot{x}_{2,3} = -\alpha\left(\Gamma\, x_{2,3} + \beta\, y_{2,3} + \xi\, z_{2,3} - \sigma(x_1 - x_{2,3})\right), \\ \dot{y}_{2,3} = -\alpha\left(-x_{2,3} + \upsilon_b\, y_{2,3}\right), \\ \dot{z}_{2,3} = -\alpha\left(-g\left(x_{2,3}\right) + z_{2,3}\right). \end{cases} \tag{3.10}$$

[6] A time window of 5×10^5 time units is considered after an initial transient of 5×10^4 time units. By keeping one 3D-point every 100 integration steps, the resolution of the time series is $dt = 0.5$ and the total number of points in each atttactor is 10^6. For the time-delayed vectors (reconstruction) we choose embedding dimension $d = 7$ and time delay $T = 1$. The parameters of SPP algorithm are the number of points inside codomain neighborhoods $n = 300$ (fixed over the attractor) and the threshold for statistical comparison $\Theta < 0.1$.

[7] A time window of 10^5 time units is considered after an initial transient of 2×10^3 time units. Even though the integration is performed with a time resolution of 0.005, only one time point every 0.5 time units is considered in the computation, so as to avoid temporal correlations. Finally, the computation of N-index is performed over the resulting 2×10^5 phase-space points. The procedure is repeated 30 times from random initial conditions.

where the piecewise part is:

$$g(x_i) = \begin{cases} 0 & \text{if } x_i \leq 3 \\ \mu\,(x_i - 3) & \text{if } x_i > 3 \end{cases} \tag{3.11}$$

Here, $\alpha = 10^4\,\mathrm{s}^{-1}$ is a time factor, and the other parameters are: $\Gamma = 0.05$, $\beta = 0.5$, $\xi = 1$, $\mu = 15$ and $\upsilon_{a,b} = \frac{10}{R_{a,b}} - 0.02$. The resistance mismatch ($R_a = 70\,\mathrm{k\Omega}$, $R_b = 39\,\mathrm{k\Omega}$) accounts for the difference between system 1 and systems 2 and 3, the latter being identical (this time, however, only up to tolerances of the electronic components and noise).

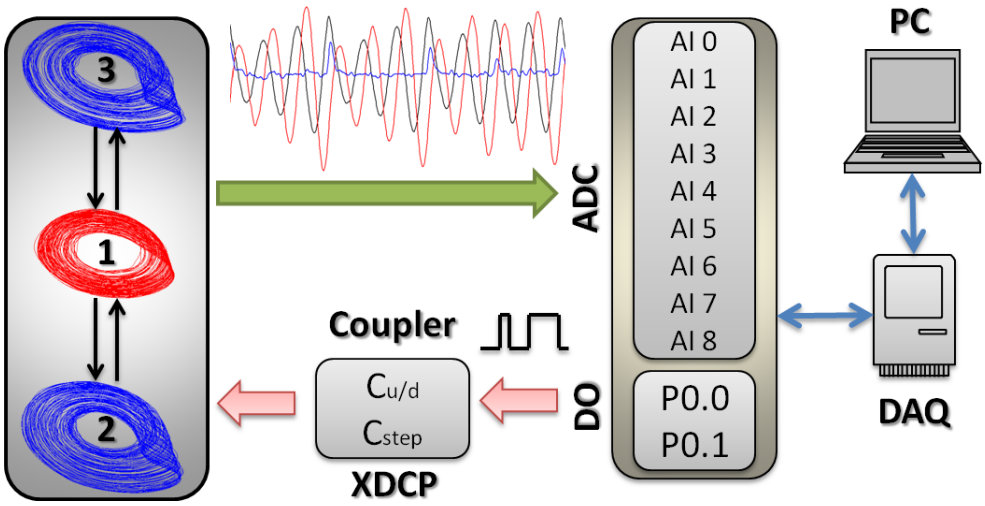

Figure 3.4: Schematic representation of the experimental setup. The bidirectional coupling is adjusted by means of three digital potentiometers X9C104 (Coupler-XDCP) whose parameters $C_{u/d}$ (Up/Down Resistance) and C_{step} (increment of the resistance at each step) are controlled by a digital signal coming from a DAQ Card. See text for the full details of the experimental system.

The coupling strength σ is controlled by a digital potentiometer (used as a voltage divisor), whose range is such that $\sigma \in \{0.00, 0.01, \ldots, 0.25\}$. We use three digital potentiometers (X9C104) which guarantee that the parameter σ is changed simultaneously for all nodes. They are adjusted by a digital signal coming from ports P0.0 and P0.1 of a NI Instruments DAQ Card (DAQ). The output of each circuit is connected to a voltage follower that works as a buffer. All 9 signals are acquired by the analog ports (AI 0 ; AI 1; ... ; AI 8) of the same DAQ Card, and recorded on a PC for further analysis. The incoming signal of the analog inputs (ADC) and the signal sent through the digital outputs (DO) are controlled and recorded by Labview.

Fig. 3.5 shows the values for the synchronization error (top), and the SPP and N-index (bottom) as functions of σ for the experimental data. In particular, panel (a)

indicates that the system achieves RS for $\sigma > 0.13$. Admittedly, the synchronization error $\langle e \rangle$ between systems 2 and 3 can never vanish, not even within experimental error limits in a low-precision experimental setup. However, it becomes very low as compared to the considerably higher values of $\langle e \rangle_{1,2}$. On the other hand, Fig. 3.5(b) confirms that both SPP and N-index give clear indication on the existence of GS between systems 2 and 3 and system 1 for this experimental setup. The critical coupling observed in the synchronization error curves again matches very well with the point where SPP and N-index become very close to 1, confirming the appearance of GS.

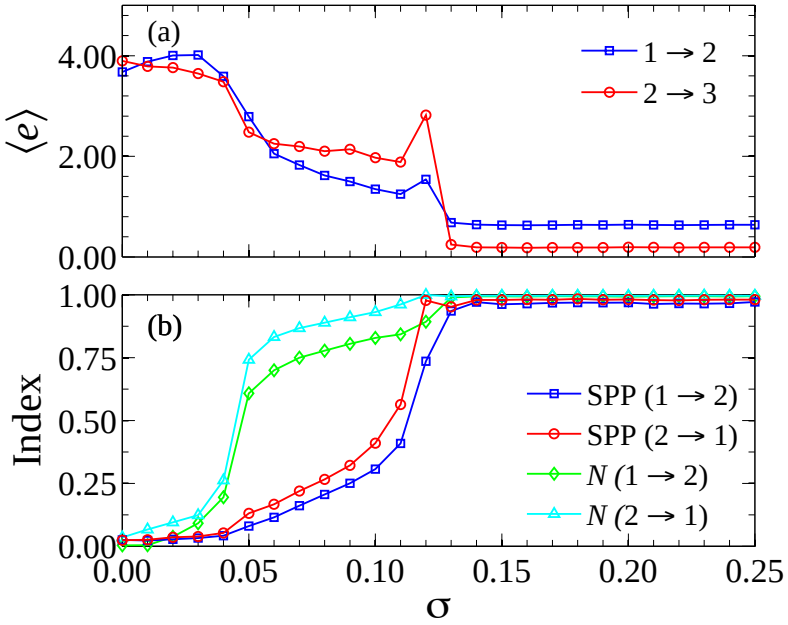

Figure 3.5: (a) Synchronization error between systems 1 and 2 (blue line) and between systems 2 and 3 (red line) as a function of σ. (b) SPP and N-index (see text for definitions) vs. σ, with the same color code described in the caption of Fig. 3.3.

3.5 Discussion

We have studied and characterized our numerical and experimental relay systems by means of measures that indicate the presence of diverse regimes of activity, including synchrony. In this regard, our results on Lyapunov exponents show that the 9-dimensional Rössler system displays two regimes of activity across a wide range of values of the coupling: Chaotic behavior is present for most of the values considered, while periodic activity can also appear (where all the Lyapunov exponents are $\lambda_i \leq 0 \, \forall i$), even for relatively large values of the coupling. Likewise, these transitions

between regimes are confirmed by the abrupt changes that both SPP and N-index exhibited for those periodic-related coupling values. As to synchrony detection, our two indicators provided strong evidence that one can correlate that the onset of the relay synchronization between the outer –identical– units is indeed associated to the occurrence of the generalized synchronization between both of them and the relay oscillator. Particularly, it can be observed that both SPP and N-index experience relatively smooth transitions across the coupling (except, of course, for the periodic instances mentioned above), but only SPP displays a steep growth right at the critical coupling σ_c (where complete synchronization is achieved by the identical nodes for the first time). We believe that this observation constitutes additional confirmation that SPP is the only direct evidence there is on the existence of generalized synchronization (because, by definition, this is an approach that aims exclusively to proof there is a single global function between the states of the subsystems) and, as far as we know, this is the first time such claim on GS for the relay configuration has been made.

Turning to the experimental settings, we can say that the implemented electronic version of the coupled Rössler system shows the robustness of the results despite the inherent presence of noise and parameter mismatch. In this case it can also be observed that both indicators provide evidence of GS as they both exhibit sooth transitions, but again only SPP displays transitions to synchrony at the critical coupling σ_c (where the error function between the identical oscillators –almost– vanishes). Putting all these aspects together, and in order to better understand how the elusive generalized synchronization works, we believe it is no sufficient for an indicator of synchrony to shed light only on the fact that such phenomenon does happen, but also on the location where it happens (that is, at the critical coupling value) and how the systems organizes itself to achieve such state (i.e. the shape of the transition). Thus, SPP indicator is better suited for this task than the N-index.

Moreover, from all of the results that the present Chapter contains, we have unquestionably established a link between the emergence of relay synchronization in instantaneously coupled chaotic systems and the existence of generalized synchronization with the relay oscillator, which opens the possibility of using relay units for practical applications. As an illustration, this approach has been used in a technique called optical encryption [62]. Briefly, the general concept of such cryptography procedure is that a content can be masked or hidden into the noise-like output of a chaotic transmitter semiconductor Laser, and that the content recovery is achieved by

relaying on the chaos synchronization between the transmitter semiconductor Laser and the receiver semiconductor Laser. Understanding the intricate mechanisms that explain relay synchronization is thus essential for the implementation of long distance, bidirectional chaos communication. We hope that the work presented in this Chapter may be helpful to formulate new research along the line of such secure technologies.

Now, there are a few aspects of our model that deserve further attention. A lot of research have been devoted, over the past few decades, to study synchronization between two chaotic units for diverse types of couplings (instantaneous, delayed, noisy, directed, etc.) [41, 42], and only until recent years some works have been published on relay systems that involve three or more chaotic oscillators [130, 131, 60, 61, 50, 63, 64, 68]. However, we still lack a complete understanding of synchronization of chaotic elements at the network level (and in particular for GS) [55, 57]. Certainly, there lies great opportunity for researchers to develop new knowledge because, when it comes to random networks, size matters indeed. Though our observation is not just about the size of the system but, more importantly, about the complexity related to it[8], which arises naturally in many real systems . One of such –paradigmatic– complex system is the brain. In the brain there has been observed that two arbitrarily separated regions or neuronal populations exhibit synchronized firing activity despite long axonal delays [65]. To explain this phenomenon of neuronal populations a relay configuration has been proposed: Their spiking signals are mediated by a third population, and the redistribution of the dynamics performed by this relay unit leads to a robust and self-organized synchrony among the outer brain regions [67]. Clearly, to approach and model realistically this phenomenon both dynamical and structural complexities have to be taken into account.

Along these lines, in Chapter 4 we review several models of neurons and study, in depth, one of them on heterogeneous complex networks. To our surprise, again, a form of synchronization arises in such neural systems as a coherent periodic activity, which confirms once more the ubiquitous nature of this prominent phenomenon.

[8]Provided the right type of topology to reflect this property, as we have explained in Chapter 2.

Chapter 4

Neural dynamics on heterogeneous sparse networks

As mentioned in the previous Chapter, coupled nonlinear elements often display complex behavior for a wide variety of interaction rules and diverse underlaying structures that channel them. For instance, several types of synchronization can be found in systems that involve continuous couplings, delays, noise, relays and, of course, oscillators [42, 41]. Though, for practical reasons, no all of these dynamics are well suited to model large-scale systems. A good example of such restrictions can be found in real neural systems, for which one might ask whether it si possible to model, for instance, the human brain as a set of coupled chaotic oscillators. Clearly such an approach would involve dealing with a dynamical system having $\sim$ 300 billion coupled equations (i.e. at least 3 times the number of neurons in an average human brain), an unmanageable task for most practical purposes. Thus, to model larger systems –in most cases– the introduction of simplifications is required (aspect that should never be regarded as a disadvantage). In physics, and particularly in statistical physics, this strategy has proven quite fruitful for a long time. Consider the *Ising model* as an illustration of this point; a simplified mathematical description of magnetic materials that was proposed almost a century ago and that created an entire research field which is still active nowadays. This observation highlights an interesting aspect of Science: It is not about capturing reality in great detail and more about decomposing phenomena into their most fundamental constituents.

Following these ideas, we note that there are different paths to provide a system with the elements that lead to complexity and, in what follows, we consider two of such aspects: Dynamical and topological complexity. Note that in the last Chapter we studied a complex dynamics in a simple configuration and here, in contrast,

we investigate a large number of simpler dynamical units in a complex structure of interactions[1]. This resolution allows: (i) to consider random topologies (with arbitrary degree distribution), (ii) to perform extensive simulations in large populations of excitable elements ($\sim 10^5$) and (iii) to compute, analytically, meaningful statistical quantities (impossible to achieve for systems of small size).

The present Chapter is divided like this: First, we review several models of neurons that can be found in the literature, and then we describe the specific ingredients of the neural heterogeneous system of interest, including an introduction to the notation and basic definitions required for our analytics. Second, we provide a full characterization of the dynamics, focusing on the effects of the parameters and its robustness against both dynamical and structural perturbations. Third, we develop an analytical approach to decompose the activity and predict the average behavior of the population using a mean-filed-like approach. In last part of the Chapter we report on a form of synchronization that emerges –unexpectedly– under couplings heterogeneity and provide a brief discussion on the main results. Regarding our methodology here we have two approaches: Extensive computer simulations, as in the previous Chapter, and a novel analytical framework derived from a few simple considerations and using elementary mathematical tools.

4.1 Models of neurons

There is a great number of models that are closely related to the problem of describing the behavior of biological neurons. Concretely, most of them try to reproduce the electrophysiology observed in individual living cells by taking into account a wide variety of known responses and properties of such units. Some other models do not account for individual features and remain at the population level, so only describe global features like the firing rate and other average behaviors. Whichever the case, this set of models is commonly known as neural models, and it is possible to find among them detailed descriptions of microscopic activity within each cell or macroscopic ones for clusters of cells. In the present Chapter, we study in depth only one of such models, a dynamics that allow us to perform computer simulations on large networks (ranging from 10^3 to 10^5 nodes) without having to sacrifice too many relevant aspects of the description of actions potential generation.

[1] In either case non-trivial behaviors emerge.

4.1.1 Integrate and fire

Integrate-and-fire (I&F, for short) models are the simplest mathematical approximation to a spiking neuron. As stated at the beginning of this Thesis, they have a very long history [132], more than a century of significant developments, and since their original introduction many novel related versions have been proposed. In spite of being so simple, this family of models still receives a great deal of attention by the scientific community [32, 33, 34, 75, 35], which may be explained by its versatility. More concretely, the main idea behind the basic version of this dynamics is that the membrane potential of a neuron can be described as a simple circuit (see Fig. 4.1), thought this assumption that does not stand alone. Let us review some other key ingredients of the model [77, 70, 76, 79, 87]:

- Shape and duration of spikes is assumed to be the same (often a delta function).
- There is well-defined threshold at which neurons fire.
- There is (linear) integration of pulse-inputs.
- Membrane potential is reset to a fixed value after every spike (renewal hypoThesis).
- In some cases, there is (either relative or absolute) refractory period.
- Distinction between inhibitory and excitatory pulse inputs and outputs.

Of course these assumptions are not arbitrary, they are basically simplifications of what has been observed in live neurons. Note that under this model, a neuron is considered as a single unit (which is not spatially extended) and the only relevant part to capture is the membrane.
As to the specific setting to describe mathematically the behavior of the voltagelike curve, Fig. 4.1 shows the diagram of the RC circuit (in parallel) that represents this version of the model,

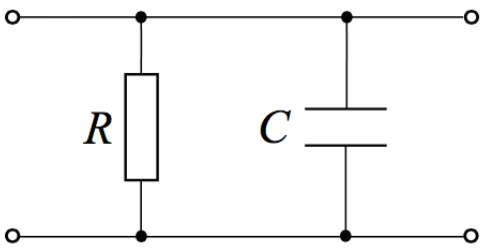

Figure 4.1: RC circuit.

More formally, let $V(t)$ represent the membrane potential of the neuron, then we have that the equation is given by Kirchhoff's current law (when the neuron is isolated),

$$C\frac{dV}{dt} = \frac{dQ}{dt} = I = -\frac{V}{R}\,, \tag{4.1}$$

which, in terms of what happens inside the neuron, states that the rate of change of the membrane potential is proportional to the rate of charge that builds up inside the cell [69]. This equation is easily integrated so we will not perform such steps here. Although the firing mechanism is not often described as part of the model, it has to be included algorithmically as follows: whenever the membrane potential reaches certain value (threshold, typically symbolized as θ), the neuron fires and its potential is reset to zero (or another fixed value).

A word of caution is in order here. Please note that in no way we believe that I&F models are detailed or accurate descriptions all the aspects displayed by actual neurons. Many limitations of such mathematical approach, especially when compared to biological systems, become quite clear if we consider what actually happens in the coupling structures, like chemical interactions in the synapse or even the way electric pulses travel along the axon. So, of course, we are fully aware that some additional phenomena are expressly neglected here, for instance non-linear effects (chaos) and adaptation, also observed in live cells. In this sense, it is obvious that our main goal is far from proposing any realistic approach to modeling neurons, but only to study a simple yet powerful model of non-linear dynamics on complex random topologies as will be shown in next sections.

4.1.2 Leaky integrate and fire

Consider the very same circuit shown in Fig. 4.1, but in this case with a driving (external) current I present. So we have that the equation for such setting is given by the expression (when the neuron is isolated, i.e. no synaptic inputs),

$$I = I_C + I_R = C\frac{dV}{dt} + \frac{V}{R} \qquad \rightarrow \qquad \tau_m\frac{dV}{dt} = -V + IR\,,$$

where $\tau_m = RC$ is the time constant, the terms $-V$ and IR on the right hand side (RHS) are often called leak and resting potential respectively. Since we will follow Ref. [72] in the rest of the Chapter, we represent the resting potential as I_{ext} and the last expression becomes,

$$\tau_m\frac{dV}{dt} = -V + I_{ext}\,. \tag{4.2}$$

After integrating, the solution of Eq. 4.2 is simply (again, in the absence of synaptic inputs),

$$V(t) = I_{ext}(1 - e^{-\frac{t}{\tau_m}}) \quad \text{where} \quad V(t_0 = 0) = 0\,,$$

and from this it can be seen that $V \to I_{ext}$ as $t \to \infty$, hence the name "resting potential". Depending on the specific values of the firing threshold and the resting potential the neuron might behave as an oscillator ($I_{ext} \geq \theta$) or as an excitable element ($I_{ext} < \theta$).

4.1.3 Hodgkin-Huxley model

As an example of a different type of mathematical neuron, here we present a model originally introduced by Alan Lloyd Hodgkin and Andrew Fielding Huxley in 1952 [24]. Just like for the I&F model, we start with Eq. 4.1 but here we consider that the total current consists of three different types of ion currents (sodium, potassium and leak, which is mainly Cl^- ions fir live cells). Such currents are given by the expression (using Ohm's law):

$$\begin{aligned} I &= I_{Na} + I_K + I_{leak} + I_{input} \\ &= g_{Na} m^3 h (V - V_{Na}) + g_K n^4 (V - V_K) + g_{leak}(V - V_{leak})\,, \end{aligned} \tag{4.3}$$

where $g_{Na,K,leak}$ are the electric conductances of each type of ion channel and $V_{Na,K,leak}$ the equilibrium (reversal) potentials, all of them empirical parameters [76, 77]. Now, n, m, and h, commonly known as gating variables, are dimensionless quantities between 0 and 1 that are related to potassium channel activation, sodium channel activation, and sodium channel inactivation respectively. A set of ordinary differential equations determines the time dependences of n, m, and h [70]:

$$\begin{aligned} \frac{dn}{dt} &= \frac{1}{\tau_n(V)}(-n + N(V)) \\ \frac{dm}{dt} &= \frac{1}{\tau_m(V)}(-m + M(V)) \\ \frac{dh}{dt} &= \frac{1}{\tau_h(V)}(-h + H(V))\,, \end{aligned} \tag{4.4}$$

where N, M and H are the equilibrium values and $\tau_{n,m,h}$ the relaxation times. Obviously all of the equations of set 4.3 share the same mathematical form, having all of them a dependency on the membrane potential V. A chief problem of the model is to

determine exactly those functions, but bear in mind that for many applications one only has to fit the experimental data to obtain them (for more details see Rinzel's, Abbott's or Wilson's simplifications in references [70, 76, 69, 36]).
Given that this model of neuron takes into account several aspects of real neurons that others ignore, and that working with it implies solving a 4D system for each neuron at every time step, it is obvious that performing computer simulations for more than a few neurons becomes quite expensive as we increase the size of the system. Since our main goal here is to study populations of neurons at the large network level, rather than the behavior of individual cells, we will have to assume a simplified version of the neuron model as we will be introduced in Sect. 4.2.

4.1.4 FitzHugh-Nagumo model

In the line of the previous model, this one also includes ingredients not present in I&F models [133, 134]. It can be derived as a simplification of the Hodgkin-Huxley (HH) model by replacing n and h by a single variable W, which leads to a system of 2D coupled equations that explains the firing mechanism (activation and deactivation) of the membrane [76]:

$$\begin{aligned} \frac{dV}{dt} &= f(V) - W + I_{input} \\ \frac{dW}{dt} &= a(bV - cW)\,, \end{aligned} \tag{4.5}$$

here V is, as usual, the membrane potential, $f(V)$ a polynomial of third degree, W is called recovery variable and I_{input} an external current. The constants a, b and c are experimental parameters.

4.1.5 Other models

As already stated, the number of neuron models that can be found in the literature is quite hight, which can be explained –partly– due to the fact that there is great number of different kinds of neurons in living organisms and also because of the rich behavior they all exhibit (which often escapes the scope of a single mathematical model). Let us review briefly a few of them:

- **Generalized Hodgkin-Huxley model:** A few generalizations of the Hodgkin-Huxley model attempt to solve problems like the low spike rates present in the

neocortex of many animals (other than the squid, on which was based their original study) [135]. In order to do that, Eqs. 4.3 and 4.4 have to be modified to include terms that explain the presence of other types of ion currents. Needless to say this is just one version we mention here, but there are many other generalizations that also have received attention in recent years [70].

- **Nonlinear integrate and fire:** Another good example of a widely used neuron model is the nonlinear I&F [77, 87], which can be defined by an expression similar to Eq. 4.2 (or even multidimensional sets of equations):

$$\tau_m \frac{dV}{dt} = F(V) + G(V) I_{ext} \,,$$

where $F(V)$ and $G(V)$ are functions that can assume any form. A stereotypical model of nonlinear dynamics is the quadratic I&F where $F(V)$ is a polynomial of second degree on V and $G(V)$ is often a constant function (again, no synaptic currents are considered here).

- **Spike response model:** A second generalization of I&F models is the so-called spike response model (SRM). In SRM models the memory of previous spikes is essential, so both parameters and equations often depend on previous activity. As for parameters in this framework we can define, for example, a dynamic firing threshold that changes in accordance with incoming pulses (same thing can be done for the refractory period, pulse delays, etc.) [76, 77].

- **Firing rate model:** A different approach, that has also received a lot of attention in recent years, is the population models [136, 69]. A population model or firing rate model is a simplification of any spiking model, since it hinges on the assumption that only average input and output spiking activity of neurons is important to describe the whole neural activity. In this case average inputs are usually interpret as currents and average outputs are called firing rates (which is defined as the probability density for the occurrence of a spike, quantity that can be approximated from a spike train in many different ways). In principle, the concept of firing rate is introduced here for individual neurons, however we can derive the model equation by averaging any of the spiking dynamics presented above over a large group of neurons [136]. In fact, they are called population models precisely because the whole point of using firing rates is to deal with networks of neurons rather than single cells. Apart from the obvious computational advantages that entail these kinds of models, there are two

additional important aspects worth mentioning. First, in many experimental setups we can only measure or record the activity of large groups of neurons, so the idea of having a framework that models populations is convenient for comparison. Second, introducing true stochasticity to a deterministic spiking model is quite difficult, so population models are ideal to include such ingredient of neural dynamics since they do not deal with specific sets of spike trains. In spite of all of the advantages noted above, firing rate models have limitations as well, mostly associated to correlated spiking activity and synchronization, which makes useless this approach for capturing certain types of brain activity.

- **Multi-compartment model:** So far we have only mentioned single compartment models, also called point neuron models, that do not take into account the spatial distribution of real neurons (for more information on this topic see references [76, 77]). Let us describe briefly another (generalized) family of models that attempts to provide a more detailed and precise description of biological neurons. The idea of the so-called multi-compartment models is that a neuron can be divided into different parts, or compartments, and that it is possible to assign to each of them, at least, one discrete variable that represents the membrane potential of the compartment [69]. With this strategy in mind we can define any kind of multi-compartment model using, for instance, any of the dynamics mentioned above. As an example of this, a third generalization of I&F models is the multi-compartment I&F model which is simply a set of equations, similar to 4.2, but now with a script μ that represents different areas of the same neuron (no synaptic inputs):

$$\tau_m \frac{dV_\mu}{dt} = -V_\mu + I^\mu_{ext} \qquad \mu = 1, 2, 3, ..., \ .$$

  Obviously this kind of concept is very useful when it comes to modeling (single) neuron's morphology, which is why it is often used along with cable theory to approximate actual neuronal structures. Of course, this level of description requires focusing only on individual cells, and thus it is far from our goals.

Many other approaches to modeling neurons were not considered here, some of them may include multidimensional systems of equations that provide dynamical complexity, others may include stochasticity to approach experimental settings, again these also escape our goals. We strongly suggest reading references [137, 138, 135, 69, 76, 70, 87, 136, 36] for more information on models of neurons.

4.2 Leaky I&F on scale-free networks

In this Section we present a particular dynamics that has been studied on random k–regular [139] and small-world networks [72]. Most of the results already reported in the literature are based on numerical simulations and, as far as we know, there is no study on heterogeneous topologies. Our approach consists of two parts. First we generate undirected random scale-free networks ($2 \lesssim \gamma \leq 3$ and $k_{min} \geq 2$) using the configuration model described in Sect. 2.4, and prescribing three additional constraints:

i The domain of the power-law degree distribution function is restricted to the values $k_{min} \leq k_i \leq \sqrt{N}$.

ii $\sum_i k_i$ even.

iii Self-connections are forbidden.

So each node is connected to the others randomly and according to these three conditions, which ensures that our networks are uncorrelated [111]. By a straightforward integration (and normalization) one obtains the exact expression of the average degree in this case:

$$\langle k \rangle = \left(\frac{\gamma - 1}{\gamma - 2} \right) \left[\frac{k_{min}^{-\gamma+2} - N^{\frac{-\gamma+2}{2}}}{k_{min}^{-\gamma+1} - N^{\frac{-\gamma+1}{2}}} \right] \quad (\gamma > 2) \,, \tag{4.6}$$

The second part of our model is the dynamics. Given a particular network of N nodes, and for fixed values of the model parameters, i.e. τ_m, τ_D, I_{ext} and θ (which from now on will be assumed constant), each node is considered as a leaky integrate-and-fire neuron that follows the equation [139, 72]:

$$\tau_m \frac{dV_i}{dt} = -V_i + I_{ext} + g_i \sum_{j,m} a_{ij} \delta \left(t - t_j^{(m)} - \tau_D \right) \,, \tag{4.7}$$

where the time-dependent variables V_i represent the membrane potential and i the neuron index. The firing mechanism is quite simple, every time the potential of a neuron reaches or exceeds the threshold, θ, it fires and its voltage drops to zero instantly. As for the parameters in Eq. 4.7, τ_m is the time constant (that models the decay) and the term I_{ext} is the same driving current mentioned before for leaky I&F dynamics, which sets the resting potential. It is straightforward to see that all interactions between neurons are due to the third term on the RHS of Eq. 4.7 (usually called synaptic current). The amplitudes of the spikes are represented by g_i, a_{ij} are

the entries of the unweighted adjacency matrix of the network, and τ_D is a constant pulse-delay (finite speed of the pulses).

Putting all these ingredients together, the dynamics goes as follows: if node j, for instance, has fired at $t_j^{(m)}$ and $a_{ij} = 1$, then node i receives an excitatory input of strength g_i after τ_D. Clearly this model is no other than a leaky I&F with a nonlinear synaptic current.

Following Ref. [72], we chose $I_{ext} < \theta$, so neurons cannot fire by themselves (non-oscillatory regime) and it is necessary to apply some initial spike-inputs to start the activity[2]. A crucial consequence of having both pulse-delay and non-oscillator neurons is that time scale becomes discrete in the sense that there are only interactions every $\Delta t = \tau_D$. Since nothing interesting happens between consecutive interaction times, from now on we will focus exclusively on such discrete time scale.

4.3 Basic definitions and notation

Let χ_{it} be the firing state of neuron i at time t (defined to be 1 if neuron i fires at time t, or 0 otherwise), then the instantaneous firing rate of the network at t is defined by:

$$\text{Firing Rate}(t) = \frac{1}{N}\sum_{i=1}^{N}\chi_{it}\,, \tag{4.8}$$

then the average firing rate of the network over a long time window ($1 \leq t \leq t_{max}$) is given by:

$$\alpha \equiv \langle \text{Firing Rate}\rangle_t = \frac{1}{t_{max}\times N}\sum_{t=1}^{t_{max}}\sum_{i=1}^{N}\chi_{it}\,. \tag{4.9}$$

The time interval between two consecutive firings of a neuron is called an inter-spike-interval (ISI, for short). For a large time window, $1 \leq t \leq t_{max}$, let $N_t(i)$ be the number of ISIs of neuron i, and T_{ih} be the duration (number of time steps Δt) of the hth ISI ($1 \leq h \leq N_t(i)$), then $\text{ISI}_{\text{ih}} = T_{ih} \times \Delta t$. For a system that is in a stationary regime of global self-sustained activity (i.e. transient is removed from computation), then the average ISI of neuron i over a long time window is given by the expression:

$$\langle \text{ISI}(i)\rangle_t = \frac{\Delta t}{N_t(i)}\sum_{h=1}^{N_t(i)} T_{ih} \approx t_{max}/\sum_{t=1}^{t_{max}}\chi_{it}\,. \tag{4.10}$$

These definitions will be used repeatedly in Sect. 4.5, and Appendixes A and B.

[2]Depending on the specific set of values of the parameters, one or several inputs are sufficient to guarantee self-sustained activity.

4.4 Numerics (homogeneous couplings)

In order to characterize our model, in the following Sections we will analyze thoroughly several salient numerical results for homogeneous pulse strength and compare them with other findings already reported in the literature.

4.4.1 Self-sustained activity and the effects of parameters

Fig. 4.2 shows an example of typical activity on SFNs: After a short transient, in which the activity spreads rapidly across the network, the global signal reaches its stable mean value (which we may call "quiescent state") and persists around it indefinitely. This activity seems to be self-sustained and not merely prolonged because it continues, without any additional external inputs, for a long time window ($t > 10^5$) with no sign of possible spontaneous failure. The underlying mechanism that explains this self-sustained activity is, as expected, related to the scale-free topology. The relative refractory period of the neurons, modeled by τ_m, has no (or small) effect on most of the hubs because they receive many inputs (even as the reflection of their own previous spikes) at each interaction time and, therefore, they fire at every time step (leading the dynamics to a regime of high-level activity). Evidently, in Fig. 4.2, the global signal does not exhibit any periodicity nor significant oscillations are present, which means that there is no predominant fire frequency nor a large group of neurons that fire in-phase (irregular firing pattern).

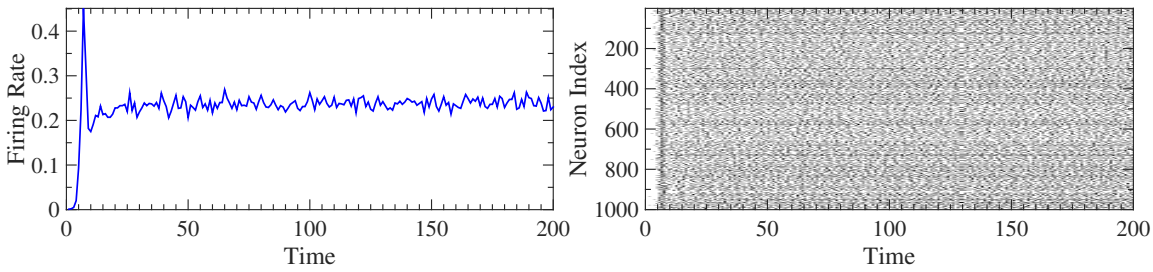

Figure 4.2: Firing rate (left) and raster plot (right) for $N = 10^3$, $\gamma = 3.0$, $k_{min} = 2$, $I_{ext} = 0.85$, $g = 0.2$ (constant $\forall i$), $\tau_m = 10$, $\tau_D = 1.0$ and $\theta = 1$. Same parameter values are used in following figures unless noted otherwise.

Taking the population firing rate in Fig. 4.2 (left panel) as our benchmark, let us now report briefly on some of the effects of the parameters in Eq. 4.7. By varying τ_m or $g_i = g$ (g constant over i) and leaving all the other parameters unchanged, for instance, we can alter the firing rate as follows: by reducing τ_m (or, equivalently, increasing $g_i = g$) the mean value of the global signal is increased, and we can even to

change its structure (for significant variations it becomes periodic with small period –see [83]). That is to say, by changing any of those parameters in the described way, a large group of neurons saturates, because of the incoming pulses, and are forced to fire within a short time window. Thus, for some values of these two parameters, and only in terms of the global behavior of the system, having neurons that are more susceptible to small inputs is equivalent to having neurons that are being stimulated by greater impulses. Similar results can be obtained by changing the speed of the pulses (and rescaling the time axis): Fast pulses ($\tau_D < 1$) reduce the mean value of the firing rate (because activity is distributed more broadly over time), while slow pulses ($\tau_D > 1$) increase it and may even change the structure of the signal (becoming periodic in the same way as explained before).

As for the specific procedure to provide the initial pulse-inputs that triggers self-sustained activity, it depends crucially on the interaction strength values g. Generally, for $g > \theta - I_{ext}$, one single external input applied to any neuron, at the time when $V_i \approx I_{ext}\ \forall i$, is sufficient to obtain self-sustained activity ($\langle \text{Firing Rate} \rangle_t > 0$). For the interval $(\theta - I_{ext})/k_{min} < g \lesssim \theta - I_{ext}$, several external inputs, or even the activation of all nodes, are required to star self-sustained activity, and there is no activity whatsoever for g values below the lower bound of this interval (since neurons with $k = k_{min}$ cannot fire). The use of a single or N initial pulse-inputs does not lead to significant differences for the average firing rate value obtained, though N initial pulse-inputs might enhance (slightly) the amplitude of signal fluctuations (because more neurons fire in-phase) and also transients are usually shorter (because the activity does not have to spread across the network). Note in Fig. 4.2 (left panel) that when a single fire is used to start the dynamics, a sharp peak appears during the transient (about $\sim 50\%$ of neurons fire at once) and then the signal decreases to the quiescent state. This feature suggests that a global (simultaneous) activation of neurons to initiate activity is a strategy that might not affect significantly the activity observed after the transient. However, for $g = [\theta - (1 - e^{-\frac{\Delta t}{\tau_m}})I_{ext}]/k_{min}$, network activity is already saturated ($\langle \text{Firing Rate} \rangle_t = 1$) for N initial pulse inputs while it might not be yet for a single one (but close).

As shown in Fig. 4.3, there is a size effect related to the structure of the firing rate and its mean value. Again, for the smallest networks illustrated in the left panels of Fig. 4.3 ($N \leq 10^3$) no predominant fire frequency in the global signal is observed, thus we say that the firing rate has no periodicity. Whereas for the largest networks considered ($N \gtrsim 10^4$), without changing any parameter of the dynamics, signal structure emerges (reported in the left column of Fig. 4.3). To corroborate the presence of such

periodicities we computed normalized spectral densities for each firing rate (displayed in the right column of Fig. 4.3), estimated using Fourier transform method, and obviously there are multiple peaks for the smallest networks whereas for the largest networks just a single peak.

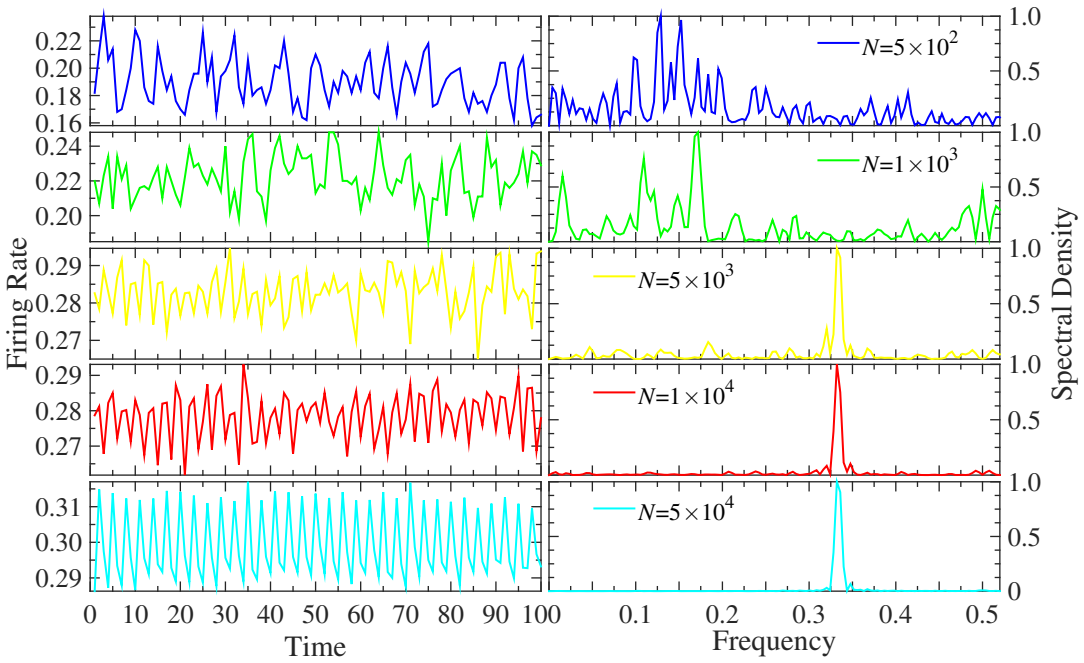

Figure 4.3: Firing rate (left column) and the corresponding normalized spectral density (right column) for five network sizes. Same parameters as Fig. 4.2, except N.

To explain this finding we have to go back to our network model. Our networks are generated following three prescriptions, one of them being $k_{max} \sim \sqrt{N}$. So the larger the network, the greater the amount of hubs and their degrees. Figure 4.4 (main) depicts $\langle \mathrm{ISI}(i) \rangle_t$ for all neurons of the network of size $N = 5 \times 10^4$, and any of them with $22 \leq k \lesssim 200$ has an average ISI equals to 1 (i.e. complete saturation, they fire at every time step). Consequently, a relevant cluster of saturated hubs arises for large networks, that do not exist for small ones, which drives the activity of small degree neurons to fire every few time steps and also increases the average value of the global signal. An additional confirmation can be obtained from the left panel of the inset in Fig. 4.4, the histogram of mean ISI, which reveals that more than one-third of the total neurons (highest bin) have $\langle \mathrm{ISI}(i) \rangle_t = 3$, value that corresponds to the frequency detected by spectral analysis. This means that the structure of the signal is formed by adding individual signals of neurons within the smallest connectivities groups ($k = 2,\ 3$, since these are the most abundant). The other signals that compose the global firing rate, neurons having $k \gtrsim 4$, just add to the mean value and not to the

periodicity. Periodic oscillations of neural populations have already been reported for different models of neurons on a few complex topologies [140, 141, 72], but specifically small period oscillations for a leaky I&F model, to our knowledge, only by reference [83].

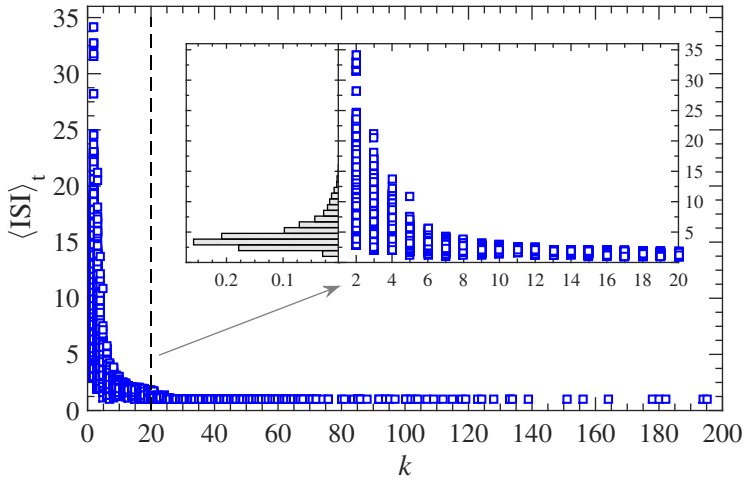

Figure 4.4: Main: Scatter plot of average ISI. The averages were computed over 10^5 time steps. Same parameters as Fig. 4.2, except $N = 5 \times 10^4$. Inset: Scatter plot of average ISI for $k \leq 20$ (right) and its corresponding histogram (left).

A most significant observation from the previous results, and from the extensive numerical simulations, is that the stationary average firing rate does not increase continuously from zero when increasing g, though it does in an abrupt way; in other words, there is a threshold value g_c (script "c" stands for critical) at which self-sustained activity starts with an average firing rate well above zero. Another relevant remark on the average firing rate with respect to the coupling is that it is a monotonically increasing function of g, but not a strictly increasing one (so for some values of g the average firing rate might not change).

Finally, the salient observation, already mentioned, that once in the self-sustained activity regime (for $g > g_c$), there is a set of extremely active neurons for which $\chi_{it} = 1$ for all time t, leads to the notion of "saturation degree" k^s (that decreases with g) such that for all neurons i with degree $k_i \geq k^s$, their ISI$(i) = 1$. Again, this core of relatively high degree/fast firing neurons is responsible for the maintenance of global self-sustained activity in SFNs and, for large networks, is also responsible for the emergence of periodic oscillations with a higher mean value of the firing rate. We will use some of these definitions and quantities in Sect. 4.5.

4.4.2 Bistability and signal control

It is possible to perturb the ongoing dynamics at any point of the quiescent state by activating or deactivating randomly chosen neurons (i.e. setting to 1 or 0 the firing states χ_{it}, respectively, and resetting to zero their membrane potentials V_i). At first glance, this procedure may seem artificial since it is "external", in the sense that does not emerge –spontaneously– from the internal dynamics of the network, but we would like to stress that it is just an *ad hoc* mechanism to test the response of the system to (synchronous) large firing signals and to assess how dynamically robust SFNs are under perturbations. On the other hand, this mechanism can be justified by arguing that it is simply the interaction between our network of neurons and, for instance, a pacemaker or even a regulatory neural network (being the latter a biologically feasible mechanism). In the next paragraphs we will describe some of the most remarkable responses of the system that we have found when using this approach:

Bistability: For the smallest networks considered here ($N \lesssim 10^3$) an inhibitory signal applied to $\gtrsim 60\%$ of all neurons is enough to extinguish the activity permanently (see Fig. 4.5), but for large networks ($N \sim 10^5$, not shown) only consecutive inhibitory global-pulses (at least two) are capable of turning "off" the dynamics. The activity can be triggered again, in the usual way, once the membrane potentials of all neurons have reached the resting value I_{ext}. Hence, the property called bistability, which is precisely the capability to switch the neural activity between "on" and "off" (resting) states, is also present in our model [72]. Of course, all these remarks are valid for the parameters used and as soon as they are modified, for instance, reducing the activity level, then less inhibition might be needed in order to cease all activity. An *ad hoc* mechanism to turn back "on" the network can be easily introduced using noise (allowing neurons to fire randomly) but will not consider this approach here (see reference [72] for more details).

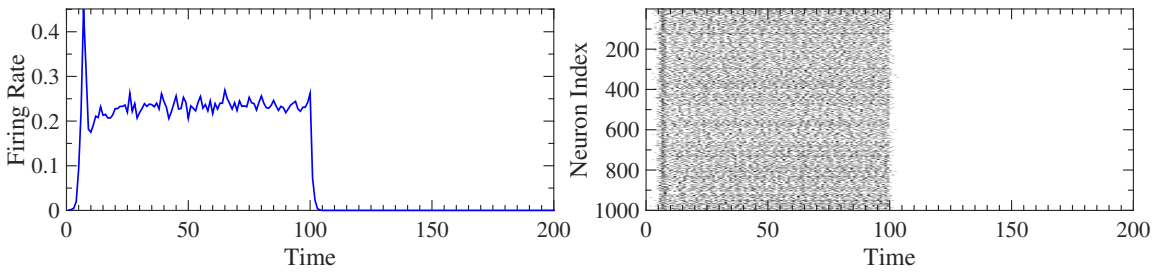

Figure 4.5: Bistability. Firing rate (left) and raster plot (right). Bistable behavior of the network. At $t = 100$ an inhibitory global signal (60%of neurons) was applied to turn off the dynamics. Same parameters as Fig. 4.2.

No signal response: Fig. 4.6 shows the same activity pattern depicted in Fig. 4.2, but in this case with a large excitatory stimulus at $t = 75$ (75% of the total neurons) and an inhibitory perturbation at $t = 125$ ($\lesssim 60\%$ of the total neurons). The first aspect to notice from it, is that for these parameters the global-pulses have no persistent effect on the global firing signal, because neither through excitatory nor inhibitory means was possible to modify the mean value or the structure of the firing rate after the perturbation' transient. The second aspect to acknowledge is that the time needed to return to the quiescent state (recovery time) for inhibitory perturbation is much longer than the recovery time for excitatory stimulus, which is reasonable because the activity has to spread across the network again. This scenario suggests that, for a given set of values of the parameters, no matter the mechanism chosen to initiate the activity (described in the previous Section), the resulting global firing rate displays the same features.

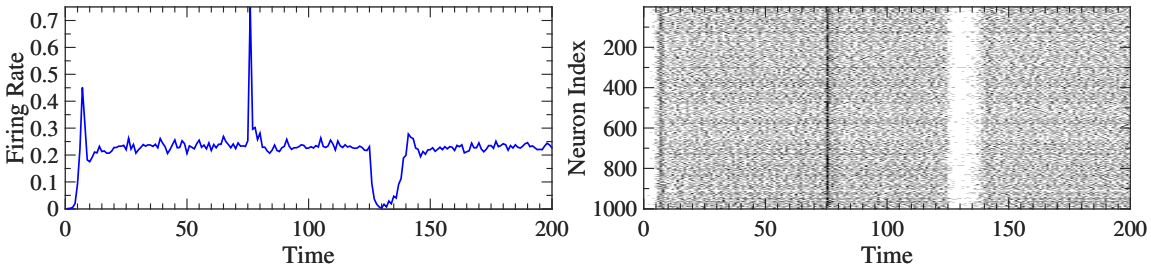

Figure 4.6: No signal response. Firing rate (left) and raster plot (right). Same parameter as Fig. 4.2. Note that in this regime of the activity large excitatory and inhibitory pulses have no effect on global features of the signal (i.e. it induces no changes to the mean value, periodicity shape and amplitude of the irregular oscillations).

Activity enhancement: Fig. 4.7 illustrates the dynamics for a stronger coupling strength. The firing rate is clearly periodic in this case (by saturation effect, described in the previous Section), and at $t = 75$ the excitatory stimulus enhances –slightly– the amplitude of the oscillations. As already explained, this enhancement is due to the fact that, after the excitatory stimulus is applied, there are more neurons (with ISI close to the period of the global signal) firing in-phase. To show that it is possible to recover the initial amplitude of the oscillations, at $t = 125$ an inhibitory perturbation is applied to 90% of the neurons and obviously it is sufficient to reduce the oscillations. Although this neural stimulus acts on randomly chosen neurons, it might be considered as a globally reversible process when using certain parameters (particularly, under homogeneous pulse-couplings). Note that the recovery time to reach the quiescent state is shorter because of the high-level activity.

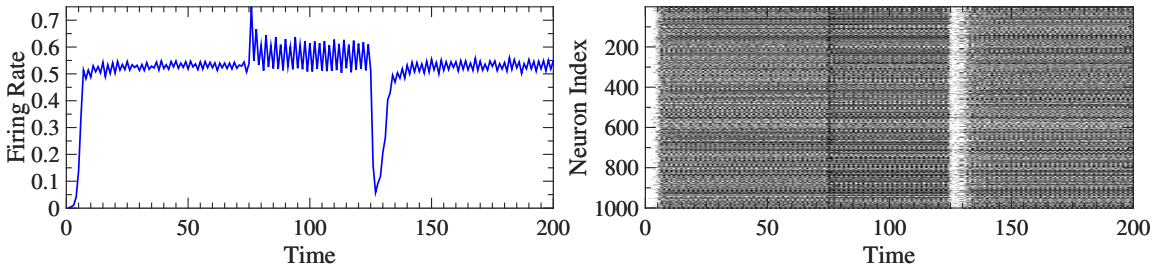

Figure 4.7: Activity enhancement. Firing rate (left) and raster plot (right) for $g = 0.35$. It is possible to change the amplitude of the oscillations of the global signal, but its structure (periodicity and shape) remains the same.

4.4.3 Activity failure and dynamical resilience

To investigate the activity failure as a result of the damaging process of the topology of the network (site percolation, reviewed in Sect. 2.5), we performed an uniformly random removal of nodes on several SFNs [105] and then we executed the dynamics on the giant component of the resulting network. Fig. 4.8 (left panel) exhibits the failure probability as a function of the removed fraction of nodes (fr), but taking into account as failure only those realizations for which all activity ceased before $t = t_{transient}+200$ time steps (each point on the curves is an average over 10^3 realizations of the random deletion of nodes). It is possible, of course, that some realizations assessed as successful using the criterion mentioned above were just prolonged activity instead of self-sustained, but such criterion turned out to be quite reliable –in most cases– because activity failure in SFNs generally occurs within a small time-window (perhaps another consequence of being ultra-small [142]). Note that the steepness of failure probability curves in the transition regime increases with the size of the network (as it should be).

Another aspect to consider here, perhaps one that describes better what occurs with the dynamics in the damaging process, is illustrated in the right panel of Fig. 4.8, where the average firing rate (of successful realizations) is shown as a function of the fraction of deleted nodes (solid curves, each point is the average over 200 non-null realizations, i.e. for $\langle \text{Firing Rate} \rangle_t > 0$). The curves of the size of the giant component (again, average over 200) are also shown for comparison in the right panel of Fig. 4.8 (dashed curves). Clearly, the average firing rate is a decreasing function in all cases when the removal is performed, but for the largest networks complete dynamical failure only occurs close to the critical value of the fraction at which the network has percolated completely ($fr \approx 0.8$). In this sense, activity on SFNs is quite resilient because, in spite of crucial changes in network' structure, it finds its way to persist

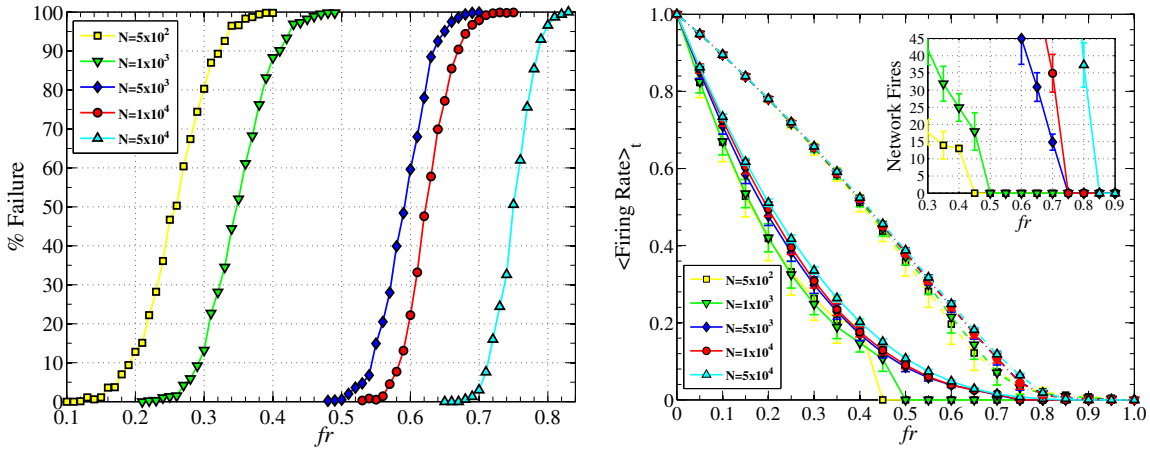

Figure 4.8: Failure activity probability as a function of the fraction of randomly removed nodes (left panel). Main (right panel): average value of the firing rate over time (solid curves, all values normalized by $\langle \text{Firing Rate} \rangle_t$ at $fr = 0$) as a function of the fraction of randomly removed nodes, and the corresponding size of the giant component (dashed curves) of the percolated network. Inset (right panel): Total fires as a function of the fraction of randomly removed nodes. Same parameters as the ones used in Fig. 4.2.

until the complete disintegration of the topology is almost achieved. The inset in the right panel of Fig. 4.8 confirms this results, but also shows an unexpected outcome of the last stages of the damaging process: Strikingly, the total number of networks fires (unnormalized) just before complete failure for all network sizes are of the same order of magnitude, which means that all SFNs are capable of sustaining activity until certain number of nodes, regardless of the original size of the network.

4.5 Analytical estimations

In an effort to provide some rationale for these salient observed features, and on the basis of some simplifying approximations, we develop in this Section some analytics whose predictions agree qualitatively, but also quantitatively in some respects, with observations on the stationary regime of self-sustained activity.

Again, let us begin by assuming that the system is in a stationary regime of global self-sustained activity on SFNs. In this framework, a recurrence relation on $V_i(t)$ can be derived by straightforward integration of Eq. 4.7:

$$V_i\left(t\right) = V_i\left(t - \Delta t\right) e^{-\frac{\Delta t}{\tau_m}} + (1 - e^{-\frac{\Delta t}{\tau_m}}) I_{ext} + g b_i\left(t\right) \ ,$$

where $b_i(t)$ is the number of pulse-inputs that neuron i receives at time t. Then the firing condition at the end of the hth ISI is expressed as,

$$\sum_{n=0}^{T_{ih}-1} \left[\left(1 - e^{-\frac{\Delta t}{\tau_m}}\right) I_{ext} + g\, b_{(T_{ih}-n)} \right] e^{-\frac{n\Delta t}{\tau_m}} \gtrsim \theta \tag{4.11}$$

where we use a simplified notation for the number of pulse-inputs received at each time step, within the hth ISI, by neuron i: b_1 are the inputs received by neuron i at $t = \Delta t \sum_{j=1}^{h-1} T_{ij}$ (the instant when the hth ISI begins), b_2 are the inputs received by neuron i at $t = \Delta t \sum_{j=1}^{h-1} T_{ij} + \Delta t$, ... , $b_{T_{ih}}$ are the inputs received by neuron i at $t = \Delta t \sum_{j=1}^{h} T_{ij}$ (the instant when the hth ISI ends).

After averaging equation Eq. 4.11 over all ISIs of neurons having degree k, as well as using a few simplifying (mean-field-like) assumptions one obtains (see Appendix A), for the average $T(k)$ of T_{ih} in the k-class:

$$T(k) \approx \frac{\tau_m}{\Delta t}\, \ln \left[\frac{\left(1 - e^{-\frac{\Delta t}{\tau_m}}\right) I_{ext} + g\alpha k}{\left(1 - e^{-\frac{\Delta t}{\tau_m}}\right) (I_{ext} - \theta) + g\alpha k} \right] , \tag{4.12}$$

where α is the average firing rate, given by Eq. 4.9. The quantity $T(k)$ provides the average ISI of neurons of degree k as:

$$\langle \mathrm{ISI}(k) \rangle_t = \begin{cases} \lceil T(k) \rceil \times \Delta t & \text{for } T(k) \leq 1 \\ T(k) \times \Delta t & \text{for } T(k) > 1 \,, \end{cases} \tag{4.13}$$

where $\lceil x \rceil$ represents the ceiling function. As expected, $T(k)$ is a monotone decreasing function of k. Using as an input the numerical results of the stationary average firing rate α in Eq. 4.12, for different values of the coupling g, one can obtain estimations of $\langle \mathrm{ISI}(k) \rangle_t$ and compare them with the numerical results (see Fig. 4.9). Clearly, Eq. 4.13 provides a good overall decomposition of the global dynamics and an accurate description of the average behavior of each k-class.

Eqs. 4.12 and 4.13 are useful to derive other properties of the model. For instance, the value $k = k^s$ can thus be estimated for any value of g (provided α), as $\langle \mathrm{ISI}(k^s) \rangle_t = 1$ (the script "s" stands for saturation, as mentioned in the last paragraph of Sect. 4.4.1):

$$k^s \equiv \frac{1}{g\alpha} \left[\theta - \left(1 - e^{-\frac{\Delta t}{\tau_m}}\right) I_{ext} \right] , \tag{4.14}$$

so that all neurons with degree $k \geq k^s$ are saturated. Note that the saturation degree value is a decreasing function of g (for α is naturally a non-decreasing function of g).

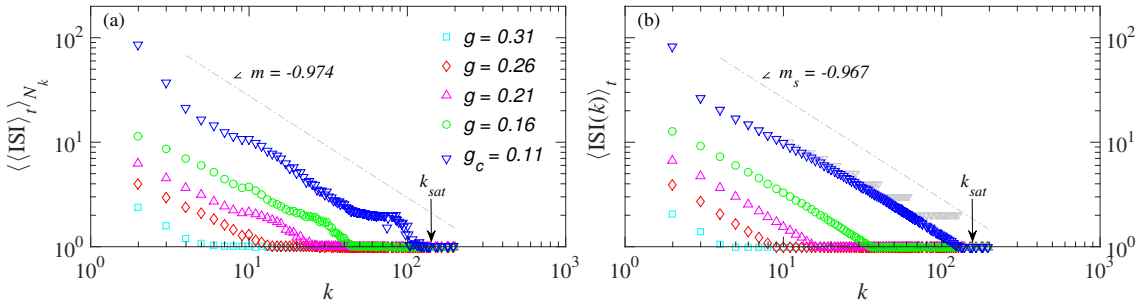

Figure 4.9: ISI heterogeneity. (a) Numerical result: average ISI (computed over 10^5 time steps) vs. connectivity and (b) Prediction of Eq. 4.13. The size of the network is $N = 5 \times 10^4$ and the critical coupling for this network is $g_c = 0.11$ (blue downward triangles). Note that some numerical curves display what we call "step effect" as a consequence of the discrete time scale imposed by pulse delays. In panel (b), only for this critical value g_c, gray triangles represent $\lceil T(k) \rceil \times \Delta t \ \ \forall k$ and are displayed for comparison. From Eq. 4.17 we estimated $k_{sat} \approx 130$ and is shown to compare with the numerical result, $k_{sat} = 128$. Finally, dashed gray lines are exhibited as a measure of agreement –they do not mean power-law behavior–, the relative error between their slopes is $E_{\%} \approx 0.7\%$.

As $T(k)$ must be a positive quantity, again from Eq. 4.12 one has that, for all g and k,

$$\alpha > \frac{1}{gk}\left(1 - e^{-\frac{\Delta t}{\tau_m}}\right)(\theta - I_{ext}) \ . \tag{4.15}$$

The RHS of this inequality is maximum at $k = k_{min}$, and therefore, as α is a non-decreasing function of the interaction strength g, one concludes that there is a lower bound g_c below which there is no global self-sustained activity, and that α jumps, at $g = g_c$, from zero to the finite value

$$\alpha_c \equiv \alpha(g_c) = \frac{\left(1 - e^{-\frac{\Delta t}{\tau_m}}\right)(\theta - I_{ext})}{(g_c \times k_{min})} \ . \tag{4.16}$$

Obviously α_c is just a lower bound for the average firing rate and, since SFNs are ultra-small [142], it just takes a few integration steps of the dynamics in order to ascertain whether there is activity or not after the transient. So in this way, from numerical simulations, we can determine easily the minimum value $g = g_c$ at which any network exhibits self-sustained activity, and thus we can estimate α_c from Eq. 4.16. As an example, the estimation of α_c for the network used in Fig. 4.9 is $\alpha_c = 0.0648$ and, from numerics, $\langle \text{Firing Rate} \rangle_t = 0.0650$ at the same coupling strength, so strikingly there is only a small relative error of $E_{\%} \approx 0.3\%$ between numerics and analytics. The fact that the expression for α_c provides, in this case, a good estimation of the average firing rate obtained from simulations means that this dynamics on SFNs is

quite resilient, because it holds until a small value of the coupling, at which most of the k_{min}-class neurons are about to fail completely their activity. From Eqs. 4.14 and 4.16 we can calculate the saturation degree (k^s) at the critical interaction strength (g_c), that we symbolize as k_{sat},

$$k_{sat} \equiv k^s(g_c) = \left[\frac{\theta - \left(1 - e^{-\frac{\Delta t}{\tau_m}}\right) I_{ext}}{\left(1 - e^{-\frac{\Delta t}{\tau_m}}\right)(\theta - I_{ext})} \right] k_{min} \ , \tag{4.17}$$

which turns out to be completely determined by the (isolated) neuron parameters and the smallest degree k_{min} of the network (then its computation does not require any input from numerics). This result for the saturated core at the critical coupling is quite surprising because it was expected to find that the larger the network, the larger k^s (since $k_{max} \sim \sqrt{N}$), but now it is clear that k_{sat} does neither depend on the size of the network nor on the specific value of g_c. See caption of Fig. 4.9 for an example of the quantitative agreement obtained, prediction that we have successfully tested for very large SFNs (up to $N = 10^5$).

Another quantity that is also completely determined by the single neuron parameters is the slope, m_s, of the curve $\langle \mathrm{ISI}(k) \rangle_t$ at $k = k^s$ for $g = g_c$ in a log-log plot (see dashed line in Fig. 4.9):

$$m_s = \frac{\tau_m}{\Delta t \theta} \left(1 - e^{\frac{\Delta t}{\tau_m}}\right) \left[\theta - \left(1 - e^{-\frac{\Delta t}{\tau_m}}\right) I_{ext}\right] \ , \tag{4.18}$$

which also turns out to be independent of the critical coupling value g_c. This slope might be useful because there is an almost-linear behavior (in log-log plot) for a wide range of k, so it can be used a measure of agreement between numerics and analytics.

From all these results it is indisputable that, even without any further development, Eq. 4.12 provides useful insight into this dynamics and also allows us to predict a few significant consequences of our model from a single input from numerics. Nevertheless, we have derived an approximate relation (see Appendix B) for the average firing rate α and the average ISI of the k-class:

$$\alpha = \langle \text{Firing Rate} \rangle_t \approx \sum_{k=k_{min}}^{k_{max}} \frac{p(k)}{\langle \mathrm{ISI}(k) \rangle_t} \ , \tag{4.19}$$

which is only approximate due to the finite value of t_{max}. Eqs. 4.12, 4.13 and 4.19 constitute a set of coupled non linear equations which can be solved to estimate $\langle \mathrm{ISI}(k) \rangle_t$ and α without the recourse to simulations.

4.5.1 Accuracy of our approach

In order to examine how accurate the assumptions and approximations made in deriving Eq. 4.19 are, we introduce the following implicit equation (that can be solved without performing any computer simulation of the dynamics):

$$f(\alpha) = \alpha - \sum_{k=k_{min}}^{k_{max}} \frac{p(k)}{\langle \mathrm{ISI}(k) \rangle_t} = 0 \tag{4.20}$$

Note that α as a function of g is constrained by Eq. 4.14 and by the minimum degree of the network, so we know exactly where to look for –real– roots of such equation. The value that Eq. 4.14 yields for the upper bound of g is $g_{sat} = \left[\theta - \left(1 - e^{-\frac{\Delta t}{\tau_m}}\right) I_{ext}\right] / k_{min}$ (at which $\alpha = 1$) and the lower bound of g is given by $(\theta - I_{ext})/k_{min}$ (below this value neurons having $k = k_{min}$ cannot fire at all).

Now, the accuracy of our theory depends crucially on having enough statistics. For large values of γ most terms in the RHS of Eq. 4.19 do not contribute significantly (even for relatively low values of k), because they are quite small ($\sim N^{-1}$) compared to the other terms and, thus, only small connectivity groups dominate the predictions provided by Eq. 4.19. In accordance to the scale free model, the larger the value of γ the less likely to have a significant amount of hubs to hold our approximations, so to have a sufficient number of nodes in most of k-classes that guarantee the contributions of most terms in the summation of Eq. 4.19, the value of γ has to be reduced. Fig. 4.10 shows evidence of this claim. In it, the behavior of $f(\alpha)$ is depicted for different couplings (six curves ranging from critical to saturation), and there is –at most– one root for each of the values of g considered. It can be observed that for low values of γ the roots of $f(\alpha) = 0$ (represented by black crosses) are quite close to their corresponding average firing rates computed from simulations (solid circles), whereas for high values of γ the theory is less accurate. In fact, our approach is quite precise when it comes to estimating the average firing rates for values of $g > \theta - I_{ext}$ when $\gamma \lesssim 2.5$ (e.g. for $\gamma = 2.0$ the predicted values in this range of the pulse strength have $E_{\%} < 5\%$ with respect to the average firing rates from numerics).

Regarding the roots of $f(\alpha) = 0$ for $g \lesssim \theta - I_{ext}$ (above g_c, though not very far from it), no matter the value of γ, clearly our theory either underestimates such values or does not provide real roots to compare with the ones computed from simulations. The reason for this is related, again, to the topology of our system. In order to fire each neurons in the largest connectivity group ($k_{min} = 2$) needs to receive excitatory inputs from all of their neighbors at the same time and when their membrane potentials is close to the resting value. Such conditions are fulfilled only occasionally

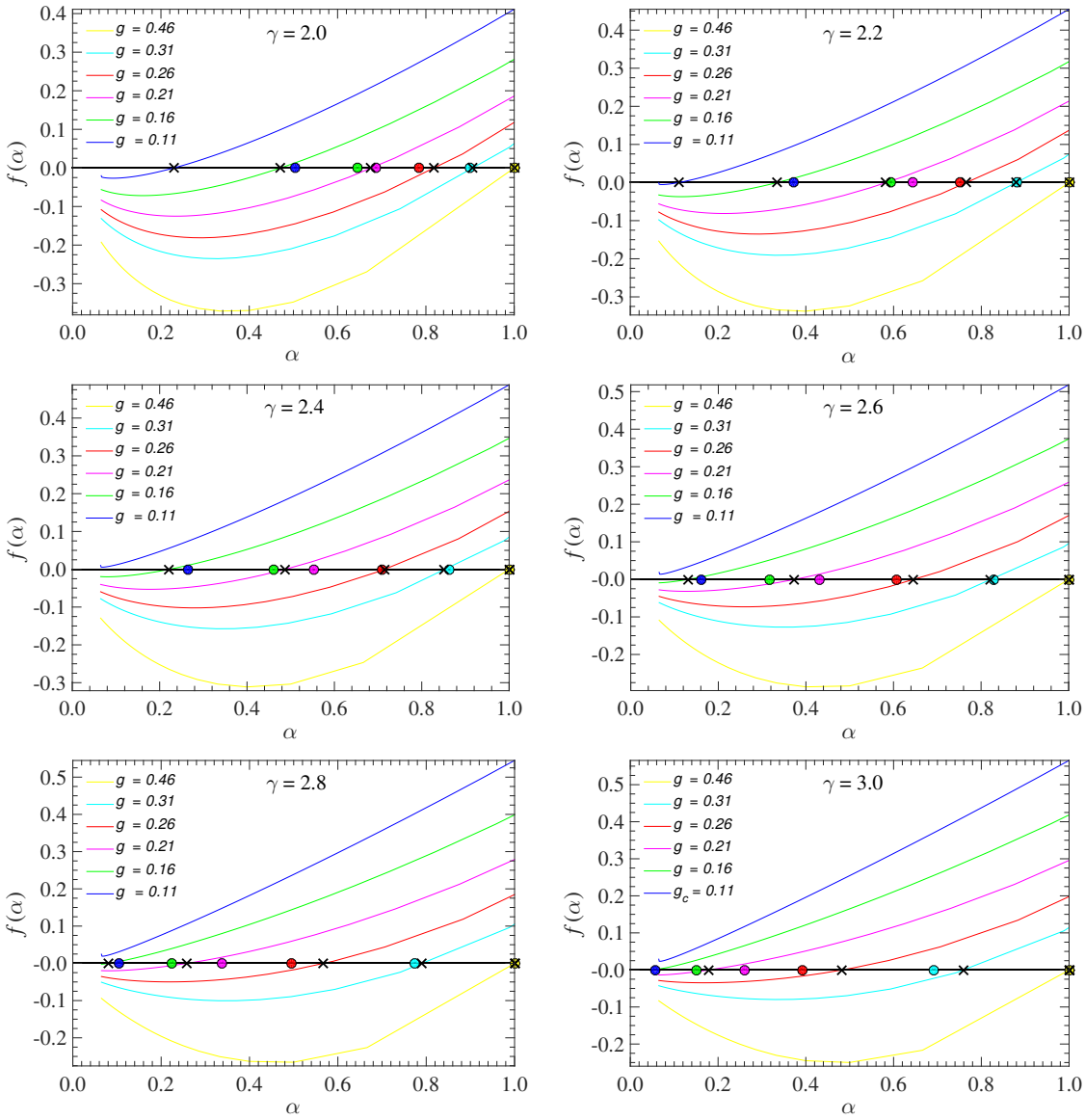

Figure 4.10: Theory performance. Each panel displays the graphical solution of Eq. $f(\alpha) = 0$ for several values of the coupling g (constant $\forall i$). Black crosses indicate the roots of $f(\alpha)$ and, for comparison, solid circles represent the average firing rate computed from numerics (both, numerical results and analytical curves are coded by color). Note that for the higher values of γ some analytical curves do not cross the x-axis (there is no -real- root). These cases are only for the smallest values of g. For larger values of g, it is possible to compute the roots and, thus, the average firing rate can be estimated. Parameters that were used are $N = 5 \times 10^4$, $k_{min} = 2$, $I_{ext} = 0.85$, $\tau_m = 10$, $\tau_D = 1$ and $\theta = 1.0$

by neurons that are not directly connected to hubs, which explains the large values of $\langle \mathrm{ISI}(k) \rangle_t$ already reported for small values of k and g. This aspect of the model is responsible for increasing the variability of ISIs of neurons having small degrees, and

some of the assumptions in the derivation of Eqs. 4.12 and 4.19 may not be valid in this regime of pathological activity.
All in all, we believe that these findings are a great success because there are not many analytical results for models of neurons at the network level and, to our knowledge, none for leaky I&F on sparse heterogeneous networks.

4.6 Inhomogeneous couplings

If the strength of the pulses that each neuron receives is inversely proportional to its connectivity (i.e. $g_i \propto k_i^{-1}$, provided that the proportionality constant is above certain value –to obtain self-sustained activity), then the firing rate becomes periodic regardless of the size of the network and the initial firing conditions (as figure 4.11 shows). In this case the period achieved by the global signal is not necessarily small, as it usually is in saturation regime for homogeneous couplings, so the activity of the network seems to be an organized collective phenomenon of neurons. This result is essentially different from the periodic oscillations displayed in Fig. 4.3, not only because in this instance it is qualitatively the same for all the network sizes considered, but also because quantitatively both period and (proportional) amplitudes are similar for all cases as well. Note the amplitude of the oscillations here $\sim 0.2N$, much greater than those exhibited by the same networks with homogeneous couplings ($\sim 0.05N$, at most). The difference in amplitudes is meaningful because it suggest that a significant amount of neurons (belonging to different k-classes) determine completely the structure of the global signal, and not just a small group with the same degree. Let us briefly comment a bit more this point. For inhomogeneous couplings most (or even all) neurons fire with similar average ISI (though not always the same instantaneous ISI), having only phase shifts between their signals. So the mechanism that explains self-sustained activity here is no longer a saturated cluster of neurons as it is for homogeneous couplings. As an average behavior, this can be confirmed by Eq. 4.12 (because all the assumptions made in deriving it remain unchanged, granted that g_i is a function exclusively of k). Thus $\langle \mathrm{ISI}(k) \rangle_t$ predicts the exact same average value for all k precisely when $g_i \propto k_i^{-1}$. To illustrate this point, using the value of α from numerics (network of $N = 10^3$), Eq. 4.12 estimates that $\langle \mathrm{ISI}(k) \rangle_t \approx 7.1$ (arbitrary time units) $\forall k$ and from spectral analysis we have determined that the period of the global firing signal is 8 (arbitrary time units).
What these findings establish is that linking $g_i \propto k_i^{-1}$ is precisely one way to

homogenize, dynamically, a system that is heterogeneous topologically (see reference [53] for another example of correlation between dynamics and topology).

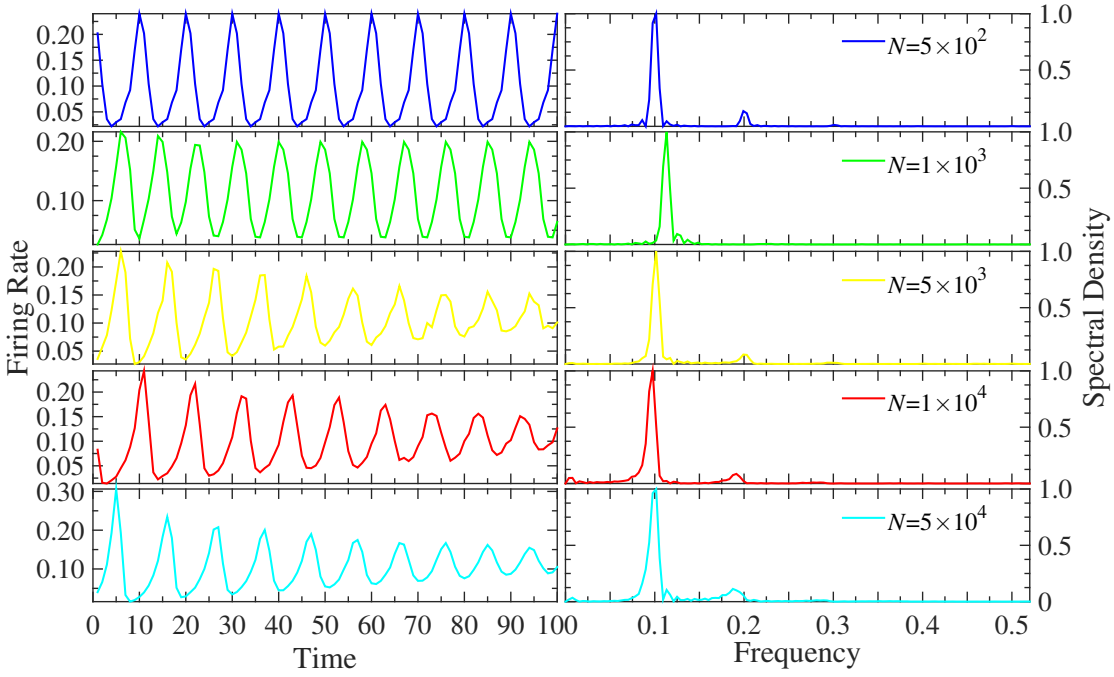

Figure 4.11: Firing rate (left column) and the corresponding normalized spectral densities (right column) for five network sizes. Same parameters as before, except $g_i = 0.89/k_i$.

Unfortunately we cannot compute –*a priori*– a precise value of α from Eq. 4.20. Essentially, inhomogeneous couplings induce a form of initial firing conditions sensitivity, in the sense that the periodic signal reached by the network after the transient depends strongly on the specific procedure used to trigger the activity [143]. This effect is so sensitive that if we change the neurons at which the activity of a network starts, it generally leads to completely different firing rates, with differences in mean value, amplitude, periodicity and shape (see an example of this claim in Fig. 4.13). Obviously Eq. 4.20 can not capture such diverse behaviors that occur for the same values of the parameters (however it may be useful to estimate some –not all– of the average firing rates resulting from precise initial conditions).

Fig. 4.12 illustrates another example of periodic oscillations, but in this instance all neurons fire exactly at the same frequency (statistically speaking). If the variance of $\{\langle \mathrm{ISI}(i)\rangle_t\}$, over the whole network, remains below $\sim 10^{-4}$ for more than a certain length of the time window considered (which, in our case, is 10^4 –arbitrary time units), we say that the system exhibits coherent oscillations (CO). For the outcome shown in Fig. 4.12 this criterion is fully satisfied, so we conclude that the system

self-organizes into one of many possible states of CO at the individual neuron level –though to achieve this state quickly initial firing conditions have to be carefully selected. Note that CO can be interpret as a form of synchronization (in spite of the fact that these dynamical elements are not –intrinsically– oscillators), thus we may call this behavior *ISI synchronization*, which have also been detected in other systems of spiking neurons (limited to homogeneous topologies) [141, 144, 145, 146].

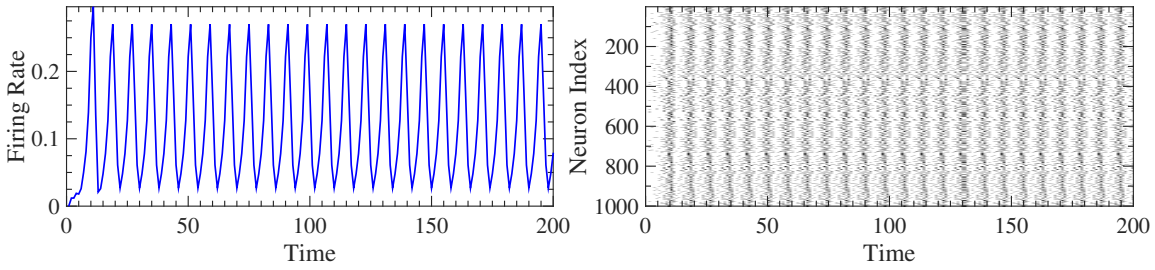

Figure 4.12: Firing rate (left) and raster plot (right). Same parameters as before, except $g_i = 0.89/k_i$.

Further evidence of the presence of CO for other network sizes is shown in Fig. 4.13, where the set of N values of $\langle \mathrm{ISI}(i) \rangle_t$ are displayed. We observe that the system's variability is quite low, in fact, at relatively small values of N (say, $N \lesssim 10^3$) the variance of $\{\langle \mathrm{ISI}(k) \rangle_t\}$ can be exactly zero (as predicted by Eqs. 4.12 and 4.13) and for $\{\langle \mathrm{ISI}(i) \rangle_t\}$ it is around 10^{-4}. Regarding larger networks ($N \gtrsim 10^3$), the variance of $\langle \mathrm{ISI}(i) \rangle_t$ is typically a bit higher (though still remains below 10^{-3}), which can ve explained as a result of the so-called *paradox of heterogeneity* (hubs are more difficult to synchronize).

From our extensive simulations, we observe that this regime of CO also exhibits longer transients that depend on the size of the system: *the larger the system the longer the transient*. As an example, we have detected that transients can be as long as 10^3 (arbitrary time units) for $N = 5 \times 10^4$. However we suspect that in certain cases it might take longer to achieve full ISI synchronization (depending on the initial firing conditions and, of course, size of the system). For now, let us express that we have not determined yet all the ingredients that guarantee the fast appearance of CO in our model (just the right coupling and careful selection of initial firing conditions), so ascertaining the rest remains a subject for future research.

Finally, in order to test the response of the system for inhomogeneous couplings, we performed the same procedure introduced in Sect. 4.4.2. As depicted in Fig. 4.13 that after the excitatory stimulus is applied (75% of neurons at $t = 100$) the mean value, the period and amplitude of the oscillations of the global signal are modified (but a

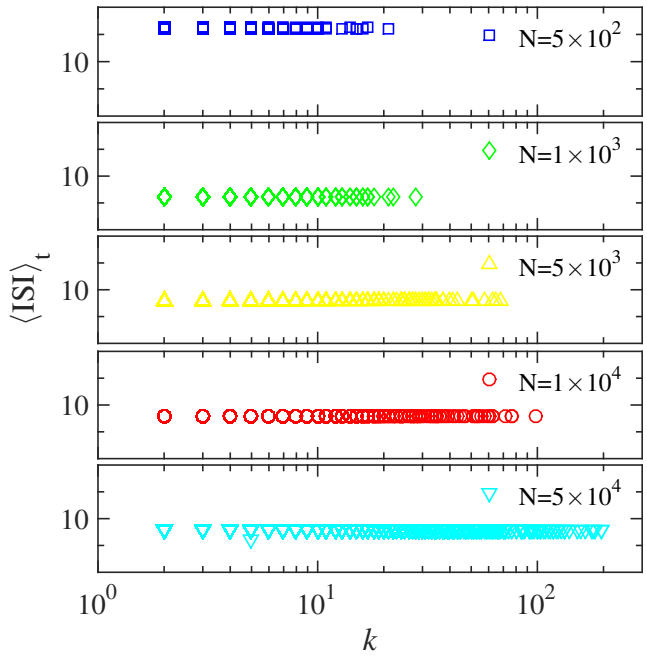

Figure 4.13: Scatter plots of average ISI for five network sizes. Same parameters as before, except $g_i = 0.89/k_i$.

periodic pattern remains). The activity of the network displays a major difference compared to previous cases seeing that we have here a full signal response. This example reveals that any stimulus applied to the SFNs under pulse heterogeneity might be globally irreversible, because there is no customary technique to restore the original state of the ongoing dynamics (but there might be a specific sequence to do it). Note also that the recovery time from the external stimulus is greater than in all previous results, which is consistent with the fact that hubs play a different roll for $g_i \propto k_i^{-1}$, as they are unable to spread the activity instantly like the do for homogeneous couplings. As for the effects of large inhibitory stimuli, we observe that global signal cease in all cases, as a result of reseting the membrane potential and the relative refractory period.

Summarizing our findings on inhomogeneous couplings:

- Correlating $g_i \propto k_i^{-1}$ is a good way to homogenize the activity of a network of excitable elements with heterogeneous topology.
- Even though the activity obtained is always well organized and can lead to the appearance of coherent oscillations, certainly it is very sensitive to initial firing conditions.

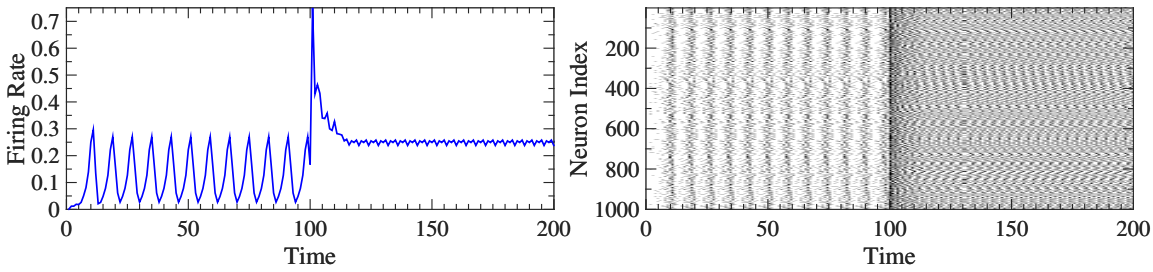

Figure 4.14: Firing rate (left) and raster plot (right) for $g_i = 0.9/k_i$. It is possible to change mean value, amplitude and structure (period and shape) by stimulating the ongoing dynamics with large excitatory signals.

- An external excitatory stimulus can alter mean value, period and shape of the global firing rate.
- As for the amplitude of the oscillations of the firing rate, a large excitatory stimulus can reduce it significantly, but there is no general procedure to enhance the oscillations of the global signal by means of trivial external firing patterns.
- If the activity is initiated using extreme initial firing conditions (e.g. N fires at the same time), it fails rapidly in all instances (the relative refractory period plays an important role here). Same reason explains why all inhibitory stimuli extinguish permanently the firing activity.

4.7 Discussion

In this Chapter we have studied a pulse-coupled dynamics of excitable elements in uncorrelated scale-free networks. Regimes of self-sustained activity were found for homogeneous couplings, in which the system displayed a wide variety of behaviors, including periodic and irregular global spiking signals. Our numerical results also show that certain properties of the population firing rate depend on specific aspects of the model, for instance the periodic signals detected are a result of either the size of the system (i.e. large cluster of dynamical hubs) or strong couplings. Furthermore, there exist two types of activity, standard and pathological, whose boundary is set by the voltage-gap between the firing-threshold and the resting potential: When the pulse-strength is larger that this gap, one obtains a kind of activity in which all neurons in the system are able to fire with one single input. On the other hand, when the pulse-strength is smaller than this gap, the neurons need to receive several inputs in order to fire. This is a dramatic condition for neurons having $k \sim k_{min}$, as it is satisfied infrequently. The system's response is also noticeable, the global

–*pathological*– patterns become irregular and the spikes are distributed more broadly. An extreme instance of this occurs when the coupling is set at the critical value (which is bounded below by the mentioned voltage-gap divided by de minimum degree of the network). For this particular state, we provided a few useful mathematical expressions that allow us to compute average behaviors and other relevant conditions.

As demonstrated before, a few straightforward dynamical and topological strategies can be introduced to perturb the dynamics. These are basic schemes to enhance or hinder global behaviors, rendering a scenario where signal control is attainable. Among the responses of the system, two of them deserve our attention. First, the mechanism to turn off the dynamics permanently has been theorized as an essential feature of neural activity[3], however its importance is associated here to the control it yields on the activity (especially when the dynamics is driven by noise). Second, the ability to control the amplitude of the global oscillations by means of trivial patterns hints at the possibility of developing an strategy to force system-wide events (i.e. a method to create large in-phase groups of neurons).

Concerning inhomogeneous couplings, coherent oscillations (an unexpected form of synchronization) appeared naturally. We observed that this regime of activity is also self-sustained as it lasts for a long time window ($\sim 10^5$). However it is a state much more sensitive to perturbations of any kind, particularly to the application of large stimuli (either as a triggering mechanism or as an ongoing perturbation). Such aspect can be difficult to work with because, among other effects, it induces very long transients. Thus determining the onset of the quiescent or stationary state may become an issue here.

As our main result, here we presented a framework to estimate, in the stationary state, the mean firing rate over a long time window and to decompose the global dynamics into average values of the inter-spike-interval of each connectivity group. Our approach provides accurate predictions of these average quantities when the network exhibits high heterogeneity. As mentioned before, most of the analytical results that can be found in the literature on neural models are focused either on single (isolated) units or on densely connected networks[4]. However, we would like to stress that the concept of sparseness of a network is not always defined precisely or it is assumed vaguely by some authors of the field [82, 139, 147]. For instance, in some of these studies the term "sparse" is used to describe random networks in which

[3]an analogous version was developed for small-world networks [72].

[4]To perform approximations impossible to achieve on sparse topologies.

each neuron receives $k = C \times N$ inputs (or connections). C is obviously a structural parameter (called connectivity level) to create an amorphous topology (i.e. random k–regular network defined in Sect. 2.3.1). However, $C \times N$ is typically assumed only one order of magnitude smaller than the size of the system ($C \sim 10^{-1}$) [28, 29, 148]. So, for example, when the structure has $N \sim 10^5$ nodes, then each of them is connected to $k \sim 10^4$ neighbors (and additional connections from outside the network are also allowed). Clearly this is not what we commonly know as a sparse graph in network science [149]. In spite of all the assumptions and approximations made in deriving our analytics, the fact that it works on sparse heterogeneous networks (where, for instance, $\langle k \rangle \sim 10^1$, quite small compared to $N \sim 10^5$) is a significant accomplishment.

Another prominent aspect of Eqs. 4.12, 4.13 and 4.19, that we want to strongly emphasize, is that these equations are valid for SFNs, but also for any topology with heterogeneous degree distribution (provided that all the other premises are satisfied as well). Using the scale-free model in the present Chapter can be interpret as an extreme example of such heterogeneity, but there is no constraint that attaches our finding to this type of network at all, and applying the same framework to other kinds of topologies (for the same dynamics) should produce accurate results as well.

Finally, along the lines expounded in the Introduction, we believe the study of spiking models is not restricted to traditional Neuroscience, and that the measure of success of such models should not be limited as to how accurate they are to reproduce what is observed in live neurons. There are many real systems where agents do not interact continuously, but in an intermittent fashion, and the lack of applications of these neural models constitutes a great opportunity to formulate novel research in the view of new progress. As a results of this observation, in the next Chapter, we introduce and develop an original approach to describe socio-technical systems in which information spreads as pulses and cascades occur naturally.

Chapter 5

Neural dynamics in socio-technical systems

In the previous Chapter we examined a nonlinear dynamics that included elementary aspects of real neurons. Among all of the properties that such systems have, spikes, pulse delays and excitability[1] stand out. These aspects are of great relevance because, as we have shown, they set a discrete time scale of events (or interactions) that enabled us to develop analytical expressions and, thus, to predict average behaviors of the system. However, these attributes also entail some restrictions. The excitatory regime imposes a dramatic feature: The population of neurons has to be triggered in order to initiate the activity. Consequently, the self-sustained activity obtained in this fashion is always linked to the initial set of fires, so any spike generated at $t > 0$ is a result of the initial inputs and can be tracked back to its source at $t = 0$. In other words, this regime of activity and its crucial triggering mechanism always leads to a form of time-constrained activity that involves the whole system. In fact, one could argue that such self-sustained dynamics of fires can be considered as one never-ending cascade[2]. These observations stress the fact that the I&F model explored in the previous Chapter can never account for a distribution of cascades observed in many real-world events, including critical phenomena.

In this Chapter, on the other hand, we propose a new framework that disentangles the mechanisms involved in the emergence of decentralized synchronization and extends prior models to accommodate the temporal evolution of interdependent cascading events. Our proposal, as an approximation to socio-technical systems, conceals in an idealized manner other desirable ingredients –such as genuine complex contagion or

[1] As opposed to the oscillatory regime, where these elements do not need to receive any input from their neighbors in order to fire.

[2] See Sect. 5.1.2 for a formal definition of this term.

self-induced motivation to participate[3]. Our goal is to characterize thoroughly this dynamics, considering wide explorations of the parameter space and to identify the conditions under which large-scale events are more likely to arise from networks that are constantly pulsating with information. As with all analytical models, ours is a simplification of what is essentially a very complex reality. But it is, we think, a less simple approximation than previous models as it moves us one step forward in our understanding of synchronization of interacting agents as it evolves over time.

The rest of the Chapter proceeds as follows. First, in Sect. 5.1, we consider prior work analyzing basic concepts like contagion, diffusion and social influence, then we review the notion of cascade and report briefly on the classic threshold model. A neural-like dynamics is introduced in Sect. 5.2, highlighting the main differences compared to previous approaches to modeling social activity and discussing the substantive implications of our departure. In Sect. 5.3 we provide the most significant results for extensive numerical simulations performed on multiple topologies. Then, under this dynamics, we develop a novel analytical approach to predict global events in Sect. 5.4 and, its application to capture the behavior of a real socio-technical system (Sect. 5.5). Finally, in the last Section of the Chapter we discuss our main findings in the context of social science, especially as they relate to previous research, and analyze future work.

5.1 Basic notions

5.1.1 Social contagion and information spreading

Social contagion and diffusion dynamics have received sustained attention since, at least, the decade of 1950s [150, 151, 152]. The use of the term "contagion" goes back to the 19th century, and the common analogy between societies and living organisms [153, 154]. Metaphors aside, when social scientists today talk about contagion they refer to cascading phenomena that is triggered by interdependence and influence [155, 156]. The object of the cascades are individual activations, which offer a conceptual shorthand for the decision to attend a protest, join a campaign, or tweet about a specific topic. The recent spike of interest in these phenomena responds partly to the irruption of networked technologies, which offer new observational windows to social interactions [157, 95, 158]; and partly to the development of new network methods to model decision making and the paths through which contagion spreads [159, 156].

[3]Ingredients captured by two simple parameters of the model.

Recent empirical efforts to dissect the mechanisms of social contagion connect with a long theoretical tradition in mathematical sociology analyzing networks and their impact on collective dynamics [160, 161, 162, 163, 164, 165, 166].

Models of interdependent decision-making have made two main contributions to the study of contagion: the first refers to individual motivations, the second to the structure of interdependence. Diversity in the motivation to become active has usually been modeled as a distribution of thresholds [167]. Prior research shows that the shape of this distribution matters greatly for the emergence of a critical mass and a successful contagion process. Diffusion or information spreading, however, depends also on links and how that underlying structure encourages or hinders spreading dynamics. Networks shape those dynamics by creating different centrality distributions (which allow specific individuals to be more or less influential, see [168]) and by opening more or less structural holes [169, 170], which constrain opportunities for chain reactions since they delimit the routes that cascades can follow [171]. The old idea that ties that link socially distant groups [160] – open the bridges for global diffusion is still central to much empirical research [172, 173]. However, recent years have also seen the development of other highly influential contributions casting light on the importance of network topology, including the theory of small world networks [94, 18]; the distinction between simple and complex contagion [174, 175]; and the identification of influencers and susceptible people in networks [176, 177]. These recent developments show that information spreading responds to structural features other than bridges, and that the mechanisms of contagion differ depending on the nature of the element being diffused. As previous studies, our view assumes that exposure to information is the driving force underlying contagion, but it is agnostic about the specific mechanism that leads to activation – it could be influence, normative pressure, learning, or some of the other mechanisms suggested by previous research [174, 175, 162, 178, 163, 179, 18, 171]. The intermittent dripping of information that social networks facilitate often leads to bursts of activity [180], as when news suddenly become trending topics [181, 182] or flash mobilizations manage to gather thousands of people in a specific location in a matter of hours, if not minutes [183, 184]. These instances of sudden hype and excitement are akin to the moments of collective effervescence identified in studies of religion [185] and other group settings [186]. The mechanism underlying these bursts of activity requires the adjustment of individual rhythms so that everybody talks about the same news or goes to the same venue at the same time. This activity – and how it leads to systemic (global) outcomes, like swift information cascades, trending topics, or massive demonstrations

– is overseen if activation is modeled as a permanent change of the state of an agent [102, 171] (see Sect. 5.1.3). We argue here that it is more realistic to model the individual propensity of an agent to be activated as an oscillating force, the direction and strength of which depends on the context, as defined by the network and the signals it transmits. This, we sustain, resembles more closely the dynamics observed in the context of large-scale mobilizations, where agents do not undergo a binary change of state, from inactive to active, but instead oscillate in their contributions to activities like spreading calls for action or increasing the salience of political issues [187, 188, 189, 190, 191].

5.1.2 Cascades: Time-constrained activity

There is a general consensus around the concept of cascade, which –in the ICT environment– can be outlined in the following way: the basic criterion to include an agent i (which, in a network is simply a node) in the cascade where j belongs to is to guarantee that:

i i and j became neighbors at t_1 (the notion of "friend" is understood broadly here).

ii i received a piece of information from j, who had sent it out, at time t_2.

iii The node i sends out a piece of information at time t_3.

Typically, no strict time restriction exists besides the fact that $t_1 < t_2 \leq t_3$: the emphasis is generally placed on whether the *same* content is flowing [101]. This content-based view is useful when considering very specific pieces of information (e-mail chain letters [192] or URL forwarding [193, 194], for instance), but renders a scenario in which the only possible transition for a node (user) is from inactive (susceptible) to active (infected).
Such vision oversees the fact that online platforms allow users to share contents, but also (more often than not) to spread behavior. Indeed, discussion over a topic typically happens not by mere information retransmission, but by iterated activity (variable units of information expressed in online text, evolving over time) [195] which influences (motivates) other users to join. A richer, time-constrained representation can then be obtained if conditions i to iii above are accepted, except that for agent i to be included in an avalanche started at j, the piece of information being transmitted may or may not be the same, and $t_3 - t_2 \leq \Delta\tau$, where τ is an arbitrary (typically small) time lapse. In other words, the condition for i and j to be included in the same cascade is to exhibit temporally correlated, synchronized or quasi-synchronized

activity [1, 2, 101]. With this slight modification, not one but multiple cascading events can be measured from an activity data set (for instance, a collection of time-stamped tweets), and a single user may participate many times in the same cascade, in different times. Empirical ans synthetic cascades hereafter refer to such time-constrained representation of the information flow.

5.1.3 The threshold model

Along the lines of content-based cascades, the reputed threshold model [102] (and its networked version [171]) mimics social dynamics, where the pressure to engage a behavior increases as more friends adopt that same behavior. Briefly, the networked threshold model assigns a fixed threshold τ, drawn from a distribution $0 \leq g(\tau) \leq 1$, to each node (individual) in a network of size N and an arbitrary degree distribution $p(k)$. Each node is marked as *inactive* except an initial seeding fraction of active nodes, typically $\Phi_0 = 1/N$. Denoting a_i the number of active neighbors, a node i with degree k_i updates its state becoming active whenever the fraction of active neighbors $a_i/k_i > \tau_i$. The simulation of this mechanistic process evolves following this rule until an equilibrium is reached, i.e., no more updates occur. Given this setup, the *cascade condition* in degree-uncorrelated networks can be derived from the growth of the initial fraction of active nodes, who on their turn might induce the one-step-to-activation (vulnerable) nodes. Therefore, large cascades can only occur if the average cluster size of vulnerable nodes diverges. This condition is met at [171, 196]

$$F = \sum_k k(k-1)\rho_k p(k) = \langle k \rangle \tag{5.1}$$

where ρ_k is the density of nodes with degree k close to their activation threshold, $p(k) = N_k/N$ is the degree probability distribution and $\langle k \rangle$ is the average degree [171].

For $F < \langle k \rangle$ all the clusters of vulnerable nodes are small, and the initial seed can not spread beyond isolated groups of early adopters; on the contrary, if $F > \langle k \rangle$ then small fraction of disseminators may unleash –with finite probability– large cascades. More recently, the cascade condition has been analytically determined for different initial conditions [196] as well as for modular and correlated networks [197, 198], while placing the threshold model in the more general context of critical phenomena and percolation theory [199].

As mentioned above, this model has a limited scope since it can account only for one-shot events, for instance the diffusion of a single rumor or the adoption of an

innovation. Also, this framework leaves no room for spontaneous initiative: even low-threshold nodes –those with higher propensity to participate in a cascade– will not be recruited unless their neighbors act upon them. Empirical evidence suggests, instead, that once an agent becomes active that behavior will be sustained, and reinforced, over time [188]. This creates a form of enduring activation that will be affected and affect other agents over time in a recursive way. Indeed, events evolve in time –and so do the cascades elicited therein [2], as a consequence of dynamical changes in the states of agents as dynamics progress. Cascades are then events that brew over time in a system that holds some memory of past interactions. Moreover, the propensity to be active in the propagation of information sometimes depends on other factors than raw social influence, e.g., mood, personal implication, opinion, etc.

5.2 Model and interpretation

In the following Sections we review briefly the model of neurons adopted to approach the problem of information spreading and cascades in ICT systems, and then we provide an interpretation of such dynamics in the context of social interactions.

5.2.1 Peskin's model

In 1975 a mathematician named Charles Peskin proposed a simple dynamics to model the synchronized behavior of cardiac cells responsible for heartbeat rhythms [14]. Later on, in 1990, Renato E. Mirollo and Stephen H. Strogatz adopted the same dynamics to study a wider scenario, the synchronization of pulse-coupled oscillators that account for a great number of phenomena, including chirping of crickets, flashing of fireflies, and, of course, pacemaker cells [71].
According to Peskin's model, given a set of N identical elements, we associate to each of them a single variable $0 \leq x_i \leq 1$ to describe their dynamics,

$$\frac{dx_i}{dt} = S_0 - \gamma_d x_i, \quad i = 1, 2, 3, ..., N. \tag{5.2}$$

Note that this equation has the same form of Eq. 4.2, so it is fair to say that these elements are identical I&F oscillators (where the voltagelike variables are represented by x_i, γ_d is the conductance and S_0 the resting potential).
The firing mechanism is introduced algorithmically as follows: When $x_i \geq \theta = 1$ the oscillator i fires and x_i is reset to zero instantly. The structure of interactions

is naturally constrained by a network of size N, so whenever node i fires then –instantaneously[4]– $x_j = min(1, x_j + \varepsilon)\ \forall j \in \mathcal{V}_i$ (where ε is the coupling strength and $\mathcal{V}_i$ denotes the set of all neighbors of node i –see Sect. 2.1).

In a more general sense, following [71], it is possible to derive a continuous function f (to describe the voltagelike curve x) that guarantees the system is always driven to synchrony (a result valid not only for the solution of Eqs. 5.2). As a simplification, given that the isolated elements exhibit periodic behavior, a phase $\phi \in [0, 1]$ is introduced here, so that $d\phi/dt = 1/T$ (where T is the natural period of the isolated elements), and the endpoint point conditions $f(0) = 0$ and $f(1) = 1$ are satisfied. If the charge curve $x = f(\phi)$ ($f : [0, 1] \to [0, 1]$) is smooth, monotonic increasing ($f' > 0$) and concave down ($f'' < 0$), then achieving full synchronization is certain (proved rigorously only for two oscillators). Thus, the mathematical expression of these ideas follows this functional form[5]:

$$x = f(\phi) = \frac{1}{\omega} ln\left[1 + (e^{\omega} - 1)\phi\right] \tag{5.3}$$

The model assumes that nodes in the network reach their firing threshold at different speeds. The speed of activation is a function of two parameters: ω, which determines how quickly each oscillator reaches the threshold zone (i.e. it defines the concavity of the curve that maps progression of x towards activation); and ε, the strength of the pulses received from the neighbors in the network when they fire (the coupling that shifts the state of the node closer towards the threshold). The timeline in Fig. 5.1 (top left) illustrates the logic of this approach. The lower panels in Fig. 5.1 (bottom left) exhibit how node i advances towards activation, both as a function of ϕ and as a response to the activation of its neighbors. When a node activates, as node i does in $t2$, it shifts the state of its neighbors with the ε signal and resets its state back to the beginning of its phase. The parameter ω determines the shape of $x = f(\phi)$. When the parameter ω is 0, the progression of nodes towards their activation threshold ($\theta = 1$) grows linearly with ϕ; as the parameter ω increases, nodes reach their activation zone faster, i.e. a signal received from their neighbors will tip their sate over the threshold, which means they will send a signal as well (thus helping other oscillators also get closer to their activation zones). In our case $\omega > 0$ (always) to make the function concave down (an illustration of the effects of ω on $x = f(\phi)$ is shown in the right panel of Fig. 5.1, a larger ω produces a more pronounced shape, making the

[4]Since the activity spreads at once, that is no pulse-delays are present, evidently the model assumes that the pulse speed is infinite.

[5]Again, this function is not an exclusive nor a general solution to the problem, any function can be used as long as they fulfill all the conditions already mentioned.

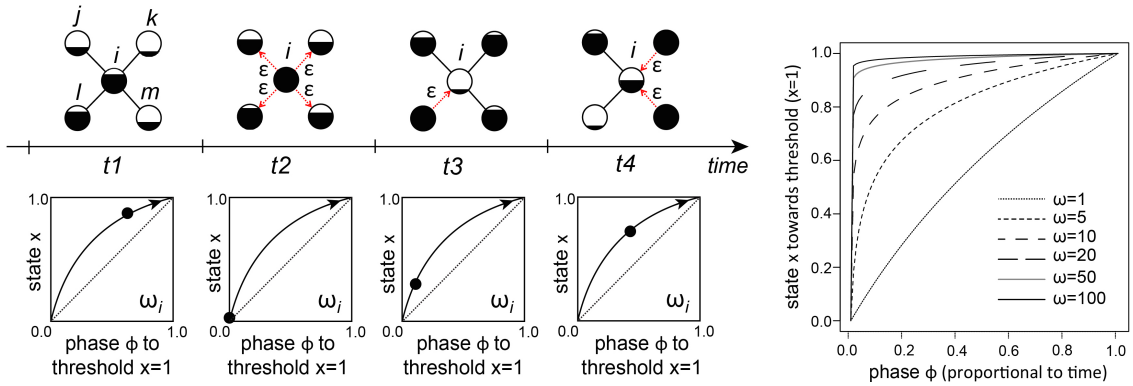

Figure 5.1: (Left) Schematic representation of the model with recurrent firing. (Right) The impact of the parameter ω on the activation buildup.

function rise very rapidly to then level off). Finally, to set initial random conditions we always distribute $\{x_i\}$ uniformly at $t = 0$, and let the system evolve until global cascades appear. Putting all these ingredients together, Fig. 5.2[6] shows the typical activity observed for random initial conditions on x. Note that at the begging of the simulation, say $t \lesssim 30$ only isolated nodes, or small groups of them, fire occasionally. Then, for $t \gtrsim 30$ a cluster of synchronized oscillators emerges abruptly until it reaches about 80% of the total nodes and continues increasing its size –slowly– for $t \gtrsim 50$ (see [73] for another example of this activity on two-dimensional square lattices).

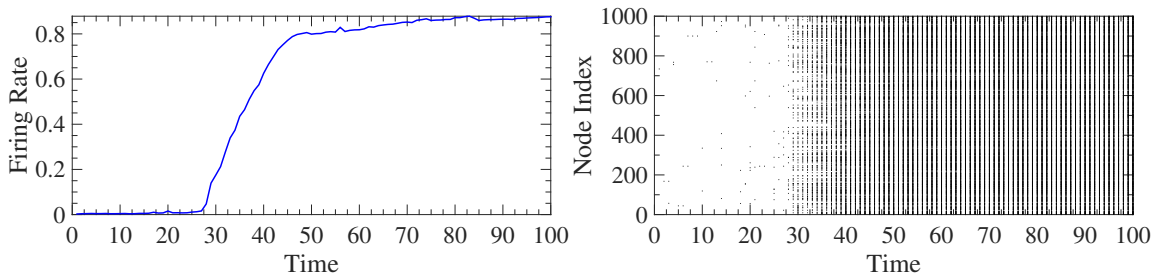

Figure 5.2: Firing rate (left) and raster plot (right) for an Erdős-Rényi network with $N = 10^4$, $\langle k \rangle = 4$, $k_{min} = 2$, $\omega = 10$ and $\varepsilon = 10^{-3}$ (threshold $\theta = 1$, always).

5.2.2 Recurrent activation

Our model relaxes the assumption that agents can only transition from an inactive to an active state. Instead of interpreting that change of state as a one-off decision that

[6]Although the network size is 10^4, the raster plot in this case only displays the activity of 10% of the population.

cannot be reversed (as most prior models do), we allow individuals to activate repeatedly as they build up momentum as they feed on collective participation. We also allow the effects of each activation to vary over time to the extent that they co-evolve with the contagion dynamics taking place in the rest of the network. Incorporating these two elements makes sense if we think about how online social networks facilitate contagion dynamics: users are constantly exposed to signals that might shift their inclination to act – for instance, send signals on their own, like messages directing attention to specific issues (e.g. #occupy); only when a large enough number of users converge in their attention to those issues, their actions become globally visible. This type of synchronization not only affects trending buzz; it actually has the potential to shape the public agenda in the same way than more traditional social movements would [200]. The difference is that synchronization happens spontaneously, from the bottom-up.

To bring these empirical intuitions into a tractable framework, we follow classic models of synchronization developed to explain the behavior of coupled oscillators. Although these models have been used extensively to study synchronization dynamics in biological and physical settings [52], they have never, to the best of our knowledge, been used to illuminate dynamics relevant for the study of social mobilization, or to extend classic threshold models as applied to sociological questions. Like threshold models, our model assumes that the motivational structure of agents can be defined by a limit that, when reached, triggers activation; unlike threshold models, we split the motivation to activate into two components: a social component, which depends on what other agents are doing (spikes); and an individual component, which defines the intrinsic propensity of agents to activate regardless of what others are doing (voltagelike curve, shaped by ω). From this line of thinking, once can observe that the parameter ε captures social influence following a similar intuition to that behind the notion of complex contagion, that is, the idea that adoption is more likely if an agent is exposed to signals sent by multiple sources [175]. Our way of modeling multiple exposure, however, differs in that we make it even more complex by making the timing of the activations be important as well. What we claim is that the activation signals sent by different sources are more consequential if they are concurrent (as shown in Fig. 5.1, see schematic dynamics at $t4$) than if they are not (diagram at $t3$). In other words: our model assumes that exposure to multiple signals matters not just because it reinforces affirmation (a process that we capture with the sudden increases in the progression towards the firing threshold zone); but also, and mostly, because it allows local activity to grow increasingly correlated over time. Introducing

this temporal correlation is a crucial ingredient to build realistic models of large-scale synchronization, especially given the available evidence on the temporal dynamics and bursts of activity characteristic of human communication [180]. Our analytical choice acknowledges the important difference between having multiple user participating in, say, discussions or encouraging actions at different, uncoordinated times than having them all converge to the same timing. Convergence in the timing of activations is more conducive to further activations, which, in turn, reinforces the feedback mechanism that makes an obscured issue suddenly jump to the spotlight of media attention (see [201] for an example of this type of process). Again, large-scale synchronization becomes visible only when the timings of individual activations become highly correlated; and this is an aspect that cannot be captured by models that disregard the effects of time on activation dynamics.

To sum up, the motivational structure of agents (nodes, users, individuals, etc.) in our model is thus determined by the parameter ω, which defines how quickly they reach the activation zone; and by the parameter ε, which determines the strength of social influence. In a system of dynamically isolated agents, ε would be equal to 0; in a system where external influence overrides the rhythms of individual activation, ε would equal to 1. Likewise, in a system of identical agents, ω would be distributed homogeneously; the more heterogeneous the distribution, the more unequal agents are in their propensity to activate. These two parameters, along with the structural properties of the network, open the basic experimental space of our model.

5.3 Numerical results

5.3.1 Regimes of activity

We already showed the activity on an ERN in Fig. 5.2, which was performed for a very small value of ε. At this value of the coupling, attaining full synchronization is still possible because there is a large set of nodes that fire in-phase (for $t \gtrsim 50$) and its size increases over time. However that is not always the case. Given a particular topology and a value of ω, there is a limiting value of $\varepsilon = \varepsilon_c$ (that we call "critical", thus the script) below which full synchronization (or even a cascade of size $\sim N$) does not occur. This is a prominent observation because it contradicts completely what was stated in the original paper by Mirollo and Strogatz [71], where the authors claim: "*We therefore suspect that our system would end up firing in unison for almost all initial conditions, no matter how the oscillators were connected*". Fig. 5.3 provides evidence of the existence of ε_c. It can be seen in the top panels that, for instance,

even for a system of agents with low intrinsic motivation ($\omega = 3$), having a strong coupling (influence) pushes the dynamics to complete synchronization within a small time window. On the other hand, bottom panels suggest that a system where agents are strongly motivated ($\omega = 48$) and favorable –to achieve synchronization– initial conditions are set[7], there are values of the coupling for which the population of oscillators not only does not sustain its cluster of synchronized agents (which can happen for values $\sim \varepsilon_c$) but it tends to desynchronize rapidly the global activity.

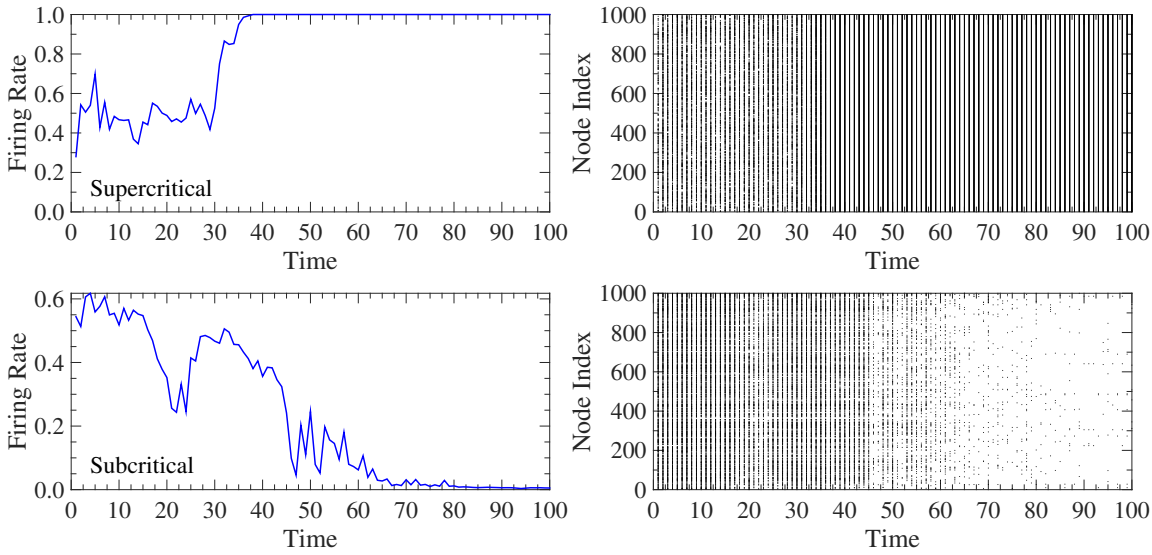

Figure 5.3: Firing rates (left column) and raster plots (right column) for a SFN with $N = 10^4$, $\gamma = 3.0$, $k_{min} = 2$. In the top panels supercritical activity is shown for $\omega = 3$ and $\varepsilon = 0.233$, and bottom panels display subcritical activity for $\omega = 48$ and $\varepsilon = 10^{-3}$.

Another relevant aspect that different regimes of activity produce is the one regarding the time scale to synchronization. Fig. 5.4 shows what happens with the levels of synchronization as the system evolves for a fixed $\varepsilon = 0.01$ on a SWN of size $N = 10^4$ (with edge-adding probability $p = 0.1$ and $\langle k \rangle = 4$). The curves track the fraction of agents that activate simultaneously, represented by peak of the voltagelike x distribution $p(x)$. As expected, high ω values (which, in this example, is the same for all agents) lead to faster large-scale synchronization. As ω decreases, the time to full synchronization increases. At low values (i.e. $\omega = 6$), system-level synchronization is unattainable: this is a condition under which only small clusters of synchronized

[7]Having $\omega = 48$ and $\{x_i\}$ distributed uniformly at random leads to a favorable state to achieve synchronization because of the way $\{x_i\}$ are mapped by f^{-1} onto the phases at $t = 0$. The conjunction of large ω and a uniform initial distribution of $\{x_i\}$ results in a sharp distribution of phases ϕ_i (that explains the large cascades observed in the bottom panels of Fig. 5.3 for $t \lesssim 50$).

nodes emerge. These observations allows us to conclude that for different values of the parameters ω and ε, even when the activity is constrained by the same network, the times to achieve full synchronization can be widespread (which can be a problem when comparing results for different regimes of activity).

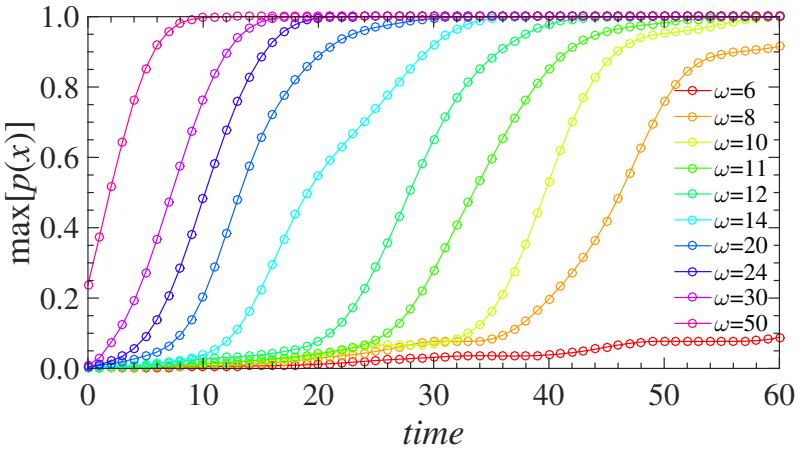

Figure 5.4: Maximum number of synchronized nodes as a function of time across ω values (for fixed $\varepsilon = 0.01$) on a SWN. Note that this value of the coupling corresponds to different regimens of activity depending on the value of the intrinsic propensity of the oscillators. For instance, at $\omega = 6$ it results in subcritical activity, whereas for $\omega \geq 8$ at the same value of the coupling the activity is critical or supercritical.

5.3.2 The concept of cycle

The main motivation guiding our analyses is to determine what conditions need to be in place for large-scale synchronization to emerge. Given that the time to full synchronization depends on the specific combination of ω and ε, and also on the underlying network, we measure time in terms of *cycle*: a cycle is complete when every agent in the network has activated at least once. This coarse-grained definition brings different time scales to a common and allows us to compare the synchronization dynamics that emerge under the different conditions we consider. In Fig. 5.5 three illustrative activation matrices are shown for an undirected ring network of size $N = 10$ and $k = 2$ (regular ring). According to our definition of cycle, all of these diagrams represent one cycle. Note that the larger the number of cycle, the fewer the number of events (or cascades) as a result of the synchronization process. However, in terms of the time scale of the system, the duration of each cycle is independent from the others (i.e. if $\Delta t = t_{10} - t_1$, $\Delta t^* = t^*_6 - t^*_1$, and $\Delta t' = t'_4 - t'_1$ are the widths of cycle 0, 10 and 15 respectively, the relation $\Delta t > \Delta t^* > \Delta t'$ does not necessarily

holds –although it is generally expected to).

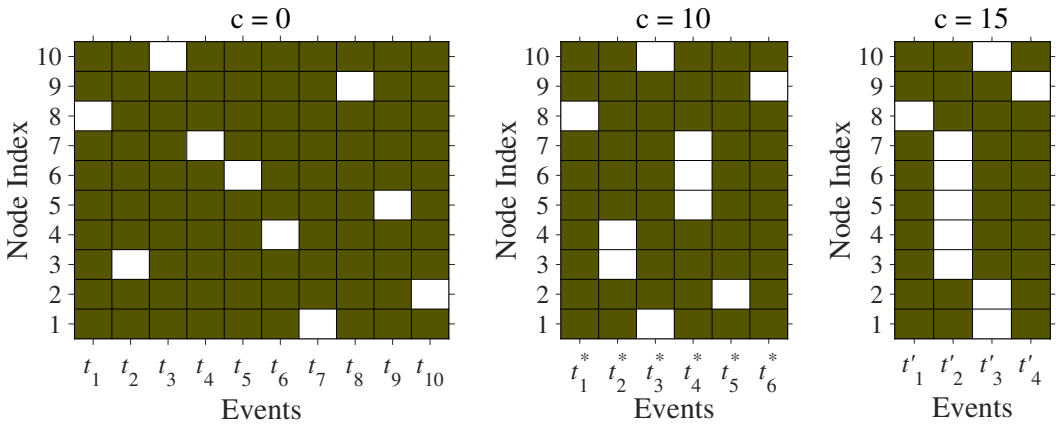

Figure 5.5: The concept of cycle. Activation matrices of a 1D lattice (undirected ring network) with $N = 10$ and $k_i = 2$. In this illustration white squares represent activations (or fires), and inactivation otherwise. Three examples of cycles are shown, $c = 0,\ 10,$ and 15.

Empirically, every time-step in our model (or every cycle) can be interpreted as a different time window, e.g. hourly, daily, weekly, or monthly activity. Finding the appropriate temporal resolution to analyze evolving dynamics in real networks is not a trivial issue [202, 203]. Our model does not make any specific assumptions about the right resolution to aggregate observed activation data; the time it takes for a cycle to complete can correspond to different empirical windows – and, in fact, the appropriate width for that window is likely to change as periods of bursts in activity unfold in chronological time.

Within a cycle, nodes activate in continuous time as they reach their thresholds. When an activation happens, the simulation enters a "frozen time" loop[8] to allow for cascading effects to unfold (a consequence of having infinite pulse speed). Once the chain reaction stops, all node phases are increased $\phi_i \ \rightarrow \ \phi_i + \Delta\phi$ (where $\Delta\phi = \theta - max\,[\phi_i]$) and the node that was closest to the threshold activates and, again, cascades are allowed to spread. At the end of every cycle, i.e. once every node has activated at least once, we count the number of nodes that activated within each cascade. Large-scale synchronization arises when small local islands of nodes firing in-phase start merging together through the cascading effects of influence, as captured by the parameter ε (and as channeled by the network).

[8]In which phases (and x_i states) can only change as a results of pulse interactions and not time-evolution.

5.3.3 Effects of network topology

Agents in our model respond to their neighborhood, which varies locally as determined by a network of interdependence. The topology on which interactions take place is, therefore, a crucial element in the dynamics we want to model. These networks determine how oscillators influence each other via pulse-like couplings of strength ε, and also capture different hypothetical scenarios where interactions might unfold empirically (as reported in next paragraph).

Here, we focus our attention on four distinct network topologies: (i) In Erdős-Rényi network, for instance, edges connecting the agents are formed at random. Although we know that social networks are never formed at random, this topology could account for a scenario where actors are connected through their online search patterns, i.e. by looking at what others are posting on websites or blogs beyond social media platforms. This network also offers a standard benchmark with which to assess the performance of the other three topologies. (ii) The ring network offers a way of mapping interdependence when it is highly structured by logistical or space constraints (e.g. mesh networks created with Bluetooth on cellphones, that require physical proximity, are widely used during protests) [204, 205, 206]. (iii) Small world and (iv) scale free topologies can be used to approximate many networks observed in the real world, particularly in social contexts. There is sufficient evidence that social networks exhibit the small world property [156] and, especially those that emerge online, they also tend to have a very skewed degree distribution [207]. Twitter, for instance, has a long tail in the allocation of connections, with a minority of accounts being disproportionately better connected than the vast majority [208]. Similar properties have been found in other social media platforms like Facebook or the Chinese Sina Weibo [209, 210, 211]. We reproduce these structural features in our simulations because ICT environment have been shown to play an important part in the emergence of large-scale coordination of agents, from agreeing on trivial opinions to organizing massive demonstrations [187, 190, 1, 212, 213].

Fig. 5.6 displays the results of expanding our analysis to a wider range of parametric combinations on four network topologies of size $N = 10^4$: (a) Erdős-Rényi ($\langle k \rangle = 4$ and $k_{min} = 2$), (b) small-world ($p = 0.1$ and $\langle k \rangle = 4$), (c) 1D lattice ($\langle k \rangle = k_i = 4$), and (d) scale-free ($\gamma = 3.0$ and $k_{min} = 2$). In these panels each point is an average computed over 100 realizations of the simulation[9].

[9] Averages over both networks and random initial conditions on x_i.

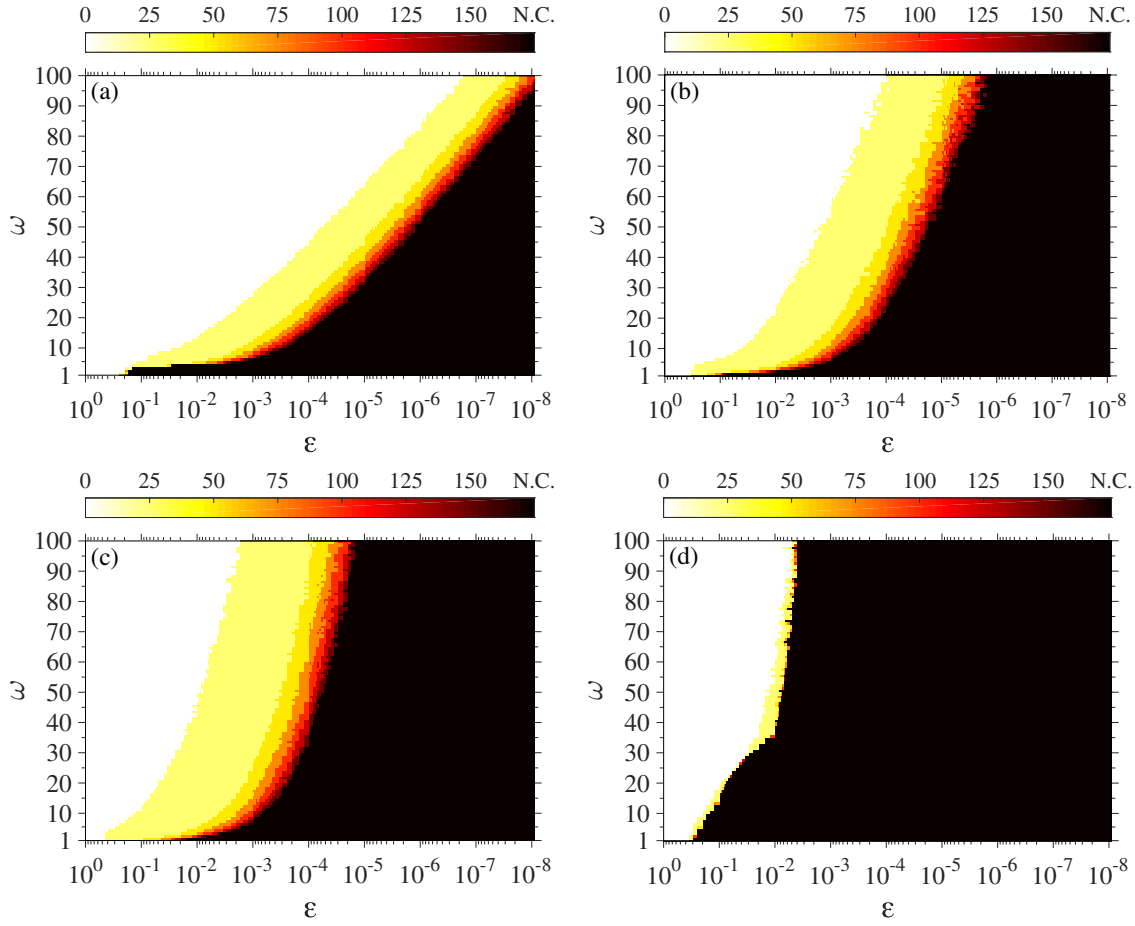

Figure 5.6: The impact of coupling or influence on large-scale synchronization across ω values for different networks of size $N = 10^4$ and $\langle k \rangle = 4$). Panel (a) ERN, panel (b) SWN, panel (c) 1D lattice, and panel (d) SFN. The findings suggest that among these topologies random homogeneous networks are more conducive to large-scale synchronization. Small world networks are also less restrictive in the emergence of synchronization than regular networks, and heterogeneous networks, in the last place, do not allow large-scale synchronization soon after the coupling weakens.

Every dot in the heatmaps corresponds to a combination (ε, ω). On the left of the horizontal axis we have systems where influence or coupling is very strong; as we move to the right, the impact of neighbor activations on agents starts diminishing. At the bottom of the vertical axis, we have agents that progress slowly towards the activation zone; at the top, we have those that get very quickly into a tipping-point state. In this set of simulations, the propensity to activate (the ω value) is distributed homogeneously across all agents in the network. The color scheme indicates the time it takes for each parameter combination to reach large-scale synchronization. Time, as explained above, is measured in cycles; and the color bar at the top of each panel indicates how cycles are coded by color (e.g. white corresponds to cycle=0 and black

to cycle=200). We define large-scale synchronization as having at least $s_c = 0.75N$ (s_c stands for "cascade size threshold") of the nodes activating simultaneously. So in this scheme, lighter colors indicate earlier synchronization; as the colors get darker, synchronization takes longer to emerge. Black signals mean that no synchronization was possible within the limit of 200 cycles (labeled as N.C., "no cascades", in the color bar), when the simulations stopped.

These results suggest that all of the topologies considered here are capable of generating synchronization in scenarios with strong to moderate coupling or influence ($0.5 < \varepsilon < 1.0$), regardless of the propensity to activate of the agents (that is regardless of the ω value). As ε starts getting smaller (i.e. as the strength of the influence diminishes), agents need to have steeper inclinations to reach the tipping point for synchronization to emerge. A network where links channel small pulses takes more time, and requires more motivated agents (larger ω), to generate the same level of synchronization than a network with stronger coupling. After some critical point, no amount of agent predisposition can overcome the lack of substantive interaction, which constitutes an additional confirmation of the existence of ε_c (as the black regions in all of these parameter spaces show). This critical point changes across networks: in the random, Erdős-Rényi network, large-scale synchronization emerges for most coupling values when ω is high, even when the impact of each neighbor activation is really low (where ε_c can be as low as $\sim 10^{-8}$). In the case of the small world networks $\varepsilon_c \sim 10^{-6}$ at $\omega \approx 100$ and, at the same value of ω, for the 1D lattice the critical coupling can get to values near $\varepsilon_c \sim 10^{-5}$. So we can see that a pattern emerges for homogeneous networks: *The more randomness in the network structure the better to attain synchronization*[10].

As for heterogeneous networks, this conclusion is not true. In panel (d) of Fig. 5.6 one can see that $\varepsilon_c \sim 10^{-3}$ for $\omega \approx 100$), so scale free networks are way more restrictive in their support to spontaneous synchronization. The scale-free network is particularly limiting: it either allows synchronization to emerge fast (white region) or, very abruptly, it prevents it (black region). The existence of hubs, so characteristic in the structure of these networks, explains why such an abrupt transition takes place: because hubs are so much better connected than the other nodes, they have a wide impact when they activate; but hubs, which are surrounded by many structural

[10]Recalling the small world model described in Sect. 2.3.3, there is a probability of rewiring p that controls the structure of the resulting network. At $p = 0$ one obtains a 1D lattice, for $0 < p \ll 1$ a small world network and at $p = 1$ nodes are connected independently at random, which is an Erdős-Rényi graph. Thus, under this model, one can observe that given the same value of ω, the higher the value of p the smaller the value of the critical coupling ε_c.

holes [169], also restrict the pathways for contagion, and for the alignment of local dynamics. In any case, we suspect that hubs are not easily synchronizable, as it is claimed by the so-called *paradox of heterogeneity* [20, 214].

Another interesting aspect, related to these parameter spaces, is that some combinations of ε and ω produce the same results in terms of the time it takes to achieve full synchronization. In particular, Fig. 5.7 exhibits the time to synchronization as a function of $\varepsilon \times \omega$ on a SWN of size $N = 10^4$ (with edge-adding probability $p = 0.1$ and $\langle k \rangle = 4$). To obtain each curve, one has to fix one parameter and allow variations on the other. Clearly in this log-log plot all the curves collapse onto a single one, which confirms that some regions of the parameter space can be interpret as equivalent[11], though the process involved to reach the global synchronized state can be very different [215].

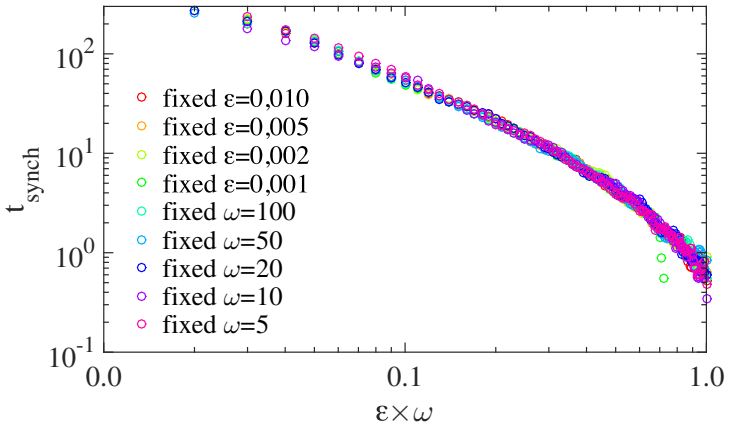

Figure 5.7: Time to achieve full synchronization as a function of $\varepsilon \times \omega$.

Turning to the social sphere, we could think of the ε value as a proxy to the strength of ties [160]. In scenarios where ties are very weak and the impact of the signals they transmit is small, the model needs agents that reach their threshold zone quickly – that is, agents that are ready to act regardless of what others are doing. When social influence is strong, synchronization emerges even when agents are slower in reaching their threshold: they are just forced to respond by their neighbors (this could be a situation where agents operate under strong social pressure). Given that most social media networks are well represented by the scale free structure, our simulations suggest two possibilities: either online ties are stronger than traditionally acknowledged (e.g., see [216]); or users are so ready to activate that synchronization

[11] Constrained by the rule $\varepsilon \times \omega =$ constant and exclusively for the time to achieve full synchronization.

is possible even with weak social influence (but not too weak). This is indeed what seems to happen during the emergence of campaign hashtags. Online users tend to be proactive in their behavior to facilitate synchronization; in fact, the use of hashtags in Twitter emerged itself as a user-driven convention (see [217]). In the context of protest mobilization, the specific signal transmitted through the edges matters greatly to understand its impact on the decision to activate. For instance, when the signal has the form of dramatic images of events happening on the ground, agents might be prompted to react out of solidarity, even if they have a low propensity to participate in a collective effort.

5.3.4 Effects of agent heterogeneity

From the point of view of modeling social systems, it is a big simplification to assume that all agents have the same propensity to reach their activation zone. In a third set of simulations, we introduced diversity in the distribution of the $\omega > 0$ parameter, given by the normal distribution:

$$f_G(\omega; \mu, \sigma) = \frac{1}{\sqrt{2\pi\sigma^2}} e^{-\frac{(\omega-\mu)^2}{2\sigma^2}},$$

where μ is the mean value of the set $\{\omega_i\}$ and σ its standard deviation.

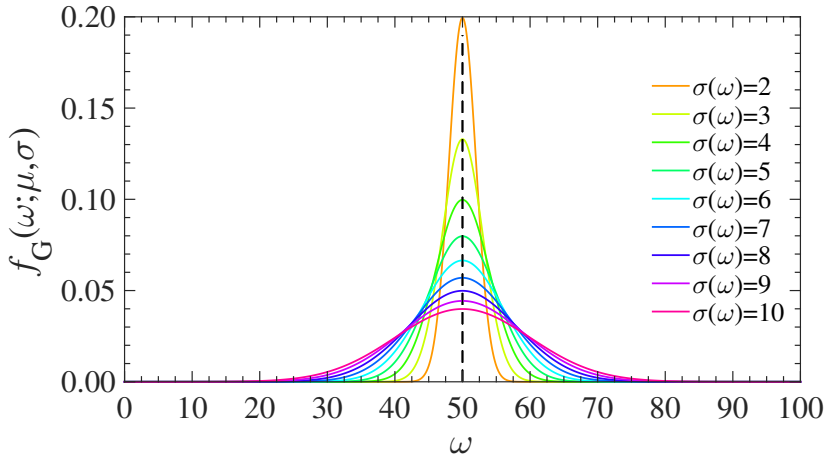

Figure 5.8: Illustrative diagram of the distributions of the speed-to-activation parameter ω. The standard deviation of ω is represented by σ and constrained to the interval $1 \leq \sigma(\omega) \leq 10$ (the curve corresponding to the lower bound is not shown).

As illustrated in Fig. 5.8, we allow different levels of heterogeneity by setting $\mu = 50$ and the interval $1 \leq \sigma(\omega) \leq 10$. The results in Fig. 5.9 show that, as reported in the previous Section, among homogeneous topologies ERNs are the less restrictive,

whereas RNs are the most. So, once again, the more randomness in the network structure the better to achieve synchronization (which do not hold for SFNs).

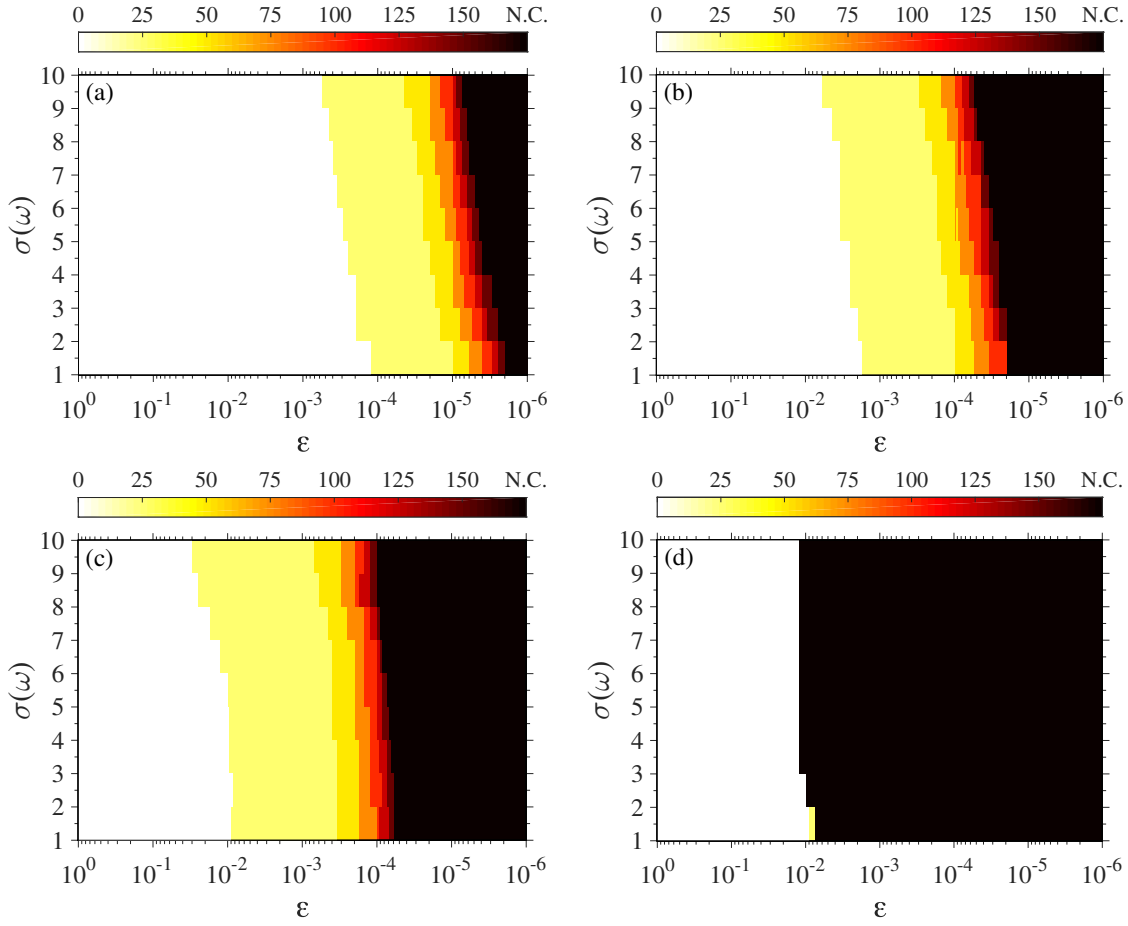

Figure 5.9: The impact of agent heterogeneity on large-scale coordination across ε values. On panel (a) results for ERN, panel (b) SWN, panel (c) 1D lattice, and panel (d) SFN. The panels summarize synchronization dynamics for different distributions of ω and ε values. The distribution of ω depends on the standard deviation (vertical axis); ε is homogeneous across nodes. The color scheme indicates, again, the time it takes to reach large-scale synchronization (i.e. at least $s_c = 0.75N$ of the nodes activating simultaneously); time is averaged over 100 realizations. The results show that, once more, all networks are less efficient in allowing large-scale synchronization than the random benchmark provided by the Erdős-Rényi topology. Overall, low to mild heterogeneity of ω increases the probability of global synchronization, whereas high heterogeneity hinders it.

In general, the simulations also reveal that allowing heterogeneous ω results in a considerable reduction of the region of system-size cascades across all networks. As an instance of this observation, let us analyze the parameter space (ε, $\sigma(\omega)$) for ERNs –displayed in panel (a) of Fig. 5.9– and compare it with (ε, ω) for the same

networks –panel (a) of Fig. 5.6: At $\sigma(\omega) = 1$ (low agent diversity) the critical value of the coupling $\varepsilon_c \sim 10^{-6}$, which completely agrees with the value reported for $\omega = 50$ when agents are identical. In contrast, at $\sigma(\omega) = 10$ (high agent diversity) $\varepsilon_c \sim 10^{-5}$, thus the narrower zone of global events. In the particular case of SFNs under agent heterogeneity, although the effect seems to be more subtle it is also present. Panel (c) of Fig. 5.9 shows that $\varepsilon_c \lesssim 10^{-2}$ regardless of the $\sigma(\omega)$, which is near the value reported in panel (c) of Fig. 5.6 at $\omega = 50$.

On the social side, a condition where agents differ slightly in their predispositions could correspond to scenarios where there is a widely acknowledged window of opportunity. A condition where agents are very heterogeneous, on the other hand, could correspond to situations where the level of commitment to a cause varies in the population (for a real-live example, see the Hong Kong protests [205]). These outcomes support the intuition that, for a cascade to grow large, agents need to share the intrinsic dynamics, that is, they need to be as similar as possible in their willingness to act. The scale-free network is, again, the most restrictive graph – but as long as the structure channel some social influence, synchronization arises fast, which is important for time-sensitive mobilizations (for instance, during the first hours of protests, when mainstream media are not broadcasting news of the events on the ground, see [187]). Given that large-scale synchronization emerges repeatedly (and swiftly) in social media platforms, our results form simulations provide further evidence that online ties weave relevant interdependence, that is, they are a significant source of social influence. This is consistent with experimental evidence on the mobilizing potential of online networks [218], which shows that exposure to information through social media has a positive and significant impact on political behavior. This positive impact is what we capture with the ε parameter; our results show that as long as it is not too low, social influence drives the network towards synchronization even when agent heterogeneity is high.

5.4 Analytical approach

Here we capitalize on the classic integrate-and-fire oscillator (IFO) introduced in Sect. 5.2.1, where system-wide events emerge as microscopical conditions become increasingly correlated. Within this framework, spontaneous propensity –activation regardless exogenous factors– is guaranteed; while contagion is genuinely complex, i.e. the number of necessary external influences (if any) to show activity varies in

time. Remarkably, activity is purely periodical only if the oscillators are either isolated (disconnected), dynamically uncoupled ($\varepsilon = 0$) or once they have reached full (irreversible) synchronization (see Fig.5.2). These three scenarios are irrelevant for our goals. On the other hand, some traces of periodicity in users' activity in socio-technical platforms –like Twitter– have been widely studied at the aggregate level (see for instance [219]), and they exist also at the individual level as will be shown in the next Section (see Fig. 5.12).

As explained above, our model comprises two parameters, ω and ε, which are closely related. Again, ω may be interpreted as the willingness or *intrinsic propensity* of agents to participate in a certain diffusion event: the larger ω, the shorter it takes for a node to enter the tip-over interval $1 - \varepsilon < x < 1$. Conversely, ε quantifies the amount of influence an agent exerts onto its neighbors when it shows some activity. Larger ε's will be more consequential for agents, forcing them more rapidly into the tip-over region. Both quantities affect the voltagelike variable x of a given agent, which can be interpret as its level of *motivation*. ε in the current framework evokes τ in the classical threshold model (see Sect. 5.1.3), in the sense that both determine the width of the tip-over region. Finally, the phase can be translated back into time steps by the prescribed rule $d\phi/dt) = \text{constant}$.

To gain some analytical insight, we use Eq. 5.1 to derive the cascade condition in this new approach. Note that now the distribution of activity is governed by $\rho(t) = 1 - \int_0^{1-\varepsilon} g(x,t)\,dx$ where $g(x,t)$ corresponds to the states' probability distribution at a certain time t. For an initial uniform distribution of the states x and a fixed ε, the condition for the emergence of cascades reads at time $t = 0$

$$\varepsilon \sum_k k(k-1)p(k) = \langle k \rangle \,, \tag{5.4}$$

(see inset (a) in Fig. 5.10). And in general for any time:

$$\rho(t) \sum_k k(k-1)p(k) = \langle k \rangle, \tag{5.5}$$

which implies that the cascade condition depends on time in our proposed framework. Clearly, in this scenario $\rho(t)$ is not a function of the node degree k, as opposed to ρ_k in Watts' proposal (reviewed in Sect. 5.1.3).

As the dynamics evolves in time, the states of the nodes progressively correlate and, consequently, the distribution of states changes dramatically. The evolution of the states distribution is depicted in Fig. 5.10. The initially uniform distribution

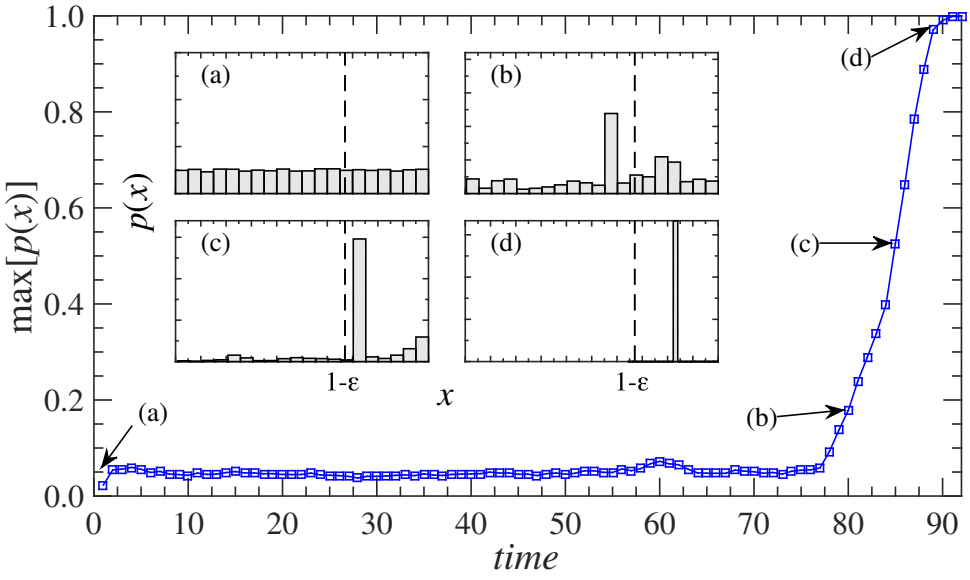

Figure 5.10: Inset (a)-(d): x probability distributions of four different representative times along the synchronization window. Each snapshot depicts the x-state histogram of the N oscillators. The dynamics begins with a random uniform distribution of x-states –inset (a)– and it progressively narrows during the transition to synchrony –inset (d). Main: largest fraction of synchronized nodes across time. The path to synchronization evolves steadily at a low level, and eventually suffers an abrupt transition.

$g(x, 0)$ (inset (a)) evolves towards a Dirac δ function (inset (d)) as the network approaches global synchronization, i.e. global cascade. We have not been able to find a closed analytical expression for the consecutive composition of the function $g(x, t)$ after an arbitrary number of time steps to reveal the evolution of $\rho(t)$, nonetheless it can be solved numerically. Eq. 5.5 reduces to:

$$\rho(t)(\langle k^2 \rangle - \langle k \rangle) = \langle k \rangle. \tag{5.6}$$

The cascade condition is thus,

$$\frac{\rho(t)}{1 + \rho(t)} = \frac{\langle k \rangle}{\langle k^2 \rangle}, \tag{5.7}$$

that exactly corresponds to the percolation critical point on uncorrelated networks (see Sect. 2.5) [220, 221, 222]. For the case of random Poisson networks $\langle k^2 \rangle \sim \langle k \rangle^2$, then

$$\frac{\rho(t)}{1 + \rho(t)} = \frac{1}{\langle k \rangle}. \tag{5.8}$$

It is worth highlighting that Eqs. 5.7 and 5.8 represent an advance in our understanding of non-linear, pulse-coupled dynamics, regardless of our (social) interpretation of

the model.

We can now explore the cascade condition in the $(\varepsilon, \langle k \rangle)$ phase diagram in Fig. 5.11, for the two topologies that exhibited radically different behavior[12] under our model, and compare the analytical predictions with results from extensive numerical simulations. Since the time to full synchronization (global cascade) is different for each $(\varepsilon, \langle k \rangle)$, again, we use cycles to compare results for different time scales. The regions where cascades size s above a prescribed threshold ($s_c = 0.25N$, in Fig. 5.11) are possible are color-coded for each cycle $0, 25, 75, 100, \ldots$, and, once more, black is used in regions where cascades do not reach s_c. Note that if global cascades are possible for a cycle c, they will be possible also for any $c' \geq c$ (provided that the effects of favorable initial condition have dissipated at c). This figure renders an interesting scenario: on the one hand, it confirms once again the existence of critical ε_c values[13] below which the cascade condition is systematically frustrated (black area in the phase diagram). On the other, it establishes how many cycles it takes for a particular $(\varepsilon, \langle k \rangle)$ pair to attain macroscopic cascades (or even full synchronization) –which becomes an attractor thereafter, for undirected connected networks. Given the cumulative dynamics of the current framework, in contrast to Watts' model, the region in which global cascades are possible grows with $\langle k \rangle$.

These results open the door to predicting how long it takes for a given topology, and a certain level of inter-agent influence, to achieve system-wide events. Furthermore, the existence of a limiting ε_c determines whether such events can happen at all.

Additionally, the predictions resulting from Eq. 5.7 are represented as dashed lines in Fig. 5.11. For the sake of clarity, we only include predictions for $c = 0$ (dashed black), $c = 25$ (dashed gray) and $c = 150$ (dashed white). Projections from this equation run close to numerical results in both homogeneous (Fig. 5.11a) and inhomogeneous networks (Fig. 5.11b) with degree distribution $p(k) = k^{-\gamma}$, although some deviations exist. Noteworthy, Eq. 5.7 clearly overestimates the existence of macroscopic cascades in the case of scale-free networks at low cycles (e.g. $c = 0$). Indeed, $\rho(0) = \varepsilon$ does not yet incorporate the inherent dynamical heterogeneity of a scale-free topology, thus Eq. 5.7 is a better predictor as the dynamics loose memory of the hardwired initial conditions. In the general case $c > 0$, deviations are due to the fact that the analytical approach in the current work is not developed beyond first order.

[12] In the sense that ERN exhibit wider cascade zones in (ε, ω) and SFN the most limited cascade zones.

[13] Though now for $\langle k \rangle$ instead of ω.

Second order corrections to this dynamics (including dynamical correlations) should be incorporated to the analysis in a similar way to that in [198], however it is beyond the scope of the current presentation.

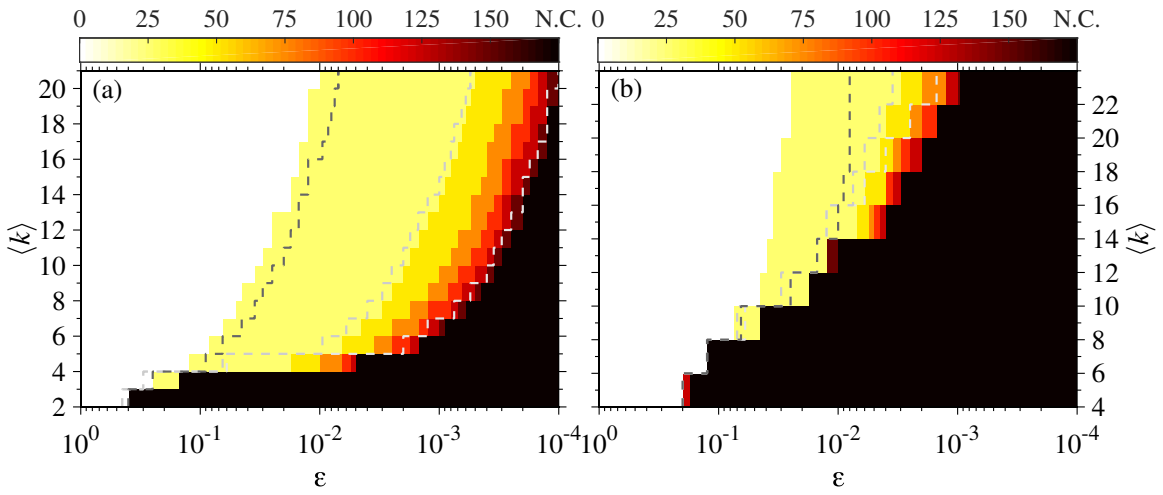

Figure 5.11: $(\varepsilon, \langle k \rangle)$ cascade diagram for different cycles (coded by color), with fixed $\omega = 3$. Vertical axis and each dashed line define a confined region in which global cascades might occur according to Eq. 5.7 and for a specific cycle (here we show only the expected zones for $c = 0$ –dashed white, $c = 25$ –dashed gray– and $c = 150$ –dashed black). Results are obtained for synthetic Erdös-Rényi (a) and scale-free with $\gamma = 3$ (b) uncorrelated networks of size $N = 10^4$. A cascade is considered "macroscopical" if the synchronized cluster $s_c \geq 0.25N$. Color codes indicate the existence of at least one cascade $s > s_c$ in numerical simulations; analytical predictions are averaged over 200 networks with random initial conditions. Note that the cascade condition in (a) often underestimates the actual cascade regions because it does not take into account second order interactions; the same applies in the lower panel (b), except for $c = 0$ where the analytical prediction overestimates the results because the inclusion of a hub into the cascade is improbable starting from a uniform distribution.

According to Mirollo & Strogatz [31], synchronicity emerges more rapidly when ω or ε is large; then the time taken to synchronize, i.e. to observe global cascades, is inversely proportional to the product $\varepsilon \times \omega$ (see Fig. 5.7). In our simulations in the next Section, we use this cooperative effect between coupling and intrinsic propensity to fix ε, which is set to a set of values (slightly above or below) $\varepsilon \simeq \varepsilon_c$, and empirically estimate ω to attain a good matching between observed cascade distributions and our synthetic results.

5.5 Application to real data

To illustrate the explanatory power of this dynamical threshold model, we use data[14] from `http://www.twitter.com`. This dataset comprise ~ 0.5 million Spanish messages publicly exchanged through this platform from the 25th of April to the 25th of May, 2011. In this period a sequence of civil protests and demonstrations took place, including camping events in the main squares of several cities beginning on the 15th of May and growing in the following days. Notably, a pulse-based model suits well with the affordances of this social network, in which any emitted message is instantly broadcasted to the author's immediate neighborhood –its set of *followers*. For the whole sample, we queried for the list of followers for each of the emitting users, discarding those who did not show outgoing activity during the period under consideration. The set of $N = 87569$ users plus their following relations constitute the topological support (directed network) for the dynamical process running on top of it. The average number of followers of this network is $\langle k_{out} \rangle = 69$ and its degree distribution scales like $p(k_{out}) \sim k^{-1.5}$. Note that, unlike other substrates, friendship networks exhibit a high level of reciprocity. In particular, $r = 0.45$ (as defined in [223]) for this network of followers, which implies that many links can effectively be regarded as undirected. This is why the theory –developed for undirected networks– is a reasonable approach for this particular case (for more information on this dataset see [1, 2]).

As a first step to model this activity, we regard this social system as a complex network of IFOs, representing the time evolving activation of users. At first glance this assumption may seem rather strong[15], but in fact traces of periodic activity of individual users can be detected as already mentioned. An example of this is shown in Fig. 5.12, where individual message signals of two users (top panels) and their spectral densities (bottom panels) are displayed. Certainly the presence of predominant frequencies constitutes evidence of the assumed behavior.

On top of the described network, we measure the empirical *time-constrained activity cascade* (or simply "cascade") size distribution for different periods, as explained in Sect. 5.1.2. To test the proposed model, we run the dynamics on the same topology, the network of followers, for some given parameters (ε, ω). To determine which

[14] `http://15m.bifi.es/index_en.php`

[15] We acknowledge that the model is an idealization, an over-simplified approach to these phenomena. For instance, the "oscillator assumption" is taken further as every node obeys the exact same dynamics (same ω); which is admittedly an unrealistic scenario. Studying this dynamics on inhomogeneous agents is part of future work.

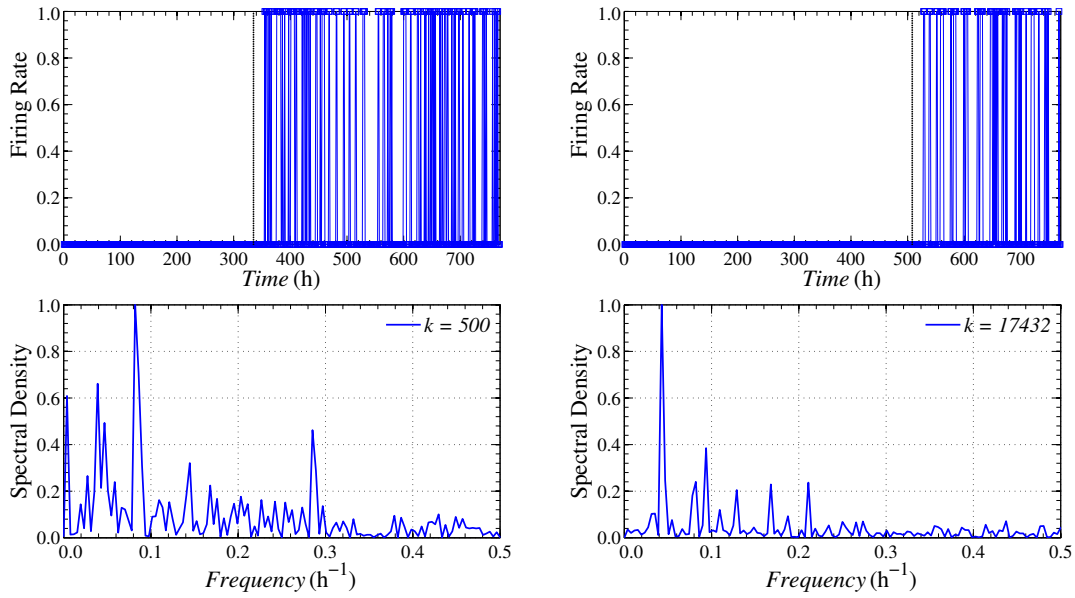

Figure 5.12: Firing rates (top panels) of two twitter users and their corresponding spectral densities (bottom panels). Dotted lines indicate the onsets of activity for these particular users.

values of ω can adequately represent the evolving nature of events, we analyzed the inter-event intervals in the data. In Fig. 5.13, Ψ represents the average inter-event times in the data for each 32 days of activity around the 15M movement. Grand averages $\langle\Psi\rangle$ are computed for 8-day windows, roughly corresponding to the periods for which we offer model fittings (see below). As expected, Ψ drops abruptly in the first days –when the movement is brewing[16]– and smoothly decreases afterwards, until $\Psi \approx 0$. Intuitively, the willingness of an individual to participate in the protest is proportional to real-world excitation level, i.e. it scales like the inverse of Ψ, and thus we envisage that $\omega \sim 1/\Psi$. On the other hand, ε is set by locating the subcritical regime at the estimated $\omega \sim 1/\Psi$ in order to fit the activity during the first time window. Surprisingly, once the coupling was set for the first period of time, it was not necessary to adjust it in order to fit the other periods. The reason for this is simply that the prescribed values of the intrinsic propensity $\omega \sim 1/\Psi$ for the other periods were sufficient to adjust the critical and supercritical behavior of the system. This observation is in agreement with the results depicted in Fig. 5.7, that suggest that under this dynamics only one parameter, $\varepsilon \times \omega$, might be sufficient to obtain a wide range of behaviors.

Putting all these ideas together, in Fig. 5.14 we compare empirical *versus* synthetic

[16]A period during which agents build up momentum.

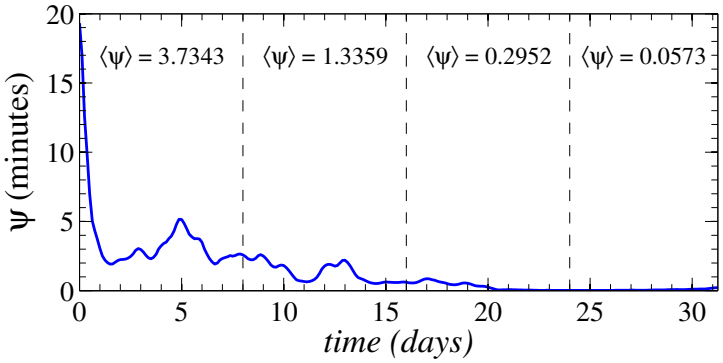

Figure 5.13: Average inter-event times Ψ of the whole collection of data. To measure them, an overlapping sliding window scheme has been used (windows span 1 day, the offset between windows is 12 hours). To estimate ω for 2 different periods of the protests, we take their corresponding time slices and compute inter-event times grand averages $\langle\Psi\rangle$. Thus, in Fig. 5.14 a $\omega \sim 10^{-1}$ will be used for the first period and $\omega \sim 20$ for the last one. The scaling $\omega \sim 1/\Psi$ is merely an heuristic estimation. Some fine-tune is necessary to determine ε and achieve a satisfactory matching.

cascade size distributions for different periods of the protests: the "slow-growth" phase (25th April to 3rd May; blue squares in the upper panel) for the first days, when the protest is limited to some online activists; and the "explosive" phase (19th to 25th May; blue squares in the lower panel), which comprehends the most active interval –the reaction to the Spanish government ban on demonstrations around local elections on the 22nd May. The proposed dynamics is run on the same topology for different ω values, with remarkable success (red circles), though the bottom panel does not show so good of an agreement as the top one. In particular, a small range around $\omega \sim 1/\langle\Psi\rangle$ values was tested in the simulations, seeking a minimization of the relative error of the slope in the linear region of $p(s)$, i.e. the cascade size distribution. Admittedly, the gap observed in the data (Fig. 5.14, right panel) is reminiscent of a super-critical regime (thus the chosen name), in which one either has small-size events or system wide cascades. The change between regimes, namely, from the sub-critical one represented in Fig. 5.14, top panel, and the super-critical phase needs the activity of the system to be long-lived, as this is a transition that takes place at different time windows. Note that this is a quite relevant feature of the model here introduced, since existing threshold models do not allow that individuals engage in more than one cascade (recall that once one individual is active remains so forever) and therefore cannot lead to the same kind of temporal transition observed in the real data.

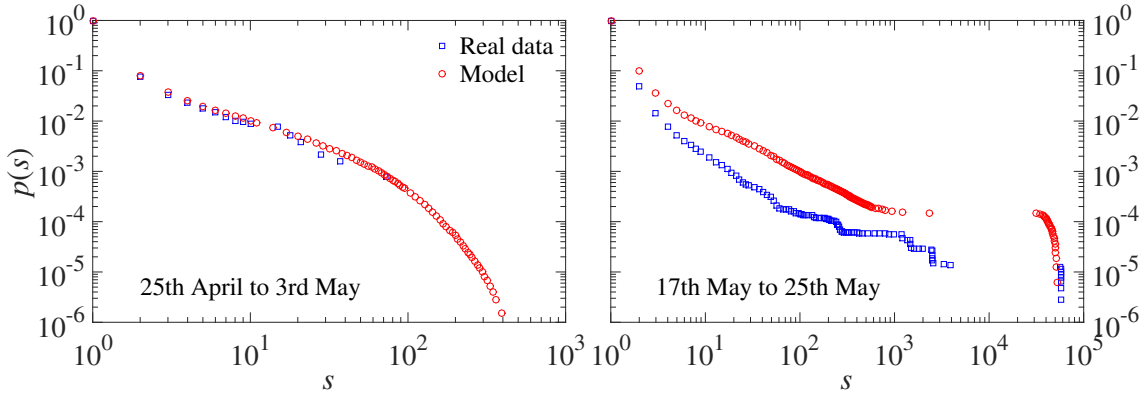

Figure 5.14: Cascade size cumulative distributions $p(s)$ of real data (blue squares) and the model counterpart (red circles). We have considered two time windows which significantly differ: first eight days (left) for which we have set $\omega = 0.1$; last eight days (right) for which we have $\omega = 30.0$. Note that $\varepsilon_c \approx 10^{-3}$. The model performs well in both periods, the relative error of the slope in the linear region is $< 1\%$ (not shown). Real data distributions are measured as described in the main text, see also [1, 2].

5.6 Discussion

The question behind many analytical models of collective action is: What makes collective efforts become self-sustained in the absence of central organizations? Interdependence, or the acknowledgment that agents do not decide in isolation but react, instead, to what other agents are doing was central to the first approaches to that question [102, 224]. Since then, researchers have treated with increasingly sophisticated tools the nature of that interdependence. In the last few decades, network science has produced numerous theoretical and empirical insights into why interdependence matters to understand collective dynamics, including contagion effects and the diffusion of information [159, 225, 226, 18, 156]. An increasing body of observational evidence is also shedding light on how decentralized networks help coordinate the actions of many [187, 190, 1, 212], often generating spillover effects [218, 213]. This evidence suggests that prior to large-scale synchronization, there is always a brewing period during which agents build up momentum and reinforce their opinions. Time-varying dynamics in networks, however, have so far been largely disregarded by analytical approaches to collective action – and yet those dynamics are crucial, we argue, to understand the feedback mechanisms that activate a critical mass, that is, a number of activated agents large enough to trigger a self-sustaining chain reaction or cascade. Prior research has shown that attaining this critical mass depends on the

network topology, in particular the density and the centralization of ties [227]. That work suggested that centralization always has a positive effect on collective action because it increases the probability that involved agents will be tied to a large number of contributors, allowing for more efficient synchronization. Our model suggests that highly centralized networks (in the form of scale-free structures) can indeed be very efficient in coordinating efforts (and thus, achieving synchronization) but only when certain conditions are met. The strength of social influence, and the distribution of propensities to activate need to be conducive to the critical mass. Compared to other network topologies, however, centralized structures perform significantly worse. Our findings also qualify the theory of complex contagion [175]. According to this theory, the activation of thresholds (which are modeled as a stepwise change of state) responds not only to the fraction of neighbors that are active but to their actual number. The assumption is that reinforcement from multiple sources is necessary when activation involves some risk, for instance, taking part in a protest against an authoritarian state. Our model also acknowledges the importance of multiple exposures from multiple sources, but it adds an additional element to the equation: the timing of activations. Large-scale synchronization depends on these timings aligning over time, which in turn depends on the ability of the underlying network to spread the chain reaction. These dynamics are disregarded by the complex contagion model which, following previous approaches, assumes that activation is a one-off event. By allowing activation to re-occur, we shift attention from the diffusion of activations to their synchronization. What we find is that for a range of parametric combinations (ω, ε), the four network topologies we analyze are equally successful at generating synchronization. What makes them differ is the impact that social influence has on collective dynamics. As networks grow more heterogeneous in their connectivity, and as they open more structural holes, the space for large-scale synchronization to emerge diminishes. This is consistent with some of the findings drawn from the complex contagion model, but it responds to the operation of a completely different feedback mechanism. Regarding our analytics to predict the emergence of global cascades, given a previous knowledge of x states distribution, we conclude that it works reasonably well on homogeneous topologies for any cycle. As for heterogeneous networks we note that predictions can be less accurate for initial cycles, though precise when far from the effects of initial conditions.

There are three aspects of our model that deserve future consideration: the distribution of ε (which we keep constant across nodes) and the way in which ω values

are distributed (randomly, when inhomogeneous).There are a number of reasons why these two choices could be modified. We know that in social networks not all couplings are worth the same: the actions of relatives, friends and acquaintances, for instance, do not have the same effect on an agent's behavior. Our model assumes that all ties channel the same amount of influence; although some ties activate more often than others (and are de facto more influential), that responds to changing local events in the network, not to an attribute of the tie. Future work should consider synchronization dynamics under different distributional assumptions of ε. Likewise, future research should analyze scenarios where the propensity to activate (ω) or the coupling are not distributed randomly but as a function of the network topology itself (say, linking them to the degree). For instance, there is wide empirical evidence to suggest that the values of ω might be more similar within clusters in a network – if we assume that this is another dimension on which homophily operates [228]. Students, for example, are more likely to share the same predispositions and be better connected to each other compared to other demographic groups. Critical mass dynamics and the timing of synchronization are likely to differ if we constrain the distribution of ω to the position of nodes in the network.

Another important topic for future research is finding a temporal scale that is the most appropriate to empirically analyze synchronization dynamics. As with all analytical models, ours is developed on a level of abstraction that allows generalizing across possible scenarios but does not give precise guidelines as to how to aggregate empirical data. Digital technologies are providing richer sources of data that could help test these models empirically [157, 95, 158] but this requires a systematic approach to the analysis of time-evolving networks and time-dependent activations [202, 203]. In many demonstrations, weeks offer the natural unit of analysis; in social media activity, on the other hand, this could be days, hours, or minutes – and the characteristic temporal scale might not even remain constant during the observation window [229]. Bringing closer the results of simulation models with the patterns observed in empirical data will first require solving the temporal resolution problem. The third aspect we suspect it is possible to develop further is a recursive composition of the x-states probability distribution to capture the time-evolution of the system. Of course, such an ambitious task can be quite difficult to achieve because many ingredients, like the dependence with the underlying structure, must be included.

Summarizing, this model of pulse-coupled oscillators and the results we presented

here aimed to illuminate what happens when agents are allowed to activate repeatedly and contribute intermittently to the buzz around a collective cause. The theory of a critical mass emphasizes the importance of interdependence, and highlights that collective action is not about obtaining unanimous participation but about mobilizing enough people to make the effort self-sustaining. Our model contributes to that line of research by emphasizing the importance of temporal correlations in network activity, so far largely disregarded – but apparent in recent examples of large-scale synchronization. What our model shows is that in many contagion conditions, synchronization does not emerge; in others, it takes some time – which, from an empirical point of view, might not always be available. But when social influence has a moderate to strong force, large-scale synchronization emerges regardless of the underlying network. To the extent that digital technologies are inserting communication networks in every aspect of social life, our results suggest that we should expect to see more instances of large-scale synchronization cascading from the bottom-up.

Chapter 6

Conclusions

This last Chapter is devoted to summarizing the chief findings that the present research work comprises, including a discussion on their expected impact and forthcoming scientific endeavors.

In the Chapter named *Complex Networks* we reviewed several topics of the standard *Graph Theory*. Particularly, the introduction of basic concepts, definitions, descriptors and topologies was essential con build the foundation and further developments of this investigation. Most of these formal contributions, that have been used repeatedly throughout this Dissertation, were formulated over the past few decades by numerous researchers and constitute key parts of the standard framework of Network Science. Although, we must remark that in spite of adopting such an approach, we did not attempt to develop any new insight or knowledge into structural properties of the network models related to this work, as our interest lies exclusively on the dynamical aspects and some of their applications to real-world systems.
Needless to say, network-like systems emerge naturally when considering populations of discrete units that interact according to a well-defined set of rules. The studies presented here are no exception, once more, networks fit exceptionally well the need for a structure of interactions. Interesting enough, random networks with an arbitrary degree sequence can be treated analytically to derive many prominent structural-related aspects (in a relatively simple manner). Of course, we refer to the *generating function formalism*, and more concretely to its algorithmic implementation as the configuration model. With two exceptions, that is the ring network and the small world graph, all of the synthetic topologies on which we studied our dynamics were generated using this versatile method. The last topic reviewed in this Chapter was a combinatorial process related to the structure of graphs, called *percolation*, and its significant consequences when it comes to damaging real networks.

At the end of this –first– journey through the network science literature, we can say with no hesitation that graphs have proven to be, over again, a useful yet simple framework to study not only the dynamics and the topology of complex systems, but also their close relationship (key to understanding them).

The third Chapter of this Dissertation addresses the problem of generalized synchronization in relay systems of chaotic oscillators. In order to study this salient and ubiquitous phenomenon, we discussed the notion of synchronization and several different types of synchrony observed in dynamical systems. The first aspect to point out, is that such behaviors can be quite difficult to capture in one simple definition. After reviewing many references on the subject we believe that, rather than a formal and restrictive definition, one should simply follow a general notion that enables us to account for all types of synchrony (which, as discussed, always involves three attributes; a form of oscillation or periodicity, coupling and rhythms). In the particular case of the generalize synchronization (GS), as the name indicates, it is a type of synchrony for which there is no specific or explicit form of the relation between the global states of two (sub)systems. By definition, we can say that as long as a global one-to-one state-mapping exists this behavior takes place. From these ideas one can see why GS is so elusive. Most measures of synchrony are designed to detect concrete traits (e.g. coordination of amplitude, phase, etc.), and thus most of them are just worthless when it comes to detecting GS. We, on the other hand, considered two indicators: the synchronization points percentage (SPP) and the non-linear interdependence (N-index). The former measures the number of local functional dependencies between two subsystems, and the latter compares the average size of the neighborhoods in one of the subsystems with the average size of its mapping in the other subsystem.

Concerning the relay configuration, here it is regarded as a network motif whose purpose is to provide a bridge of communication between two units, that are not connected directly. This structural setting can either amplify or interfere with synchronization, depending on the nature of the systems and the type of couplings. In our case, for undirected, continuous and instantaneous couplings between chaotic oscillators, we showed that the two identical unconnected units achieve complete synchronization at a critical coupling strength and remain fully synchronized for larger values of it. Using the Lyapunov spectrum, the SPP and the N-index we were able to prove that: (i) the 9D Rössler system exhibits two regimes of activity, switching between chaotic and periodic behavior, and, more importantly, (ii) the onset of relay

synchronization (between the two outer oscillators) indicates the regime where GS actually occurs. However, not all of these tools displayed the same features. Clearly the Lyapunov spectrum showed that the appearance of relay synchronization (and GS) is characterized by one single positive exponent (the rest are either zero or negative), but no further insight could be extracted from it. As for the N-index, it experiences a smooth transition across coupling values that starts at a value much lower than the critical one. In contrast, SPP reveals the right critical value of the coupling as its steeper transition to synchrony takes place right where the second largest Lyapunov exponent vanishes. From all of these observations, we conclude that between the two indicators of synchrony, SPP is undoubtedly a better choice to study generalized synchronization.

Considering now the experimental setting, that is three coupled Rössler circuits operating in chaotic regime, the exact same observations stated in the previous paragraph hold. The idea behind this approach was to demonstrate our results beyond plain numerical models and, thus, the robustness of our findings in an experimental implementation, which was achieved indeed.

We hope these results on relay systems and generalized synchronization help in the understanding of the intrinsic mechanisms underlying such phenomena (also present in diverse real-world systems), and in this manner encourage other researchers to develop better techniques on synchrony detection and promote incipient technologies (e.g. optical cryptography and acoustic communications).

Chapter number 4 deals with concepts traditionally associated to Neuroscience. In its first part, the notion of mathematical neuron is introduced, as well as several emblematic models of neurons (proposed over the last century). After learning there are too many different representations of the same biological units, the main aspects we want to highlight on this regard are: (i) All of these models have, obviously, similar fundamental traits, for instance most of them include spikes (pulse-couplings), voltagelike curves (to capture the membrane potential), ion currents and firing thresholds. Therefore they can be easily categorized into distinct families. (ii) The most relevant differences between these families of models are essentially focused on the level of detail to account either for the behavior or the structure of neurons. As an illustration, among these families, there can be found many models that do no include spatial structure (e.g. point neurons), though they typically provide detailed description of the dynamics of the membrane potential (e.g. Hodgkin-Huxley model for a realistic model). Whereas on the other hand one can find multi-compartment

models that add an extra ingredient regarding the spatial distribution of real neurons and how these parts behave individually, which means that a single neuron can be described as an elaborate assembly of inter-dependent compartments. In any case, as stated in the Introduction, our view of neural dynamics, or models of neurons, is simply as a set of units whose internal behavior follows a voltagelike curve (shaped according to some generic parameters) and whose interactions are characterized by pulse-couplings (defined by a given shape, amplitude, duration, delay, etc.). Such scenario renders a great possibility to introduce these mathematical representations to diverse systems where the interactions among their elements occur sporadically, without having to assume the constraints that the activity of live neurons impose to the features of the model.

Concerning the specific approach to study population of neurons studied in the fourth Chapter, it incorporates a set of leaky I&F elements on a scale-free structure of interactions (with pulse-delays). From the numerous computer simulations performed we noted there are two regimes of self-sustain activity (for homogeneous coupling): First, when the pulse-strength is greater than the voltage-gap between the firing threshold and the resting potential, one obtains what may be called *standard* or *normal* activity. In this state, all neurons in the system are able to fire whenever they receive one single input (regardless of the degree). The behavior of the global firing signal ranges from irregular patterns at relatively low values of the coupling to periodic ones at larger values (including the eventual full saturation of fires). Second, when the pulse amplitude is smaller than the voltage-gap between the firing threshold and the resting potential, then we have an *abnormal* or *pathological* activity where most neurons in the smallest degree-class can only fire occasionally, when they receive inputs from all of their neighbors at once. In this regime, the initial mechanism required to triggering the dynamics has, necessarily, to be extreme (i.e. involving multiple sources, or even all nodes, to fire at the same time) and there is a value of the coupling, that we call *critical*, defined as the smallest pulse-strength for which the set of excitable elements exhibits activity (lasting longer than a certain time-window). This critical value is bound below by the voltage-gap mentioned above divided by the minimum degree of the network. The extreme firing initial conditions described previously enables the system, at the critical coupling, to reach a global state of irregular spikes where the mean firing rate is very small (which hints the possibility that the activity only involves certain parts of the network, those that are better connected).

Under this model, two distinct strategies to perturb the system were performed:

(i) Dynamical perturbation: An *ad hoc* mechanism that involves applying a large/global stimulus to the ongoing dynamics and observe its response. Particularly, we detected three scenarios; inhibitory stimulus to cease all activity, no signal response to stimuli in the irregular-pattern regime, and the enhancement (hindrance) of oscillations' amplitude for excitatory (inhibitory) stimuli in the regular-patterns regime (associated to strong couplings). Thus, we observed that there exist some external firing perturbations that may help to control the global activity by means of trivial mechanisms. **(ii) Structural perturbation:** After performing a random removal of nodes (site percolation) the dynamics was executed in order to measure both the probability of activity failure and the average population firing rate. From this strategy one can confirm, once again, that scale-free networks are quite resilient. The threshold to activity failure depends on the size of the system as: *the larger the network, the greater the fraction of removed nodes needed to achieve full activity failure*. Furthermore, we demonstrated that the average firing rate remained positive almost until the complete structural disintegration is achieved, hard evidence of its tolerance to random failures.

From some basic assumptions and with an elementary mathematical approach we managed to derive several analytical expressions that allow us to predict diverse aspects of the dynamics. First of all, the time-average of the inter-spike-interval for the k-class proved to be an accurate method to decompose the dynamics and to shed some light on the roles the different connectivity groups play. The activity ranges from saturation to critical behavior, and with this method we provided formal equations to compute the precise boundaries of the coupling strength and their corresponding average firing rates. A striking result of this formulation was the fact that at the critical value of the couping there is always a minimum saturated degree that can be calculated analytically and it only depends on the single neuron parameters and the smallest degree of the network. Finally, we also derived an expression that links the mean firing rate with the time-average of the inter-spike-interval (as a function of the connectivity), which lead us to an implicit equation that can be solved without the recourse to simulations. This rigorous finding is accurate for standard activity on scale-free networks having high heterogeneity (i.e. lower values of the exponent of the degree distribution). The failure of the approximations on low heterogeneous graphs is an statistical issue, whereas for abnormal activity one obtains unprecise estimations as a results of not having enough activity in the smallest-connectivity groups.

At the end of Chapter 4, we analyzed the activity under inhomogeneous couplings.

As predicted by our analytics, correlating the pulse-strength of the inputs that a neuron receives with its degree is a way to homogenize the activity of a network of excitable elements with heterogeneous topology: The activity becomes well-organized and periodic, that is all neurons exhibit similar inter-spike-interval. However, under this assumption, the system becomes quite sensitive to initial firing conditions. In other words, different mechanisms to trigger the dynamics lead to distinct activity patterns. As an extreme instance of this behavior, one can obtain a salient outcome: a type of synchronization, named coherent oscillations, by carefully selecting initial firing conditions (though further research is needed on this phenomenon).
As for future work, diverse aspects remain to be explored; being the most relevant the oscillatory regime on complex –sparse– topologies and the applications of time-delayed interactions to cascading processes.

In Chapter 5 we studied a second model of neurons in the context of socio-technical interactions. The essential difference compared to the previous dynamics is that instead of having excitable elements we incorporated phase oscillators with instantaneous pulse-couplings (a simpler model whose dynamics comprises only two parameters). The first part of the Chapter was devoted to reviewing essential concepts like information spreading, complex contagion and cascades, as well a short report on prior work on social modeling (namely the threshold model). In order to introduce our proposal, which may be called the dynamical threshold model, we described in great detail the Peskin's model, and the further developments by Mirollo and Strogatz. As mentioned above, the dynamics only includes two parameters, which, in the context of social interactions, can be interpreted as follows: the homogeneous pulse-strength represents social influence and the shape of the voltagelike curves typifies the *intrinsic propensity* of each individual to join collective events (or *willingness*). It has been proved, for an all-to-all graph, that this model leads to full synchronization when interactions take place and under certain conditions on the voltage curve. Provided that, at the individual level, such voltage-curve conditions are satisfied, the numerous interactions needed for these oscillators to achieve synchrony mimic the mechanism of complex contagion.

The first significant finding we presented on this dynamics is the one regarding the regimes of activity. In contradiction with the original statements by Mirollo and Strogatz, we found there is indeed a critical value of the coupling below which complete synchronization can never occur (not even system-wide events). This conclusion is based on the observation that for certain complex graphs the system evolves towards

a desynchronized global state, even when favorable conditions to attain synchronization are set (i.e. large intrinsic propensity and an initial large group of in-phase oscillators).

The exploration of two kinds of parameter spaces (corresponding to uniform and distributed intrinsic propensity) on four network topologies revealed that among them Erdős-Rényi networks are the most tolerant to attain synchronization under adverse conditions, whereas scale-free graphs are the most restrictive (which can be explained as a result of the *paradox of heterogeneity*). In fact, for the latter, we showed that synchronization is either achieved fast or not achieve at all (perhaps a consequence of being ultra small), while homogeneous topologies demonstrated that synchrony can be the result of a slow process. Another related outcome is a pattern detected in homogeneous networks: *The more randomness in the network structure the better to attain synchronization.* In other words, given a specific value of the intrinsic propensity of the oscillators, the critical coupling in Erdős-Rényi networks is smaller than the one obtained in small-world networks, which in turn is smaller than the one found in 1D lattices (similar results hold for distributed intrinsic propensity).

Again, in this case we managed to derive analytically a cascade condition that connects a structural-related feature of the network (the threshold for the existence of the giant component) with a dynamical measure that quantifies the fraction of oscillators that need to receive only one single input to fire. Although such measure cannot be computed as a function of time (up to this point), it can be estimated at least one step ahead of the occurrence of a global cascade, which provides useful predictions (even for practical purposes). As an illustration of this approach we performed extensive computer simulation on both types of graphs that displayed opposite –extreme– behaviors in terms of the time to synchronization: Erdős-Rényi networks (most tolerant) and scale-free networks (most restrictive). We showed that the proposed method renders accurate predictions on both of them across a wide range of average degree values. Once more, trough this exploration we confirmed that, given an intrinsic propensity, there is a critical value of the coupling that decreases with the average connectivity.

The last part of the Chapter is the application of our model to reproduce the traits of real activity in a socio-technical phenomenon: The spanish 15M movement on Twitter. We analyzed the time-constrained activity of users and extracted three main results: (i) Most active individuals exhibit activity patterns that have periodicities, in agreement with our assumption regarding the oscillatory nature of our elements. (ii)

The intrinsic propensity of the model can be estimated from the inter-event-interval, as these quantities are –approximately– inversely proportional. (iii) The dynamical threshold model enabled us to perform simulations on the network of followers and we obtained subcritical and supercritical cascade-size distributions that closely resemble those extracted from the dataset. Consequently, our proposal extends considerably prior works as it incorporates ingredients like recurrent activation and parametric variety, which may be used to fit a broad range of behaviors observed in diverse real-world phenomena.

Finally, there are unexplored aspects of the model that deserve further research. Firstly, from the empirical point of view, coupling heterogeneity (or, equivalently, weighted edges) could provide a more realistic scenario to model social influence (e.g. the information received from a known person should have greater impact than the one from a stranger). Secondly, another aspect to examine in the future is finding a temporal scale that is the most appropriate to empirically analyze synchronization dynamics, which means a strategy to extract from real activity a proper characterization of cycles. Thirdly, additional rigorous developments are needed to derive a recursive composition of the state probability distribution that allows to follow the evolution of the system without inputs from numerics.

– –

A final personal note: After some years devoted to this research project, I came to understand one or two things about our line of work. Perhaps one of the most significant and apparently trivial observations is that sacrifices are always required (yet not everyone in *Academia* agrees). Most of the effort that one invests to obtain relevant results vanishes during those long hours when numerous attempts are made with little or no success at all. I am convinced this is the hidden story behind every honest scientific endeavor, and it is mine as well. Fortunately, every now and then, the relentless struggle pays off and one gets to discover/develop something –hopefully– novel. Rest assured it never matters whether our findings may seem as a little progress or as a monumental breakthrough, any advancement is always fulfilling. I am thankful for this.

"*Physics is like sex: sure, it may give some practical results, but that's not why we do it.*" –Richard Feynman.

Appendix A

Approximations involved in the estimation of $\langle \mathrm{ISI}(k) \rangle_t$

Let us assume that the system is in a stationary regime of global self-sustained activity. For a long time window, $1 \leq t \leq t_{max}$, let $N_t(i)$ be the number of ISIs of neuron i, and T_{ih} be the duration (number of time steps –given by $\Delta t = \tau_D$–) of the hth ISI ($1 \leq h \leq N_t(i)$). The firing condition at the end of the hth ISI is expressed as,

$$\sum_{n=0}^{T_{ih}-1} \left[\left(1 - e^{-\frac{\Delta t}{\tau_m}} \right) I_{ext} + g\, b_{(T_{ih}-n)} \right] e^{-\frac{n\Delta t}{\tau_m}} \gtrsim \theta \,, \tag{A.1}$$

where $b_{(T_{ih}-n)}$ is the number of pulse-inputs received at the corresponding time step by neuron i. We will consider the set of ISIs of all the neurons of degree $k_i = k$, whose cardinal is $M_k \equiv \sum_{j \in in(k)} N_t(j)$, where $in(k)$ denotes the set containing indexes of all neurons in the k-class.

We will call $T(k)$ the average of T_{ih} over this set, i.e.

$$T(k) = \frac{1}{M_k} \sum_{j \in in(k)} \sum_{h=1}^{N_t(j)} T_{jh} \,. \tag{A.2}$$

By averaging the inequality (A.1), one obtains

$$\frac{1}{M_k} \sum_{i \in in(k)} \sum_{h=1}^{N_t(i)} \sum_{n=0}^{T_{ih}-1} \left[\left(1 - e^{-\frac{\Delta t}{\tau_m}} \right) I_{ext} + g\, b_{(T_{ih}-n)} \right] e^{-\frac{n\Delta t}{\tau_m}} \gtrsim \theta \,. \tag{A.3}$$

Except for neurons at saturation, i.e. $T_{ih} = 1$ for all h, or very close to it, one expects that both sides of this inequality should be approximately equal in most instances. Therefore, for values of k below the degree of saturation, we will assume an approximate equality for equation (A.3), i.e.

$$\frac{1}{M_k} \sum_{i \in in(k)} \sum_{h=1}^{N_t(i)} \sum_{n=0}^{T_{ih}-1} \left[\left(1 - e^{-\frac{\Delta t}{\tau_m}} \right) I_{ext} + g\, b_{(T_{ih}-n)} \right] e^{-\frac{n\Delta t}{\tau_m}} \approx \theta \quad \text{for } k < k^s \,. \tag{A.4}$$

The number of pulse-inputs a neuron receives at a given instant of time is obviously bounded by its degree. Besides, as our networks do not possess degree correlations, the numbers $b_{(T_{ih}-n)}$ inside the sums in equation (A.3) above are expected to be evenly distributed with an average αk, where α is the average firing rate, which suggests the following (mean-field-like) approximation:

$$\alpha k \approx \frac{\sum_i \sum_h \sum_n b_{(T_{ih}-n)} e^{-\frac{n\Delta t}{\tau_m}}}{\sum_i \sum_h \sum_n e^{-\frac{n\Delta t}{\tau_m}}} \,. \tag{A.5}$$

Inserting this into equation (A.4) one obtains

$$\left[\left(1-e^{-\frac{\Delta t}{\tau_m}}\right) I_{ext} + g\alpha k\right] \left[\frac{1}{M_k} \sum_{i\in in(k)} \sum_{h=1}^{N_t(i)} \sum_{n=0}^{T_{ih}-1} e^{-\frac{n\Delta t}{\tau_m}}\right] \approx \theta \quad \text{for } k < k^s, \tag{A.6}$$

where the quantity in the last brackets can be rewritten (after summation of the truncated geometric series) as follows:

$$\frac{1}{M_k} \sum_{i\in in(k)} \sum_{h=1}^{N_t(i)} \sum_{n=0}^{T_{ih}-1} e^{-\frac{n\Delta t}{\tau_m}} = \frac{1}{1-e^{-\frac{\Delta t}{\tau_m}}} \left[1 - \left(\frac{1}{M_k} \sum_{i\in in(k)} \sum_{h=1}^{N_t(i)} e^{-\frac{T_{ih}\Delta t}{\tau_m}}\right)\right] \,. \tag{A.7}$$

Now, using the Taylor expansion of the exponential function, we can write the average inside the parenthesis of RHS in this equation as

$$\frac{1}{M_k} \sum_{i\in in(k)} \sum_{h=1}^{N_t(i)} e^{-\frac{T_{ih}\Delta t}{\tau_m}} = e^{-\frac{T(k)\Delta t}{\tau_m}} \left(1 + \frac{1}{2}\sigma^2_{T,k} + \cdots\right) \,, \tag{A.8}$$

where $\sigma^2_{T,k}$ denotes the variance of the distribution of ISI duration on the set of neurons of degree k, and $T(k)$ is the ISI average defined in equation (A.2). From equations (A.6), (A.7) and (A.8) we can solve for $T(k)$:

$$T(k) \approx \frac{\tau_m}{\Delta t} \ln\left[\frac{\left(1-e^{-\frac{\Delta t}{\tau_m}}\right) I_{ext} + g\alpha k}{\left(1-e^{-\frac{\Delta t}{\tau_m}}\right)(I_{ext}-\theta) + g\alpha k}\right] + \frac{\tau_m}{\Delta t} \ln\left(1 + \frac{1}{2}\sigma^2_{T,k} + \cdots\right) \,. \tag{A.9}$$

Provided the ISI' duration variability on the k-class is small enough, one can neglect the second term on the RHS of equation (A.9):

$$T(k) \approx \frac{\tau_m}{\Delta t} \ln\left[\frac{\left(1-e^{-\frac{\Delta t}{\tau_m}}\right) I_{ext} + g\alpha k}{\left(1-e^{-\frac{\Delta t}{\tau_m}}\right)(I_{ext}-\theta) + g\alpha k}\right] \,, \tag{A.10}$$

which is Eq. 4.12 of the Chapter 4.

Appendix B

Approximate relation between α and $\langle \mathrm{ISI}(k) \rangle_t$

Let us first rewrite (and rearrange a bit) equation (A.2) in time units:

$$M_k \langle \mathrm{ISI}(k) \rangle_t = \sum_{j \in in(k)} \sum_{h=1}^{N_t(j)} T_{jh} \, \Delta t \; . \tag{B.1}$$

The RHS of this equation is bounded above by the time window width, t_{max}, times the number N_k of neurons in the k-class, and therefore

$$M_k \langle \mathrm{ISI}(k) \rangle_t \leq N_k t_{max} \; . \tag{B.2}$$

However, for large values of t_{max}, one expects that this inequality holds as an approximate equality

$$M_k \langle \mathrm{ISI}(k) \rangle_t \approx N_k t_{max} \; , \tag{B.3}$$

except, perhaps, in those cases when the ISI duration is extremely large, which may happen at low values of k and g.

On the other hand, we have defined (Eq. 4.9) the average firing rate as the average over the whole network of the time average of the firing state, χ_{it}, of neurons

$$\alpha = \frac{1}{N \, t_{max}} \sum_{t=1}^{t_{max}} \sum_{i=1}^{N} \chi_{it} \; . \tag{B.4}$$

Using the degree probability distribution $p(k) = N_k/N$, the RHS can be rewritten as

$$\sum_k p(k) \frac{1}{N_k \, t_{max}} \sum_{t=1}^{t_{max}} \sum_{j \in in(k)} \chi_{jt} \; . \tag{B.5}$$

Now, recalling that $N_t(j)$ is the number of ISIs of neuron j, we can write,

$$N_t(j) \equiv \left(\sum_{t=1}^{tmax} \chi_{jt} \right) - 1 \tag{B.6}$$

which gives way to,

$$M_k \equiv \sum_{j \in in(k)} N_t(j) = \sum_{j \in in(k)} \left[\left(\sum_{t=1}^{t_{max}} \chi_{jt} \right) - 1 \right] = \left(\sum_{t=1}^{t_{max}} \sum_{j \in in(k)} \chi_{jt} \right) - N_k \tag{B.7}$$

so the double sum in t and j of equation (B.5) is just the number, $(M_k + N_k)$, and therefore the average firing rate can be written as

$$\alpha = \sum_k \frac{p(k)}{N_k \, t_{max}} (M_k + N_k) = \frac{1}{t_{max}} + \sum_k \frac{p(k)}{N_k \, t_{max}} M_k \ , \tag{B.8}$$

for large values of t_{max}, this expression can be approximated as,

$$\alpha \approx \sum_k \frac{p(k)}{N_k \, t_{max}} M_k \ , \tag{B.9}$$

which, together with the approximate equality (B.3) gives the desired approximate relation between α and $\langle \mathrm{ISI}(k) \rangle_t$:

$$\alpha \approx \sum_{k=k_{min}}^{k_{max}} \frac{p(k)}{\langle \mathrm{ISI}(k) \rangle_t} \ . \tag{B.10}$$

which is Eq. 4.19 of the Chapter 4.

Bibliography

[1] Sandra González-Bailón, Javier Borge-Holthoefer, Alejandro Rivero, and Yamir Moreno. The dynamics of protest recruitment through an online network. *Scientific reports*, 1, 2011.

[2] Javier Borge-Holthoefer, Alejandro Rivero, and Yamir Moreno. Locating privileged spreaders on an online social network. *Phys. Rev. E*, 85(6):066123, 2012.

[3] Péter Érdi. *Complexity explained*. Springer Science & Business Media, 2007.

[4] Philip W. Anderson. More is different. *Science*, 177(4047):393–396, 1972.

[5] Elena Castellani. Reductionism, emergence, and effective field theories. *Studies in History and Philosophy of Science Part B: Studies in History and Philosophy of Modern Physics*, 33(2):251–267, 2002.

[6] Alexander Rosenberg. *Darwinian reductionism: Or, how to stop worrying and love molecular biology*. University of Chicago Press, 2008.

[7] S. H. Strogatz. *Sync: How Order Emerges from Chaos in the Universe, Nature, and Daily Life*. Hyperion Books, 2004.

[8] S.H. Strogatz. *Nonlinear Dynamics and Chaos: With Applications to Physics, Biology, Chemistry, and Engineering*. Studies in nonlinearity. Westview Press, 2008.

[9] Edward N. Lorenz. Deterministic nonperiodic flow. *Journal of the atmospheric sciences*, 20(2):130–141, 1963.

[10] Benoit B. Mandelbrot and Roberto Pignoni. *The fractal geometry of nature*. W.H. freeman New York, 1983.

[11] Arthur T. Winfree. Biological rhythms and the behavior of populations of coupled oscillators. *Journal of theoretical biology*, 16(1):15–42, 1967.

[12] David Ruelle and Floris Takens. On the nature of turbulence. *Communications in mathematical physics*, 20(3):167–192, 1971.

[13] Arthur T. Winfree. Spiral waves of chemical activity. *Science*, 175(4022):634–636, 1972.

[14] Charles S. Peskin. *Mathematical aspects of heart physiology*. Courant Institute of Mathematical Sciences, New York University, New York, 1975.

[15] Horst Sachs, Michael Stiebitz, and Robin J. Wilson. An historical note: Euler's königsberg letters. *Journal of Graph Theory*, 12(1):133–139, 1988.

[16] P. Erdős and A. Rényi. On random graphs. *Publicationes Mathematicae Debrecen*, 6:290–297, 1959.

[17] Frank Harary. *Graph theory*. Addison-Wesley, 1969.

[18] Duncan J. Watts. *Small worlds: the dynamics of networks between order and randomness*. Princeton university press, 1999.

[19] A. Barabasi and R. Albert. Emergence of scaling in random networks. *Science*, 286(5439):509–512, 1999.

[20] A. Barrat, M. Barthelemy, and A. Vespignani. *Dynamical Processes on Complex Networks*. Cambridge University Press, Cambridge, 2008.

[21] M. E. J. Newman. *Networks: An Introduction*. Oxford Univ. Press, New York, 2010.

[22] L. Lapicque. Recherches quantitatifs sur l'excitation des nerfs traitee comme une polarisation. *J. Phys. Pathol. Gen.*, 9:620–635, 1907.

[23] D. O. Hebb. *The Organization of Behavior*. Wiley, New York, 1949.

[24] Alan L. Hodgkin and Andrew F. Huxley. A quantitative description of membrane current and its application to conduction and excitation in nerve. *The Journal of physiology*, 117(4):500, 1952.

[25] Wilfrid Rall. Theory of physiological properties of dendrites. *Annals of the New York Academy of Sciences*, 96(4):1071–1092, 1962.

[26] Wilfrid Rall. Theoretical significance of dendritic trees for neuronal input-output relations. *Neural theory and modeling*, 7397, 1964.

[27] D. Marr. A theory of cerebellar cortex. *The Journal of physiology*, 202(2):437–470, 1969.

[28] Daniel J. Amit and Nicolas Brunel. Dynamics of a recurrent network of spiking neurons before and following learning. *Network: Computation in Neural Systems*, 8(4):373–404, 1997.

[29] Daniel J. Amit and Nicolas Brunel. Model of global spontaneous activity and local structured activity during delay periods in the cerebral cortex. *Cerebral cortex*, 7(3):237–252, 1997.

[30] Nicolas Brunel and Vincent Hakim. Fast global oscillations in networks of integrate-and-fire neurons with low firing rates. *Neural computation*, 11(7):1621–1671, 1999.

[31] Renato E. Mirollo and Steven H. Strogatz. Synchronization of pulse-coupled biological oscillators. *SIAM Journal on Applied Mathematics*, 50(6):1645–1662, 1990.

[32] Diego Pazó and Ernest Montbrió. From quasiperiodic partial synchronization to collective chaos in populations of inhibitory neurons with delay. *Phys. Rev. Lett.*, 116:238101, Jun 2016.

[33] Jie Zhang and Remus Osan. Analytically tractable studies of traveling waves of activity in integrate-and-fire neural networks. *Phys. Rev. E*, 93:052228, May 2016.

[34] Zhixin Lu, Shane Squires, Edward Ott, and Michelle Girvan. Inhibitory neurons promote robust critical firing dynamics in networks of integrate-and-fire neurons. *Phys. Rev. E*, 94:062309, Dec 2016.

[35] Romi Mankin and Neeme Lumi. Statistics of a leaky integrate-and-fire model of neurons driven by dichotomous noise. *Phys. Rev. E*, 93:052143, May 2016.

[36] Priscilla E. Greenwood and Lawrence M. Ward. *Stochastic neuron models*, volume 1. Springer, 2016.

[37] Michela Fratini, Nicola Poccia, Alessandro Ricci, Gaetano Campi, Manfred Burghammer, Gabriel Aeppli, and Antonio Bianconi. Scale-free structural organization of oxygen interstitials in La_2CuO_{4+y}. *Nature*, 466(7308):841–844, 2010.

[38] Nicola Poccia, Alessandro Ricci, Gaetano Campi, Michela Fratini, Alessandro Puri, Daniele Di Gioacchino, Augusto Marcelli, Michael Reynolds, Manfred Burghammer, Naurang Lal Saini, et al. Optimum inhomogeneity of local lattice distortions in La_2CuO_{4+y}. *Proceedings of the National Academy of Sciences*, 109(39):15685–15690, 2012.

[39] S. Boccaletti, V. Latora, Y. Moreno, M. Chavez, and D.-U. Hwang. Complex networks: Structure and dynamics. *Physics Reports*, 424(4-5):175–308, 2006.

[40] R. Albert and A. Barabasi. Statistical mechanics of complex networks. *reviews of Modern Physics*, 74:47–97, 2002.

[41] A. Pikovsky, M. Rosenblum, and J. Kurths. *Synchronization: A Universal Concept in Nonlinear Sciences*. Cambridge Nonlinear Science Series. Cambridge University Press, 2003.

[42] Alex Arenas, Albert Díaz-Guilera, Jurgen Kurths, Yamir Moreno, and Changsong Zhou. Synchronization in complex networks. *Physics Reports*, 469(3):93–153, 2008.

[43] S. Boccaletti, J. Kurths, G. Osipov, D.L. Valladares, and C.S. Zhou. The synchronization of chaotic systems. *Physics Reports*, 366(1–2):1 – 101, 2002.

[44] Louis M. Pecora and Thomas L. Carroll. Synchronization in chaotic systems. *Phys. Rev. Lett.*, 64:821–824, Feb 1990.

[45] Louis M. Pecora, Thomas L. Carroll, and James F. Heagy. Statistics for mathematical properties of maps between time series embeddings. *Phys. Rev. E*, 52:3420–3439, Oct 1995.

[46] Nikolai F. Rulkov, Mikhail M. Sushchik, Lev S. Tsimring, and Henry D.I. Abarbanel. Generalized synchronization of chaos in directionally coupled chaotic systems. *Phys. Rev. E*, 51(2):980, 1995.

[47] Reggie Brown and Ljupčo Kocarev. A unifying definition of synchronization for dynamical systems. *Chaos: An Interdisciplinary Journal of Nonlinear Science*, 10(2):344–349, 2000.

[48] S. Boccaletti, Louis M. Pecora, and A. Pelaez. Unifying framework for synchronization of coupled dynamical systems. *Phys. Rev. E*, 63:066219, May 2001.

[49] L. Pastur, S. Boccaletti, and P. L. Ramazza. Detecting local synchronization in coupled chaotic systems. *Phys. Rev. E*, 69:036201, Mar 2004.

[50] R. Banerjee, D. Ghosh, E. Padmanaban, R. Ramaswamy, L.M. Pecora, and Syamal K. Dana. Enhancing synchrony in chaotic oscillators by dynamic relaying. *Phys. Rev. E*, 85(2):027201, 2012.

[51] Steven H. Strogatz. From kuramoto to crawford: exploring the onset of synchronization in populations of coupled oscillators. *Physica D: Nonlinear Phenomena*, 143(1):1–20, 2000.

[52] Steven Strogatz. *Sync: The emerging science of spontaneous order*. Hyperion, New York, 2003.

[53] Jesús Gómez-Gardeñes, Sergio Gómez, Alex Arenas, and Yamir Moreno. Explosive synchronization transitions in scale-free networks. *Phys. Rev. Lett.*, 106:128701, Mar 2011.

[54] Stefano Boccaletti, Ginestra Bianconi, Regino Criado, Charo I Del Genio, Jesús Gómez-Gardenes, Miguel Romance, Irene Sendiñá Nadal, Zhen Wang, and Massimiliano Zanin. The structure and dynamics of multilayer networks. *Physics Reports*, 544(1):1–122, 2014.

[55] Lucia Valentina Gambuzza, Mattia Frasca, Luigi Fortuna, and Stefano Boccaletti. Inhomogeneity induces relay synchronization in complex networks. *Phys. Rev. E*, 93:042203, Apr 2016.

[56] S. Boccaletti, J.A. Almendral, S. Guan, I. Leyva, Z. Liu, I. Sendiña-Nadal, Z. Wang, and Y. Zou. Explosive transitions in complex networks' structure and dynamics: Percolation and synchronization. *Physics Reports*, 660:1–94, 2016.

[57] J. Zhou, C. Juan, J. Lu, and J. A. Lu. On applicability of auxiliary system approach to detect generalized synchronization in complex networks. *IEEE Transactions on Automatic Control*, PP(99):1–1, 2016.

[58] L. Kocarev and U. Parlitz. Generalized synchronization, predictability, and equivalence of unidirectionally coupled dynamical systems. *Phys. Rev. Lett.*, 76:1816–1819, Mar 1996.

[59] Ingo Fischer, Raúl Vicente, Javier M. Buldú, Michael Peil, Claudio R. Mirasso, M. C. Torrent, and Jordi García-Ojalvo. Zero-lag long-range synchronization via dynamical relaying. *Phys. Rev. Lett.*, 97:123902, Sep 2006.

[60] A. Englert, W. Kinzel, Y. Aviad, M. Butkovski, I. Reidler, M. Zigzag, I. Kanter, and M. Rosenbluh. Zero lag synchronization of chaotic systems with time delayed couplings. *Phys. Rev. Lett.*, 104:114102, Mar 2010.

[61] J. Tiana-Alsina, K. Hicke, X. Porte, M. C. Soriano, M. C. Torrent, J. Garcia-Ojalvo, and I. Fischer. Zero-lag synchronization and bubbling in delay-coupled lasers. *Phys. Rev. E*, 85:026209, Feb 2012.

[62] Jia-Gui Wu, Zheng-Mao Wu, Guang-Qiong Xia, Tao Deng, Xiao-Dong Lin, Xi Tang, and Guo-Ying Feng. Isochronous synchronization between chaotic semiconductor lasers over 40-km fiber links. *Photonics Technology Letters, IEEE*, 23(24):1854–1856, 2011.

[63] Iacyel Gomes Da Silva, Javier M Buldú, Claudio R Mirasso, and Jordi García-Ojalvo. Synchronization by dynamical relaying in electronic circuit arrays. *Chaos: An Interdisciplinary Journal of Nonlinear Science*, 16(4):043113, 2006.

[64] A. Wagemakers, J.M. Buldú, and M.A.F. Sanjuán. Experimental demonstration of bidirectional chaotic communication by means of isochronal synchronization. *EPL (Europhysics Letters)*, 81(4):40005, 2008.

[65] Andreas K. Engel, Peter König, Andreas K. Kreiter, and Wolf Singer. Interhemispheric synchronization of oscillatory neuronal responses in cat visual cortex. *Science*, 252(5009):1177–1179, 1991.

[66] Peter Konigqt and Wolf Singer. Visuomotor integration is associated with zero time-lag synchronization among cortical areas. *Nature*, 385:157, 1997.

[67] Raul Vicente, Leonardo L. Gollo, Claudio R. Mirasso, Ingo Fischer, and Gordon Pipa. Dynamical relaying can yield zero time lag neuronal synchrony despite long conduction delays. *Proceedings of the National Academy of Sciences*, 105(44):17157–17162, 2008.

[68] M. Vajapeyam, S. Vedantam, U. Mitra, J. C. Preisig, and M. Stojanovic. Distributed space-time cooperative schemes for underwater acoustic communications. *IEEE Journal of Oceanic Engineering*, 33(4):489–501, Oct 2008.

[69] Peter Dayan and Laurence F. Abbott. *Theoretical neuroscience*, volume 806. Cambridge, MA: MIT Press, 2001.

[70] Hermann Haken. *Brain dynamics: an introduction to models and simulations*. Springer Science & Business Media, 2007.

[71] Renato E. Mirollo and Steven H. Strogatz. Synchronization of pulse-coupled biological oscillators. *SIAM Journal on Applied Mathematics*, 50(6):1645–1662, 1990.

[72] A. Roxin, H. Riecke, and S. A. Solla. Self-sustained activity in a small-world network of excitable neurons. *Phys. Rev. Lett.*, 92:198101, May 2004.

[73] Álvaro Corral, Conrad J. Pérez, Albert Díaz-Guilera, and Alex Arenas. Self-organized criticality and synchronization in a lattice model of integrate-and-fire oscillators. *Phys. Rev. Lett.*, 74(1):118, 1995.

[74] P. Piedrahita, J. Borge-Holthoefer, Y. Moreno, and A. Arenas. Modeling self-sustained activity cascades in socio-technical networks. *EPL (Europhysics Letters)*, 104(4):48004, 2013.

[75] Irmantas Ratas and Kestutis Pyragas. Macroscopic self-oscillations and aging transition in a network of synaptically coupled quadratic integrate-and-fire neurons. *Phys. Rev. E*, 94:032215, Sep 2016.

[76] Wulfram Gerstner and Werner M. Kistler. *Spiking neuron models: Single neurons, populations, plasticity*. Cambridge university press, 2002.

[77] Wulfram Gerstner, Werner M. Kistler, Richard Naud, and Liam Paninski. *Neuronal dynamics: From single neurons to networks and models of cognition*. Cambridge University Press, 2014.

[78] Victor M. Eguíluz, Dante R. Chialvo, Guillermo A. Cecchi, Marwan Baliki, and A. Vania Apkarian. Scale-free brain functional networks. *Phys. Rev. Lett.*, 94:018102, Jan 2005.

[79] A. N. Burkitt. A review of the integrate-and-fire neuron model: I. homogeneous synaptic input. *Biological Cybernetics*, 95(1):1–19, 2006.

[80] A. N. Burkitt. A review of the integrate-and-fire neuron model: Ii. inhomogeneous synaptic input and network properties. *Biological cybernetics*, 95(2):97–112, 2006.

[81] Alfonso Renart, Nicolas Brunel, and Xiao-Jing Wang. Mean-field theory of irregularly spiking neuronal populations and working memory in recurrent cortical networks. *Computational neuroscience: A comprehensive approach*, pages 431–490, 2004.

[82] Nicolas Brunel. Dynamics of sparsely connected networks of excitatory and inhibitory spiking neurons. *Journal of computational neuroscience*, 8(3):183–208, 2000.

[83] Bruno Cessac. A discrete time neural network model with spiking neurons. *Journal of Mathematical Biology*, 56(3):311–345, 2008.

[84] Bruno Cessac. A discrete time neural network model with spiking neurons ii: Dynamics with noise. *Journal of mathematical biology*, 62(6):863–900, 2011.

[85] Bruno Cessac and Rodrigo Cofre. Spike train statistics and gibbs distributions. *Journal of Physiology-Paris*, 107(5):360–368, 2013.

[86] James P. Keener, F. C. Hoppensteadt, and J. Rinzel. Integrate-and-fire models of nerve membrane response to oscillatory input. *SIAM Journal on Applied Mathematics*, 41(3):503–517, 1981.

[87] Eugene M. Izhikevich. *Dynamical systems in neuroscience*. MIT press, 2007.

[88] P. C. Bressloff. Mean-field theory of globally coupled integrate-and-fire neural oscillators with dynamic synapses. *Phys. Rev. E*, 60:2160–2170, Aug 1999.

[89] Nicolas Brunel and Peter E. Latham. Firing rate of the noisy quadratic integrate-and-fire neuron. *Neural Computation*, 15(10):2281–2306, 2003.

[90] Simona Olmi, Roberto Livi, Antonio Politi, and Alessandro Torcini. Collective oscillations in disordered neural networks. *Phys. Rev. E*, 81:046119, Apr 2010.

[91] Wilten Nicola and Sue Ann Campbell. Mean-field models for heterogeneous networks of two-dimensional integrate and fire neurons. *Frontiers in Computational Neuroscience*, 7:184, 2013.

[92] Agnieszka Grabska-Barwińska and Peter E. Latham. How well do mean field theories of spiking quadratic-integrate-and-fire networks work in realistic parameter regimes? *Journal of computational neuroscience*, 36(3):469–481, 2014.

[93] Matteo di Volo, Raffaella Burioni, Mario Casartelli, Roberto Livi, and Alessandro Vezzani. Neural networks with excitatory and inhibitory components: Direct and inverse problems by a mean-field approach. *Phys. Rev. E*, 93:012305, Jan 2016.

[94] Duncan J. Watts. The "new" science of networks. *Annual review of Sociology*, 30:243–270, 2004.

[95] David Lazer, Alex Sandy Pentland, Lada Adamic, Sinan Aral, Albert Laszlo Barabasi, Devon Brewer, Nicholas Christakis, Noshir Contractor, James Fowler, Myron Gutmann, et al. Life in the network: the coming age of computational social science. *Science (New York, NY)*, 323(5915):721, 2009.

[96] Rosaria Conte, Nigel Gilbert, Giulia Bonelli, Claudio Cioffi-Revilla, Guillaume Deffuant, Janos Kertesz, Vittorio Loreto, Suzy Moat, J-P Nadal, Anxo Sanchez, et al. Manifesto of computational social science. *The European Physical Journal Special Topics*, 214(1):325–346, 2012.

[97] Jim Giles. Making the links. *Nature*, 488(7412):448, 2012.

[98] Anatol Rapoport. Spread of information through a population with socio-structural bias: I. assumption of transitivity. *The bulletin of mathematical biophysics*, 15(4):523–533, 1953.

[99] Daryl J. Daley and David G. Kendall. Epidemics and rumours. *Nature*, 204(4963):1118–1118, 1964.

[100] William Goffman and V.A. Newill. Generalization of epidemic theory. *Nature*, 204(4955):225–228, 1964.

[101] Javier Borge-Holthoefer, Raquel A. Baños, Sandra González-Bailón, and Yamir Moreno. Cascading behaviour in complex socio-technical networks. *Journal of Complex Networks*, 1(1):3–24, 2013.

[102] Mark Granovetter. Threshold models of collective behavior. *American journal of sociology*, 83(6):1420–1443, 1978.

[103] James P. Gleeson, Davide Cellai, Jukka-Pekka Onnela, Mason A. Porter, and Felix Reed-Tsochas. A simple generative model of collective online behavior. *Proceedings of the National Academy of Sciences*, 111(29):10411–10415, 2014.

[104] Tad Hogg, Kristina Lerman, and Laura M. Smith. Stochastic models predict user behavior in social media. *arXiv preprint arXiv:1308.2705*, 2013.

[105] M. E. J. Newman. The structure and function of complex networks. *SIAM review*, 45(2):167–256, 2003.

[106] R. Pastor-Satorras, M. Rubi, and A. Diaz-Guilera. *Statistical mechanics of complex networks*, volume 625. Springer Science & Business Media, 2003.

[107] P. Erdős and A. Rényi. On the evolution of random graphs. *Bull. Inst. Internat. Statist*, 38(4):343–347, 1961.

[108] D. J. Watts and S. H. Strogatz. Collective dynamics of /'small-world/' networks. *Nature*, 393:440–442, June 1998.

[109] Alain Barrat and Martin Weigt. On the properties of small-world network models. *The European Physical Journal B-Condensed Matter and Complex Systems*, 13(3):547–560, 2000.

[110] Stefan Bornholdt and Heinz Georg Schuster. *Handbook of graphs and networks: from the genome to the internet*. John Wiley & Sons, 2006.

[111] M. Catanzaro, M. Boguñá, and R. Pastor-Satorras. Generation of uncorrelated random scale-free networks. *Phys. Rev. E*, 71:027103, Feb 2005.

[112] Mikko Kivelä, Alex Arenas, Marc Barthelemy, James P Gleeson, Yamir Moreno, and Mason A Porter. Multilayer networks. *Journal of complex networks*, 2(3):203–271, 2014.

[113] E. A. Bender and E. R. Canfield. The asymptotic number of labeled graphs with given degree sequences. *Journal of Combinatorial Theory, Series A*, 24(3):296 – 307, 1978.

[114] M. E. J. Newman, S. H. Strogatz, and D. J. Watts. Random graphs with arbitrary degree distributions and their applications. *Phys. Rev. E*, 64:026118, Jul 2001.

[115] Duncan S. Callaway, M. E. J. Newman, Steven H. Strogatz, and Duncan J. Watts. Network robustness and fragility: Percolation on random graphs. *Phys. Rev. Lett.*, 85:5468–5471, Dec 2000.

[116] Luc Devroye. *Non-Uniform Random Variate Generation*. Springer-Verlag, New York, 1986.

[117] Niloy Ganguly, Andreas Deutsch, and Animesh Mukherjee. *Dynamics On and Of Complex Networks: Applications to Biology, Computer Science, and the Social Sciences*. Springer Science & Business Media, 2009.

[118] A. Pikovsky and M. Rosenblum. Synchronization. *Scholarpedia*, 2(12):1459, 2007. revision 128276.

[119] Tilmann Heil, Ingo Fischer, Wolfgang Elsässer, Josep Mulet, and Claudio R. Mirasso. Chaos synchronization and spontaneous symmetry-breaking in symmetrically delay-coupled semiconductor lasers. *Phys. Rev. Lett.*, 86(5):795–798, 2001.

[120] Olga I. Moskalenko, Alexey A. Koronovskii, Alexander E. Hramov, and Stefano Boccaletti. Generalized synchronization in mutually coupled oscillators and complex networks. *Phys. Rev. E*, 86(3):036216, 2012.

[121] Alexandra S. Landsman and Ira B. Schwartz. Complete chaotic synchronization in mutually coupled time-delay systems. *Phys. Rev. E*, 75(2):026201, 2007.

[122] Otto E. Rössler. An equation for continuous caos. *Physics Letters A*, 57(5):397–398, 1976.

[123] Valery Iustinovich Oseledec. A multiplicative ergodic theorem. lyapunov characteristic numbers for dynamical systems. *Trans. Moscow Math. Soc*, 19(2):197–231, 1968.

[124] Predrag Cvitanovic, Roberto Artuso, Ronnie Mainieri, Gregor Tanner, Gábor Vattay, Niall Whelan, and Andreas Wirzba. *Chaos: classical and quantum*. Niels Bohr Institute, Copenhagen 2005, 2005.

[125] Marco Sandri. Numerical calculation of lyapunov exponents. *Mathematica Journal*, 6(3):78–84, 1996.

[126] Giancarlo Benettin, Luigi Galgani, Antonio Giorgilli, and Jean-Marie Strelcyn. Lyapunov characteristic exponents for smooth dynamical systems and for hamiltonian systems; a method for computing all of them. part 1: Theory. *Meccanica*, 15(1):9–20, 1980.

[127] R. Quian Quiroga, A. Kraskov, T. Kreuz, and P. Grassberger. Performance of different synchronization measures in real data: A case study on electroencephalographic signals. *Phys. Rev. E*, 65:041903, Mar 2002.

[128] Matthew B. Kennel, Reggie Brown, and Henry D. I. Abarbanel. Determining embedding dimension for phase-space reconstruction using a geometrical construction. *Phys. Rev. A*, 45:3403–3411, Mar 1992.

[129] A. N. Pisarchik, R. Jaimes-Reátegui, J. R. Villalobos-Salazar, J. H. García-López, and S. Boccaletti. Synchronization of chaotic systems with coexisting attractors. *Phys. Rev. Lett.*, 96:244102, Jun 2006.

[130] R. Gutiérrez, R. Sevilla-Escoboza, P. Piedrahita, C. Finke, U. Feudel, J. M. Buldú, G. Huerta-Cuellar, R. Jaimes-Reátegui, Y. Moreno, and S. Boccaletti. Generalized synchronization in relay systems with instantaneous coupling. *Phys. Rev. E*, 88:052908, Nov 2013.

[131] Olga I. Moskalenko, Alexey A. Koronovskii, and Alexander E. Hramov. Inapplicability of an auxiliary-system approach to chaotic oscillators with mutual-type coupling and complex networks. *Phys. Rev. E*, 87:064901, Jun 2013.

[132] Henry C. Tuckwell. *Introduction to Theoretical Neurobiology: Volume 1, Linear Cable Theory and Dendritic Structure*, volume 1. Cambridge University Press, 1988.

[133] Richard FitzHugh. Impulses and physiological states in theoretical models of nerve membrane. *Biophysical journal*, 1(6):445–466, 1961.

[134] Jinichi Nagumo, Suguru Arimoto, and Shuji Yoshizawa. An active pulse transmission line simulating nerve axon. *Proceedings of the IRE*, 50(10):2061–2070, 1962.

[135] Hugh R. Wilson. *Spikes, decisions, and actions: the dynamical foundations of neurosciences*. Oxford University Press, 1999.

[136] G. Bard Ermentrout and David H. Terman. *Mathematical foundations of neuroscience*, volume 35. Springer Science & Business Media, 2010.

[137] Michael V. Mascagni, Arthur S. Sherman, et al. *Numerical methods for neuronal modeling*, volume 2. MIT Press, Cambridge, MA, 1989.

[138] Yoshiki Kuramoto. Collective synchronization of pulse-coupled oscillators and excitable units. *Physica D: Nonlinear Phenomena*, 50(1):15–30, 1991.

[139] Hédi Soula, Guillaume Beslon, and Olivier Mazet. Spontaneous dynamics of asymmetric random recurrent spiking neural networks. *Neural Computation*, 18(1):60–79, 2006.

[140] D. R. Paula, A. D. Araújo, J. S. Andrade, H. J. Herrmann, and J. A. C. Gallas. Periodic neural activity induced by network complexity. *Phys. Rev. E*, 74:017102, Jul 2006.

[141] Patrick McGraw and Michael Menzinger. Self-sustaining oscillations in complex networks of excitable elements. *Phys. Rev. E*, 83:037102, Mar 2011.

[142] Reuven Cohen and Shlomo Havlin. Scale-free networks are ultrasmall. *Phys. Rev. Lett.*, 90:058701, Feb 2003.

[143] Bruno Cessac and Manuel Samuelides. From neuron to neural networks dynamics. *The European Physical Journal Special Topics*, 142(1):7–88, 2007.

[144] Lorenzo Tattini, Simona Olmi, and Alessandro Torcini. Coherent periodic activity in excitatory erdös-renyi neural networks: the role of network connectivity. *Chaos: An Interdisciplinary Journal of Nonlinear Science*, 22(2):023133, 2012.

[145] Luis F. Lago-Fernández, Ramón Huerta, Fernando Corbacho, and Juan A. Sigüenza. Fast response and temporal coherent oscillations in small-world networks. *Phys. Rev. Lett.*, 84:2758–2761, Mar 2000.

[146] Wouter-Jan Rappel and Alain Karma. Noise-induced coherence in neural networks. *Phys. Rev. Lett.*, 77:3256–3259, Oct 1996.

[147] Wilten Nicola, Felix Njap, Katie Ferguson, Frances Skinner, and Sue Ann Campbell. Mean field analysis gives accurate predictions of the behaviour of large networks of sparsely coupled and heterogeneous neurons. *BMC Neuroscience*, 15(Suppl 1):O3, 2014.

[148] Stefano Fusi and Maurizio Mattia. Collective behavior of networks with linear (vlsi) integrate-and-fire neurons. *Neural Computation*, 11(3):633–652, 1998.

[149] Charo I. Del Genio, Thilo Gross, and Kevin E. Bassler. All scale-free networks are sparse. *Phys. Rev. Lett.*, 107:178701, Oct 2011.

[150] James Coleman, Elihu Katz, and Herbert Menzel. The diffusion of an innovation among physicians. *Sociometry*, 20(4):253–270, 1957.

[151] Elihu Katz and Paul Lazarsfeld. Lazarsfeld. 1955. personal influence: The part played by people in the flow of mass communications. *Glencoe, Illinois: The Free Press. KatzPersonal Influence: The Part Played by People in the Flow of Mass Communication*, 1955.

[152] Rolf Meyersohn and Elihu Katz. Notes on a natural history of fads. *American Journal of Sociology*, 62(6):594–601, 1957.

[153] Gabriel Tarde. *On communication and social influence: Selected papers*. University of Chicago Press, 2010.

[154] Herbert Spencer. *The Study of Sociology*, volume 5. D. Appleton, 1873.

[155] Nicholas A. Christakis and James H. Fowler. *Connected: The surprising power of our social networks and how they shape our lives*. Little, Brown, 2009.

[156] Duncan J. Watts. *Six degrees: The science of a connected age*. WW Norton & Company, 2004.

[157] Scott A. Golder and Michael W. Macy. Digital footprints: Opportunities and challenges for online social research. *Annual review of Sociology*, 40:129–152, 2014.

[158] Duncan J. Watts. A twenty-first century science. *Nature*, 445(7127):489–489, 2007.

[159] Mark Newman, Albert-Laszlo Barabasi, and Duncan J. Watts. *The structure and dynamics of networks*. Princeton University Press, 2011.

[160] Mark S. Granovetter. The strength of weak ties. *American journal of sociology*, 78(6):1360–1380, 1973.

[161] Mark Granovetter. The strength of weak ties: A network theory revisited. *Sociological theory*, pages 201–233, 1983.

[162] Hyojoung Kim and Peter S. Bearman. The structure and dynamics of movement participation. *American Sociological review*, pages 70–93, 1997.

[163] Michael W. Macy. Chains of cooperation: Threshold effects in collective action. *American Sociological review*, pages 730–747, 1991.

[164] Gerald Marwell and Pamela Oliver. *The critical mass in collective action*. Cambridge University Press, 1993.

[165] Thomas W Valente. *Network models of the diffusion of innovations.* Cresskill New Jersey Hampton Press 1995., 1995.

[166] Thomas W. Valente. Social network thresholds in the diffusion of innovations. *Social networks*, 18(1):69–89, 1996.

[167] Peter Hedström and Peter Bearman. *The Oxford handbook of analytical sociology*. Oxford University Press, 2009.

[168] Linton C. Freeman. Centrality in social networks conceptual clarification. *Social networks*, 1(3):215–239, 1978.

[169] Ronald S. Burt. *Structural holes: the social structure of competition*. Cambridge, MA: Harvard University Press, 1992.

[170] Michelle Girvan and Mark E. J. Newman. Community structure in social and biological networks. *Proceedings of the national academy of sciences*, 99(12):7821–7826, 2002.

[171] Duncan J. Watts. A simple model of global cascades on random networks. *Proceedings of the National Academy of Sciences*, 99(9):5766–5771, 2002.

[172] J-P Onnela, Jari Saramäki, Jorkki Hyvönen, György Szabó, David Lazer, Kimmo Kaski, János Kertész, and A-L Barabási. Structure and tie strengths in mobile communication networks. *Proceedings of the National Academy of Sciences*, 104(18):7332–7336, 2007.

[173] Johan Ugander, Lars Backstrom, Cameron Marlow, and Jon Kleinberg. Structural diversity in social contagion. *Proceedings of the National Academy of Sciences*, 109(16):5962–5966, 2012.

[174] Damon Centola, Víctor M. Eguíluz, and Michael W. Macy. Cascade dynamics of complex propagation. *Physica A: Statistical Mechanics and its Applications*, 374(1):449–456, 2007.

[175] Damon Centola and Michael Macy. Complex contagions and the weakness of long ties 1. *American journal of Sociology*, 113(3):702–734, 2007.

[176] Sinan Aral, Lev Muchnik, and Arun Sundararajan. Distinguishing influence-based contagion from homophily-driven diffusion in dynamic networks. *Proceedings of the National Academy of Sciences*, 106(51):21544–21549, 2009.

[177] Sinan Aral and Dylan Walker. Identifying influential and susceptible members of social networks. *Science*, 337(6092):337–341, 2012.

[178] Michael W. Macy. Learning theory and the logic of critical mass. *American Sociological review*, pages 809–826, 1990.

[179] Michael W. Macy. Learning to cooperate: Stochastic and tacit collusion in social exchange. *American Journal of Sociology*, 97(3):808–843, 1991.

[180] Alexei Vázquez, Joao Gama Oliveira, Zoltán Dezsö, Kwang-Il Goh, Imre Kondor, and Albert-László Barabási. Modeling bursts and heavy tails in human dynamics. *Phys. Rev. E*, 73(3):036127, 2006.

[181] Janette Lehmann, Bruno Gonçalves, José J Ramasco, and Ciro Cattuto. Dynamical classes of collective attention in twitter. In *Proceedings of the 21st international conference on World Wide Web*, pages 251–260. ACM, 2012.

[182] Fang Wu and Bernardo A. Huberman. Novelty and collective attention. *Proceedings of the National Academy of Sciences*, 104(45):17599–17601, 2007.

[183] Paolo Gerbaudo. *Tweets and the streets: Social media and contemporary activism*. Pluto Press, 2012.

[184] Howard Rheingold. *Smart Mobs: The next social revolution*. Cambridge, MA: Perseus, 2002.

[185] Emile Durkheim and Ward Swain. The elementary forms of religious life. *AJN The American Journal of Nursing*, 16(12):1248, 1916.

[186] Randall Collins. *Interaction Ritual Chains*. Princeton University Press, 2004.

[187] Pablo Barberá, Ning Wang, Richard Bonneau, John T. Jost, Jonathan Nagler, Joshua Tucker, and Sandra González-Bailón. The critical periphery in the growth of social protests. *PloS one*, 10(11):e0143611, 2015.

[188] Javier Borge-Holthoefer, Alejandro Rivero, Iñigo García, Elisa Cauhé, Alfredo Ferrer, Darío Ferrer, David Francos, David Iniguez, María Pilar Pérez, Gonzalo Ruiz, et al. Structural and dynamical patterns on online social networks: the spanish may 15th movement as a case study. *PloS one*, 6(8):e23883, 2011.

[189] Ceren Budak and Duncan J. Watts. Dissecting the spirit of gezi: Influence vs. selection in the occupy gezi movement. *Sociological Science*, 2, 2015.

[190] Michael D. Conover, Emilio Ferrara, Filippo Menczer, and Alessandro Flammini. The digital evolution of occupy wall street. *PloS one*, 8(5):e64679, 2013.

[191] Sarah J. Jackson and Brooke Foucault Welles. Hijacking# mynypd: Social media dissent and networked counterpublics. *Journal of Communication*, 65(6):932–952, 2015.

[192] David Liben-Nowell and Jon Kleinberg. Tracing information flow on a global scale using internet chain-letter data. *Proceedings of the National Academy of Sciences*, 105(12):4633–4638, 2008.

[193] Eytan Bakshy, Jake M. Hofman, Winter A. Mason, and Duncan J. Watts. Everyone's an influencer: quantifying influence on twitter. In *Proceedings of the fourth ACM international conference on Web search and data mining*, pages 65–74. ACM, 2011.

[194] Kristina Lerman, Rumi Ghosh, and Tawan Surachawala. Social contagion: An empirical study of information spread on digg and twitter follower graphs. *arXiv preprint arXiv:1202.3162*, 2012.

[195] Jure Leskovec, Lars Backstrom, and Jon Kleinberg. Meme-tracking and the dynamics of the news cycle. In *Proceedings of the 15th ACM SIGKDD international conference on Knowledge discovery and data mining*, pages 497–506. ACM, 2009.

[196] James P. Gleeson and Diarmuid J. Cahalane. Seed size strongly affects cascades on random networks. *Phys. Rev. E*, 75(5):056103, 2007.

[197] Aram Galstyan and Paul Cohen. Cascading dynamics in modular networks. *Phys. Rev. E*, 75(3):036109, 2007.

[198] James P. Gleeson. Cascades on correlated and modular random networks. *Phys. Rev. E*, 77(4):046117, 2008.

[199] Adam Hackett, Sergey Melnik, and James P. Gleeson. Cascades on a class of clustered random networks. *Phys. Rev. E*, 83(5):056107, 2011.

[200] Khury Peterson-Smith. Black lives matter: A new movement takes shape. *International Socialist review*, 96, 2015.

[201] D. Carr. View of# ferguson thrust michael brown shooting to national attention. *The New York Times*, 2014.

[202] Petter Holme and Jari Saramäki. Temporal networks. *Physics reports*, 519(3):97–125, 2012.

[203] James Moody. The importance of relationship timing for diffusion. *Social Forces*, 81(1):25–56, 2002.

[204] Kate Knibbs. *Protesters Are Using FireChat's Mesh Networks To Organize in Hong Kong*, 2014.

[205] Emily Parker. Social media and the hong kong protests. *The New Yorker*, 2014.

[206] Aviva Rutkin and Jacob Aron. *Hong Kong protesters use a mesh network to organise*, 2014.

[207] Albert-László Barabási. Scale-free networks: a decade and beyond. *science*, 325(5939):412–413, 2009.

[208] Haewoon Kwak, Changhyun Lee, Hosung Park, and Sue Moon. What is twitter, a social network or a news media? In *Proceedings of the 19th international conference on World wide web*, pages 591–600. ACM, 2010.

[209] Lars Backstrom, Paolo Boldi, Marco Rosa, Johan Ugander, and Sebastiano Vigna. Four degrees of separation. In *Proceedings of the 4th Annual ACM Web Science Conference*, pages 33–42. ACM, 2012.

[210] Johan Ugander, Brian Karrer, Lars Backstrom, and Cameron Marlow. The anatomy of the facebook social graph. *arXiv preprint arXiv:1111.4503*, 2011.

[211] Zhengbiao Guo, Zhitang Li, and Hao Tu. Sina microblog: an information-driven online social network. In *Cyberworlds (CW), 2011 International Conference on*, pages 160–167. IEEE, 2011.

[212] Daniel M. Romero, Brendan Meeder, and Jon Kleinberg. Differences in the mechanics of information diffusion across topics: idioms, political hashtags, and complex contagion on twitter. In *Proceedings of the 20th international conference on World wide web*, pages 695–704. ACM, 2011.

[213] Zachary C. Steinert-Threlkeld, Delia Mocanu, Alessandro Vespignani, and James Fowler. Online social networks and offline protest. *EPJ Data Science*, 4(1):19, 2015.

[214] Takashi Nishikawa, Adilson E. Motter, Ying-Cheng Lai, and Frank C. Hoppensteadt. Heterogeneity in oscillator networks: Are smaller worlds easier to synchronize? *Phys. Rev. Lett.*, 91:014101, 2003.

[215] Kevin P. O'Keeffe, P. L. Krapivsky, and Steven H. Strogatz. Synchronization as aggregation: Cluster kinetics of pulse-coupled oscillators. *Phys. Rev. Lett.*, 115:064101, Aug 2015.

[216] Malcolm Gladwell. Small change. *The New Yorker*, 4(2010):42–49, 2010.

[217] Ashley Parker. Twitter's secret handshake. *The New York Times*, 2011.

[218] Robert M. Bond, Christopher J. Fariss, Jason J. Jones, Adam D.I. Kramer, Cameron Marlow, Jaime E. Settle, and James H. Fowler. A 61-million-person experiment in social influence and political mobilization. *Nature*, 489(7415):295–298, 2012.

[219] Scott A. Golder and Michael W. Macy. Diurnal and seasonal mood vary with work, sleep, and daylength across diverse cultures. *Science*, 333(6051):1878–1881, 2011.

[220] Michael Molloy and Bruce Reed. A critical point for random graphs with a given degree sequence. *Random structures & algorithms*, 6(2-3):161–180, 1995.

[221] Michael Molloy and Bruce Reed. The size of the giant component of a random graph with a given degree sequence. *Combinatorics, probability and computing*, 7(03):295–305, 1998.

[222] Sergey N. Dorogovtsev, Alexander V. Goltsev, and José F.F. Mendes. Critical phenomena in complex networks. *reviews of Modern Physics*, 80(4):1275, 2008.

[223] Diego Garlaschelli and Maria I. Loffredo. Patterns of link reciprocity in directed networks. *Phys. Rev. Lett.*, 93:268701, Dec 2004.

[224] Thomas C. Schelling. *Micromotives and macrobehavior*. London: Norton, 1978.

[225] Everett M. Rogers. Diffusion of innovations, edn. *Free Pres., New York*, 2003.

[226] Stanley Wasserman and Katherine Faust. *Social network analysis: Methods and applications*, volume 8. Cambridge university press, 1994.

[227] Gerald Marwell, Pamela E. Oliver, and Ralph Prahl. Social networks and collective action: A theory of the critical mass. iii. *American Journal of Sociology*, 94(3):502–534, 1988.

[228] Miller McPherson, Lynn Smith-Lovin, and James M. Cook. Birds of a feather: Homophily in social networks. *Annual review of sociology*, 27(1):415–444, 2001.

[229] Javier Borge-Holthoefer, Nicola Perra, Bruno Gonçalves, Sandra González-Bailón, Alex Arenas, Yamir Moreno, and Alessandro Vespignani. The dynamics of information-driven coordination phenomena: A transfer entropy analysis. *Science advances*, 2(4):e1501158, 2016.